

# Drying of Faecal Sludge using Solar Thermal Energy

Report to the  
**Water Research Commission**

by

**<sup>1</sup>Dr. Santiago Septien Stringel, <sup>1</sup>Mr. Tendayi Mugauri, <sup>2</sup>Mrs. Anusha Singh and  
<sup>3</sup>Dr. Freddie Inambao**

<sup>1</sup>Pollution Research Group, University of KwaZulu-Natal

<sup>2</sup>Chemical Engineering, University of KwaZulu-Natal

<sup>3</sup>Mechanical Engineering, University of KwaZulu-Natal

**WRC Report No. 2582/1/18  
ISBN 978-0-6392-0095-8**

**March 2019**



**Obtainable from**  
Water Research Commission  
Private Bag X03  
GEZINA, 0031

[orders@wrc.org.za](mailto:orders@wrc.org.za) or download from [www.wrc.org.za](http://www.wrc.org.za)

**DISCLAIMER**

This report has been reviewed by the Water Research Commission (WRC) and approved for publication. Approval does not signify that the contents necessarily reflect the views and policies of the WRC, nor does mention of trade names or commercial products constitute endorsement or recommendation for use.

# TABLE OF CONTENTS

---

List of Figures.....	vi
List of Tables.....	xi
Abbreviations.....	xii
1 Introduction.....	1
2 Literature review.....	5
2.1 Solar Energy.....	5
2.1.1 Solar energy resource.....	5
2.1.2 Use of solar energy in the sanitation field.....	14
2.2 Drying of faecal sludge.....	16
2.2.1 Concepts of drying process.....	16
2.2.2 Drying technologies.....	22
2.2.3 Peculiarities of faecal sludge drying.....	24
2.3 Solar drying.....	31
2.3.1 Solar thermal systems.....	31
2.3.2 Solar drying technologies.....	32
2.3.3 Solar drying of sewage sludge.....	35
2.3.4 Potential use of solar drying for faecal sludge.....	42
3 Methodology.....	43
3.1 Feedstock: faecal sludge from VIP latrines.....	43
3.2 Solar drying rig.....	43
3.2.1 Drying chamber.....	45
3.2.2 Air stream.....	46
3.2.3 Measurement of temperature and relative humidity.....	47
3.2.4 Measurement of solar irradiance.....	47
3.2.5 Interface and data logging.....	47
3.3 Experimental plan.....	49

3.3.1	Experiments in the solar drying rig .....	49
3.3.2	Characterization of the dried product.....	49
3.3.3	Solar air heating chimney .....	52
4	Results and Discussion .....	53
4.1	Solar drying.....	53
4.1.1	Effect of the weather conditions.....	53
4.1.2	Effect of size .....	60
4.1.3	Effect of air stream .....	63
4.2	Characterization of the samples.....	67
4.2.1	Moisture and ash content .....	68
4.2.2	Nutrient analysis .....	70
4.2.3	Calorific value .....	70
4.2.4	Thermal properties .....	71
4.2.5	Morphological characteristics .....	73
4.3	Summary.....	77
5	General conclusion from the project .....	80
6	Guidelines for the development of a solar drier for faecal sludge treatment .....	81
7	Perspectives .....	87
8	Capacity building .....	90
9	Transfer of knowledge .....	91
10	References .....	92
	APPENDIX A: Solar Drying Technologies.....	99
	APPENDIX B: Greenhouses to dry sewage sludge.....	111
	APPENDIX C: Ethical Clearance .....	114
	APPENDIX D: Experimental Site Solar Assessment.....	115
	APPENDIX E: Selection of the Material of the Drying Chamber .....	120
	APPENDIX F: Plans of the Drying Rig .....	122

APPENDIX G: CFD Simulations .....	129
APPENDIX H: Preliminary tests .....	135
APPENDIX I: Solar Air Heating Chimney .....	139
APPENDIX J: Risk Assessment of the Experimental Rig.....	143
APPENDIX K: Irradiance measured during the experiments.....	144
APPENDIX L: Temperatures measured during the experiments (ambient temperature and in drying chamber) .....	149
APPENDIX M: Nutrient analysis.....	154

## LIST OF FIGURES

---

Figure 1. Routes of conversion of solar energy with the associated technologies (GCEP, 2006).....	6
Figure 2. Solar radiation spectrum (source: <a href="https://en.wikipedia.org/wiki/Sunlight#/media/File:Solar_spectrum_en.svg">https://en.wikipedia.org/wiki/Sunlight#/media/File:Solar_spectrum_en.svg</a> ).....	7
Figure 3. Different paths of solar radiation propagation on earth .....	8
Figure 4. Main measurement parameters of solar irradiance .....	9
Figure 5. Photograph (left) and scheme (right) of a pyrheliometer .....	10
Figure 6. Calculation of the DNI .....	10
Figure 7. Shadow band pyranometer .....	11
Figure 8. Thermopile and silicon pyranometers .....	12
Figure 9. Solar map of Africa from the south to the equator, based on GHI (left) and DNI (right) value (source: Solargis) .....	14
Figure 10. Distribution of GIH in the world in 2016 (source: Solargis).....	15
Figure 11. Proportion of the global population using improved sanitation (source: World Health Organization).....	15
Figure 12. Distribution of GIH in Africa in 2016 (source: Solargis) .....	16
Figure 13. Sorption isotherms (Mujumdar and Devahastin, 2000) .....	17
Figure 14. Psychrometric chart of vapour water – air mixture (source: Carrier Corporation) .....	18
Figure 15. Different types of moisture (Mujumdar and Devahastin, 2000) .....	19
Figure 16. Typical drying curve (Moyers and Baldwin, 1997).....	21
Figure 17. Water distribution in the sludge (Chen et al., 2002) .....	25
Figure 18. Presentation of the different phases during conductive drying (Lowe, 1995).....	27
Figure 19. Faecal sludge drying flow diagram.....	31
Figure 20. Typical solar energy dryer design classification (Ekechukwu, 1999).....	34
Figure 21. Schematic representation of the transfer phenomena during sewage sludge solar drying in a greenhouse (Roux et al., 2010) .....	36

Figure 22. Typical greenhouse solar dryer (Huber, 2007).....	36
Figure 23. Photographs of the sludge aspect at different moisture content during solar drying (Zhao et al., 2009) .....	37
Figure 24. Solar drying rig diagram .....	44
Figure 25. Solar drying rig setup .....	44
Figure 26. Setup of the sample support in the solar drying rig .....	45
Figure 27. Drying chamber inside the protection box .....	46
Figure 28. Air heater.....	46
Figure 29. Interior of the air heater .....	47
Figure 30. Data acquisition box.....	48
Figure 31. Interface of the software used for the interface between the instruments and the computer .....	48
Figure 32. Irradiance measured during solar drying in a sunny, cloudy and overcast day.....	54
Figure 33. Temperature measured at the core and surface of the sludge during solar drying in a sunny, cloudy and overcast day.....	55
Figure 34. Mass evolution as a function of time during solar drying in a sunny, cloudy and overcast day.....	56
Figure 35. Mass evolution as a function of time, during solar drying of the enclosed sample (A) and open-air sample (B), in a sunny (1), cloudy (2) and overcast (3) conditions .....	59
Figure 36. Mass evolution as a function of time, during solar drying of the 60 and 120 mm diameter sample, in a sunny day.....	60
Figure 37. Temperature measured at the core and surface during solar drying of the 60 and 120 mm diameter samples, in a sunny day .....	60
Figure 38. Mass evolution as a function of time, during solar drying of the 5 and 10 mm thickness sample, in a sunny day.....	62
Figure 39. Temperature measured at the core and surface during solar drying of the 5 and 10 mm thickness samples, in a sunny day .....	62
Figure 40. Mass evolution as a function of time, during solar drying at different air flowrate, in a sunny day.....	64

Figure 41. Temperature measured at the core and the surface during solar drying at different air flowrate, in a sunny day .....	65
Figure 42. Mass evolution as a function of time, during solar drying at different air temperatures in a sunny day .....	66
Figure 43. Temperature measured at the core and the surface during solar drying at different air temperatures, in a sunny day .....	66
Figure 44. Moisture content of the sludge samples .....	69
Figure 45. Moisture content of the sludge samples .....	70
Figure 46. Calorific value of the sludge samples .....	71
Figure 47. Thermal conductivity of the sludge samples.....	72
Figure 48. Heat capacity of the sludge samples.....	73
Figure 49. Density of the sludge samples .....	74
Figure 50. Shrinkage of the sample after solar drying .....	75
Figure 51. Sample of 5 mm thickness before and after solar drying in sunny conditions (left and right photo, respectively) .....	75
Figure 52. Typical distributed-type natural-circulation solar energy .....	99
Figure 53. Distributed-type natural-circulation solar dryer .....	100
Figure 54. Integral-type (direct) natural-circulation solar energy dryer .....	100
Figure 55. Typical natural circulation solar energy cabinet dryer .....	101
Figure 56. Modified natural circulation solar energy cabinet dryer .....	101
Figure 57. Natural circulation solar energy cabinet dryer with chimney.....	102
Figure 58. Natural circulation glass roof solar energy dryer .....	102
Figure 59. Natural circulation polythene tent dryer .....	103
Figure 60. Natural circulation solar dome dryer.....	103
Figure 61. Greenhouse-type natural circulation solar dome dryer.....	104
Figure 62. Mixed mode natural circulation solar energy dryer.....	104
Figure 63. Mixed mode natural circulation solar dryer.....	105
Figure 64. Mixed mode natural circulation solar dryer with thermal storage.....	105

Figure 65. Multi-stacked mixed mode natural circulation solar energy dryer.....	106
Figure 66. Distributed type active solar energy dryer .....	106
Figure 67. Distributed type active solar dryer with partial air re-circulation.....	107
Figure 68. Continuous flow active grain dryer .....	107
Figure 69. Forced convection greenhouse dryer .....	108
Figure 70. Forced convection transparent roof solar barn.....	108
Figure 71. Active solar energy cabinet dryer .....	109
Figure 72. Interior drum absorber greenhouse active solar dryer.....	109
Figure 73. Typical mixed mode active solar energy dryer .....	110
Figure 74. Solar tunnel dryer with an additional auxiliary heating source.....	110
Figure 75. Solar drying plant in Palma de Mallorca, Spain (Bux, 2010) .....	111
Figure 76. Solar drying plant in Managua, Nicaragua (Meyer-Scharenberg and Pöppke, 2010).....	111
Figure 77. Solar plant in Oldenburg, Germany (Thermo-System, n.d.).....	111
Figure 78. Solar drying greenhouse in Fethiye wastewater treatment plant, Turkey (Kurt, 2014) .....	112
Figure 79. Pilot greenhouse in the East wastewater treatment plant, Turkey (Salihoglu et al., 2007) .....	112
Figure 80. Pilot greenhouse in the Kavala wastewater treatment plant, Greece (Mathioudakis et al., 2013).....	113
Figure 81. Greenhouse dryer combined with heat pump, installed in the west of France (Slim et al., 2008).....	113
Figure 82. Global Horizontal Irradiation (top) and Direct Normal Irradiation (bottom) map in South Africa (source: <a href="http://solargis.info">http://solargis.info</a> ).....	116
Figure 83. Solar maps in the region of KwaZulu-Natal .....	117
Figure 84. GIH daily sum with the diffusive and direct radiation contributions and air temperature during the day, at the roof of Chemical Engineering building (source: <a href="http://solargis.info">http://solargis.info</a> ).....	118
Figure 85. Day length and minimum solar zenith angle at the roof of Chemical Engineering building (source: <a href="http://solargis.info">http://solargis.info</a> ).....	118

Figure 86. Position of the sun along the day at the roof of Chemical Engineering building (source: <a href="http://solargis.info">http://solargis.info</a> ).....	119
Figure 87. Residuals Plot .....	133
Figure 88. CFD simulations of the airflow within the drying chamber with multi-entries inlet (top) and single entry inlet (bottom) .....	134
Figure 89. Solar irradiance measured by the pyranometer .....	135
Figure 90. Mass variation of the wet tissue in the solar drying rig .....	136
Figure 91. Temperature variation (blue plot: temperature in the protection box; orange plot: temperature of the tissue; grey plot: air temperature inside the drying chamber; yellow plot: ambient temperature) .....	138
Figure 92. Photographs of the solar drying rig .....	140

## LIST OF TABLES

---

Table 1. List of faecal sludge drying technologies .....	29
Table 2. Characteristics and performance of greenhouses for sewage sludge solar drying .....	39
Table 3. Label of the samples .....	67
Table 4. Qualitative observations .....	76
Table 5. List of students involved in the project.....	90
Table 6. Characteristics of transparent material of 2 -3 mm thickness .....	121
Table 7. Air flowrate measured at different position in the cross-section of the drying chamber, using single and multi-entry inlet .....	134
Table 8. Summary of the results obtained by the solar heating chimney from the initial design to the modified versions.....	141

## ABBREVIATIONS

---

DHI	Diffusive Horizontal Irradiance
DIFF	Diffusive Irradiance
DNI	Direct Normal Irradiance
GHI	Global Horizontal Irradiance
GTI	Global Tilt Irradiance
IWA	International Water Association
LaDePa	Latrine Dehydration Pasteurization
LTI	Latitude Tilt Irradiance
PRG	Pollution Research Group
SAURAN	Southern African Universities Radiometric Network
UK	United Kingdom
UKZN	University of KwaZulu-Natal
WEDEC	Water, Engineering and Development Centre
WISA	Water Institute of Southern Africa
WRC	Water Research Commission
YWP	Young Water Professional

# 1 INTRODUCTION

---

According to figures from the World Health Organization, 2 billion people worldwide does not have access to decent sanitation in 2017 (WHO, 2017). As a result, important quantities of excreta are annually generated from unimproved sanitation facilities or open defecation practice, which represent a public health threat and pollution source for the environment. Faecal sludge, which is the faecal waste accumulated into pits and eventually mixed with urine, water and / or greywater, needs to be safely managed in order to overcome all the hazards that it presents.

The treatment of faecal sludge is a key step in the faecal sludge management chain. It enables a suitable disposal of the waste without risks for the population and the environment, and with the possibility resource recovery in ultimate goal. Faecal sludge can be reused in different ways, as pointed out by Diener et al. (2014). Different products can be obtained from faecal sludge as fertilizer, soil container, biofuel, animal protein and building material (Kengne et al., 2014).

Drying represents a critical process for the treatment of faecal sludge. It enables to remove the moisture from the sludge and to kill the pathogen population found in the faecal material. The loss of moisture leads to the decrease of the mass and volume of the material, reducing costs related to transportation and storage. The deactivation of pathogens leads to a product safer to handle. Drying can be the final treatment before reuse or a pre-treatment step before further processing (example: pyrolysis or combustion).

Commonly, drying beds are employed for the dehydration of faecal sludge, where a thick layer of faecal sludge is spread in an open-air basin and is removed after the reduction of moisture content. The principle of this technology is based on dewatering by gravity at the bottom of the basin and evaporation of the moisture at the top surface. The drying beds are low-cost technologies but the treatment of sludge takes quite long time to be achieved (usually a few weeks), and pasteurization is not always achieved (Cofie et al., 2006; Dodane and Ronteltap, 2014).

Thermal drying technologies can be used as alternative to drying beds, after an eventual dewatering step in the case of liquid faecal sludge. This type of technology

can achieve considerably faster drying rates, so that they can treat higher throughputs of sludge at lower time. Nevertheless, conventional thermal drying demands high operation costs, which are mainly due to the high amount of moisture to evaporate in the faecal sludge and the high heat latent of vaporization of water. For example, in the eThekweni municipality, an infrared dryer, LaDePa (Latrine Dehydration Pasteurization) was developed to treat the faecal sludge from 30,000 VIP latrines (Harrison and Wilson, 2012). It consumes 8 litres of diesel per hour for its operation (equivalent to 7.9 dollar per hour in August 2017). This cost could not be afforded by many municipal entities in developing countries.

Solar thermal energy is an abundant and free source of energy in the world, particularly in major part of developing countries. Therefore, it could supplement heat for drying purposes, leading to the decrease of the operating costs. Solar drying is one of the most ancient application of solar energy, practiced particularly for food and crops conservation. Since then, there have been technological breakthrough in this area, but the deployment of solar drying technologies have not yet widely commercialized (Belessiotis and Delyannis, 2011). This may change in the near future, as the use of solar energy is gaining relevance in the actual context where efforts are made to reduce the energetic dependence to fossil fuels and to use sustainable sources of energy.

In the faecal sludge sector, the use of solar energy for drying has been minimal, with only a few cases. The use of drying beds in a greenhouse have been explored in Uganda, Ghana and Senegal (Muspratt et al., 2014; Seck et al., 2015). Muspratt et al. (2014) shown that the use of greenhouse could reduce considerable the number of days required to achieve the desired moisture content. In contrast, Seck et al. (2015) did not find that greenhouse shortened the drying period, which could be originated from a less efficient design, but they stated that a greenhouse offers protection to sludge against rehydration during rainfalls. In Rwanda, a faecal sludge treatment plant, designed and operated by Pivot, includes solar drying as a pre-drying stage prior to a rotary thermal dryer (Pivot, 2016). A few on-site sanitation technologies, consisting in a urine diversion dry toilet where the faecal fraction is dried by solar thermal energy, are commercially available, such as the MAITRI toilet (RaVikas, 2016), SANI SOLAR toilet (3P-Technik-Sanitation, 2016) and the Earth Auger (Earth-Augur, n.d.). Other applications of solar thermal energy other than drying exist for faecal sludge treatment,

such as: disinfection of the effluent from a septic tank by heating in a conventional solar water heater, developed by the Asian Institute of Technology in Thailand (Kootatep et al., 2014); disinfection of faecal sludge using steam generated by solar energy concentration in parabolic troughs, developed in Kenya by the company Sanivation (Bohnert et al., 2017); bio-char production from faeces by solar concentration in the “Char-Sol” toilet, funded by the Bill & Melinda Gates Foundation under the Reinvent The Toilet Challenge and designed by the University of Colorado Boulder (Garcia-Fine, 2015); bio-char production from faecal sludge using a mobile transparent screw conveyer and a parabolic solar concentrator in South Africa, Ubuntu-San, funded by the Water Research Commission under the Research Fund For Africa (Pillay and Bhagwan, 2014).

Possible reasons for the low use of solar drying is the lack of awareness about this type of technology, as well as a lack of knowledge and data for the design of plants that could dissuade sanitation practitioners from using solar drying technologies. Motivated from these gaps, a fundamental study was conducted in this project to characterize faecal sludge solar drying. The data obtained during the project could be used for the design of solar drying plants, improvement of existing technologies and innovation of further ones. This study will be done by the development of a thermobalance to measure the kinetics and calculate the energy balance during solar drying at different conditions. This information is crucial for the design and development of solar dryers. Moreover, a series of analyses will be conducted in the dried sample with the objectives to determine how solar drying affects the physical and chemical properties of faecal sludge, with the intention to better understand the phenomenology of the process, and to evaluate the reuse of the product in agriculture and as a biofuel. Faecal sludge from VIP latrines will be used as feedstock for this study as this type of waste is abundant in Africa (Cairncross et al., 2010; Habitat, 2008; Jain, 2011). In parallel to this study, solar drying equipment will be developed through undergraduate projects.

As expected output, this project could promote the use of solar energy for faecal sludge drying, which is a comprehensive way to conciliate sustainability and sanitation. Moreover, this project will also develop Human Capacity on the bridge between the sanitation and energy sectors. In fact, this project is congruent with the national energy strategies of the South African government with respect to beneficiation from the solar

thermal energy capacity in the country (NREL, 2014), and its constitutional obligation to provide sanitation to all citizens (Lewin et al., 2007). In the last couple of years, the South African government has facilitated a large scale installation of water solar heater households, and several projects regarding the construction of concentrating solar power plants. Recently, the largest solar power plant in the southern hemisphere with a capacity of 100 MW, KaXu Solar One, has commenced operation in Pofadder, Northern Cape.

## 2 LITERATURE REVIEW

---

This chapter presents the literature review performed in this project. It presents the theoretical background required for a better understanding of the investigation, by introducing the basic concepts of solar thermal energy, drying process and solar drying technologies. It also gives a review about the peculiarities of faecal sludge drying and the state-of-art of solar drying in the case of sewage sludge.

### 2.1 SOLAR ENERGY

#### 2.1.1 Solar energy resource

Around the world, many countries have begun to confront the challenge of sustainability by adjusting energy consumption methods in order to uphold social, ecological and financial aspects of sustainable development. Fossil fuel based energy sources such as oil, coal and natural gas have resulted in the increase of the amount of greenhouse gases released in the atmosphere, causing global warming. Besides, the depletion of fossil reserves would result in exorbitant operation costs for processes dependent on this energy source. A large interest in alternative fuels such as solar energy for power generation exists in both the developed and developing world. Solar energy is a promising renewable energy resource for power generation. As a renewable energy source, solar energy is environmentally friendly, as it has a low carbon footprint and low pollutant emission.

Solar energy represents the largest energy inflow in the ecosystems. The power density of the density emitted by the Sun is around 64 MW/m<sup>2</sup> of which around 1370 W/m<sup>2</sup> arrives at the atmosphere of Earth, without significant absorption in its way through the space. After reflection and absorption in the atmosphere, around half of the incoming solar energy reaches the surface of the Earth, and used for land heating, evaporation of water and the development of living organisms via photosynthesis.

Despite the availability of solar resource with a potential of 2.5 to 80 TW to supply energy on global scale, generation of power from solar resource is still low compared to other energy resources. The main constraints to the application of solar technologies to replace conventional energy systems have been the relative high capital cost. However, solar energy harnessing technologies are changing to be more

cost effective. The intermittent nature of solar energy results in the requirement of energy storage systems and a management system taking into account the variations of solar energy in the operation of the plant (GCEP, 2006).

Solar energy can be used in different ways:

- Photovoltaic systems which converts solar energy into electrical energy via inorganic or organic semiconductor materials;
- Thermal systems which converts solar energy into thermal energy using solar irradiance absorbents and concentrator devices;
- Photosynthetic, photo(electro)chemical, thermal and thermochemical processes which convert solar energy into fuels for chemical energy storage (example: hydrogen).

The different routes of solar energy valorisation are summarized in Figure 1.

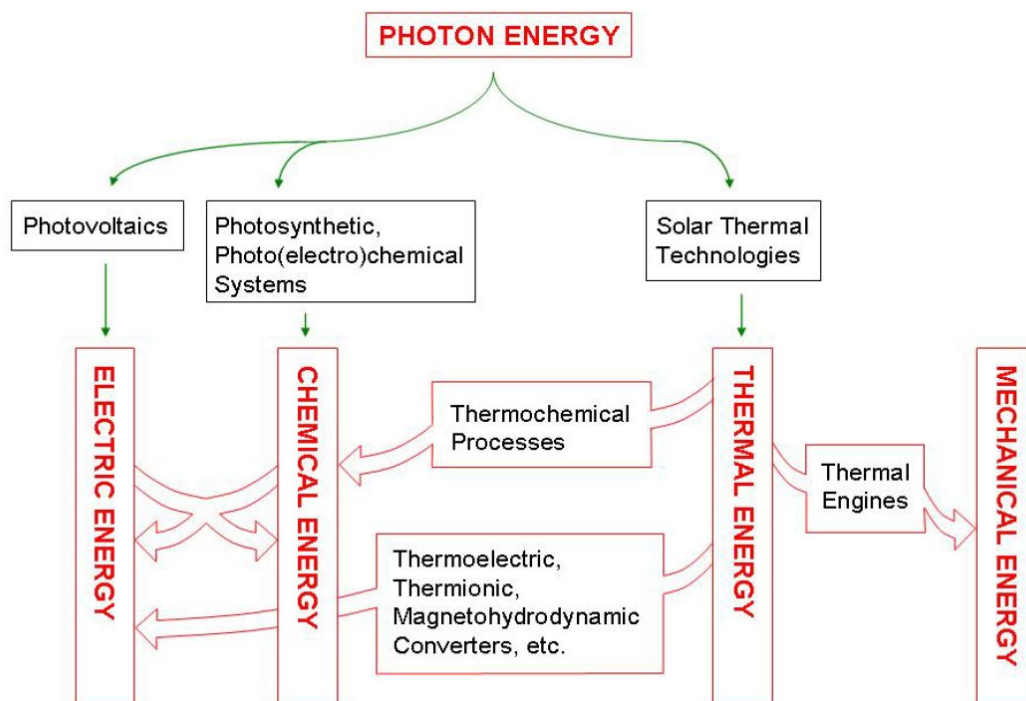


Figure 1. Routes of conversion of solar energy with the associated technologies (GCEP, 2006)

### 2.1.1.1 Solar spectrum

According to the laws of Physics, a body with a temperature greater than absolute zero emits electromagnetic radiation in the form of thermal radiation. In the case of black-body which is a perfect emitter, the intensity of the radiation emitted depends only on the temperature. The sources of radiation are usually considered to behave as a black-body, such as the Sun.

The solar irradiance spectrum is displayed in Figure 2. As expected, the solar spectrum pattern resembles closely the radiation of a black-body emitting at the same temperature than the Sun (5,778 K). Atmospheric absorption considerably lowers the solar irradiance on the surface of the Earth at sea level. Three main types of radiation are included in the solar irradiance:

- Ultraviolet radiation, with a wavelength lower than 400 nm, accounting for less than 9% of the total;
- Visible light, with a wavelength comprised between 400 and 700 nm for 39%;
- Infrared radiation, with a wavelength greater than 700 nm, for about 52%.

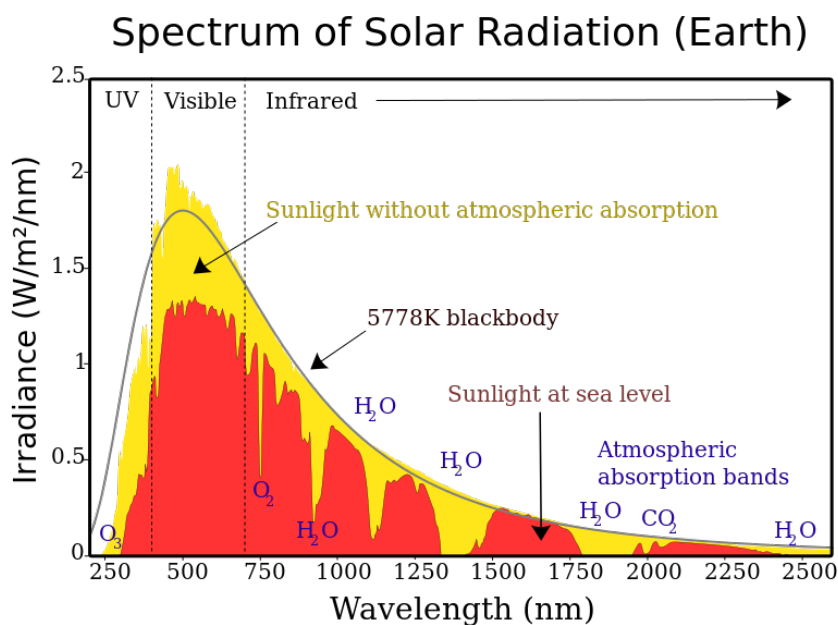


Figure 2. Solar radiation spectrum (source: [https://en.wikipedia.org/wiki/Sunlight#/media/File:Solar\\_spectrum\\_en.svg](https://en.wikipedia.org/wiki/Sunlight#/media/File:Solar_spectrum_en.svg))

### 2.1.1.2 Measurement of solar irradiance

There are different paths of how solar irradiance is propagated, leading to different types of radiation, as it can be seen in Figure 3.

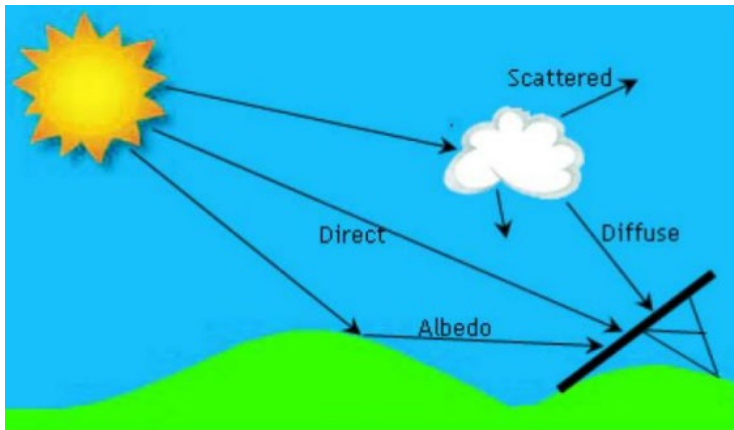


Figure 3. Different paths of solar radiation propagation on Earth

Direct radiation is the direct beam component that passes unaltered to the earth, which can be seen on a cloudless day. It has the ability to cast a shadow and can be concentrated and reflected. Diffuse radiation is the component of the solar beam that has been scattered in its way to the surface of Earth. This can be due to cloud cover, moisture in the air or other atmospheric components. Diffuse radiation cannot cause a shadow, be focused or concentrated. Surfaces can also reflect a part of the irradiance which is known as albedo.

There are different ways to quantify solar irradiance, as function of the type of radiation considered. The main types are illustrated in Figure 4.

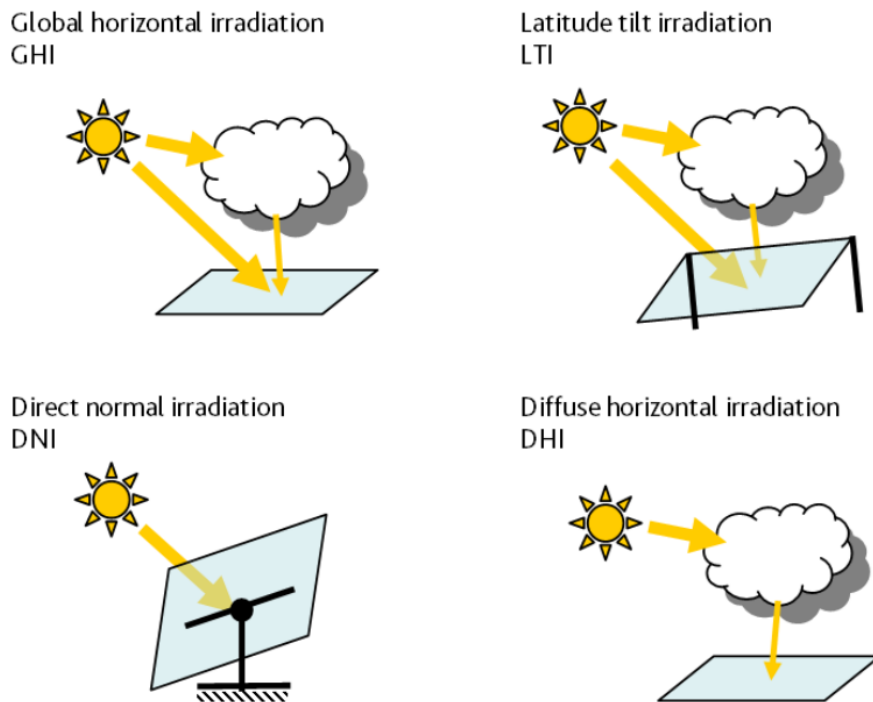


Figure 4. Main parameters of solar irradiance

- Direct normal irradiance (DNI)

The Direct Normal Irradiance (DNI) is the radiation that arrives to the earth in a normal direction to the earth's surface, without any interference (no diversion, splitting or diffusion as it passes through the atmosphere). The greatest amount of DNI is experienced on a clear day where possible interferences are minimum. Places that receive the greatest amount of DNI are mainly deserts, and locations with low humidity values. In contrast, humid areas with frequent rainfall receive relatively low values of DNI. This type of radiation has the ability to create shadows, and can be reflected and focused to a particular place through the use of mirrors, glasses, reflective materials, raindrops and other materials which can cause light dispersion.

DNI values can be measured using a pyrheliometer (Figure 5), or can be calculated from the other types of radiation through the use of the angle of elevation (Figure 6).

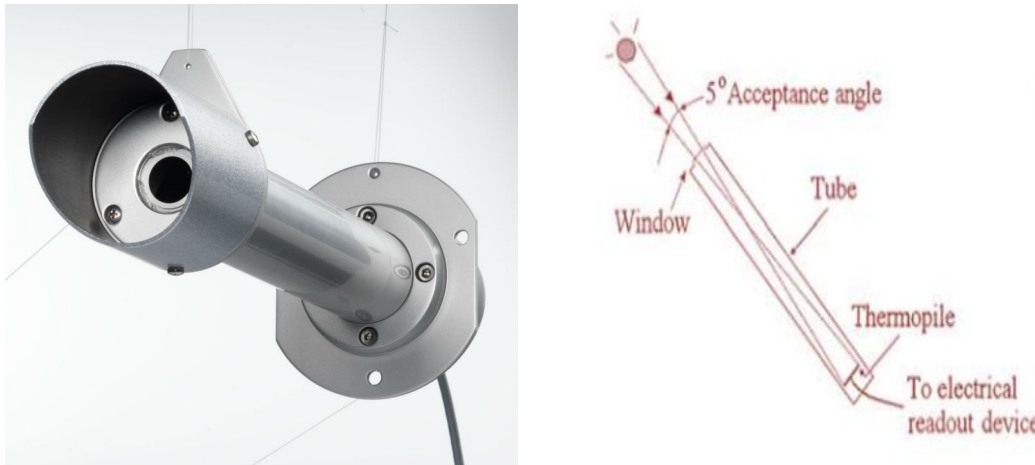


Figure 5. Photograph (left) and scheme (right) of a pyrheliometer

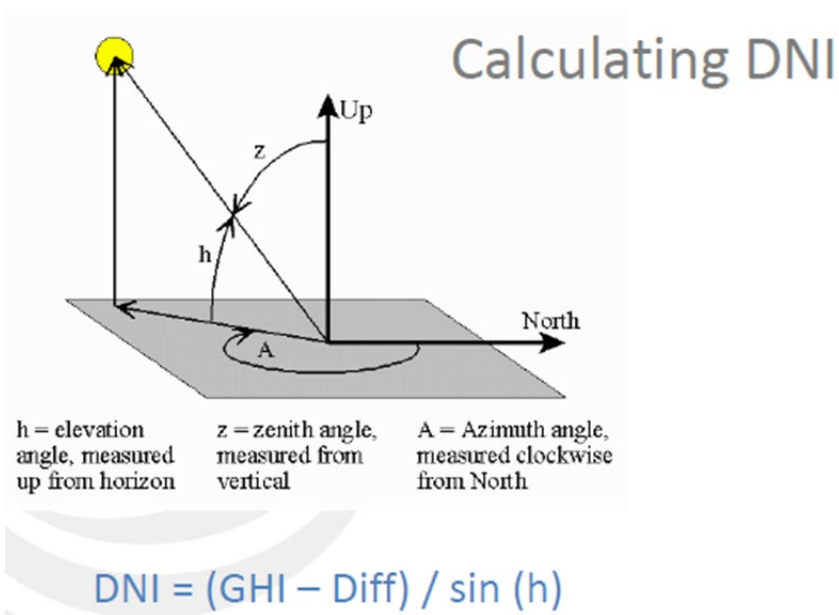


Figure 6. Calculation of the DNI

- Diffused radiation (DIFF)

Diffused radiation (DIFF), also known as Diffuse Horizontal Irradiance (DHI), is radiation that has experienced interference but eventually arrives to the earth's surface. Hence, its path is not direct to the earth, the main cause being presence of clouds in the atmosphere. The least amount of DIFF is experienced on a clear day

where interferences are at their minimum. Places that receive the least amount of DIFF are mainly deserts and locations with low humidity values, whereas humid areas with frequent rainfall receive relatively high values. DIFF radiation does not have the ability to create shadows, and cannot be reflected and focused to a particular place through the use of mirrors, glasses, reflective materials, raindrops and other materials which can cause light dispersion.

DIFF values are measured using a pyranometer with a band that is constantly rotating for blocking out the direct radiation from the sun (Figure 7).



*Figure 7. Shadow band pyranometer*

- Global horizontal irradiance

Global horizontal irradiance (GHI) is the total amount of irradiance received at a surface parallel to the earth's surface. It is a combination of DNI and DIFF. Since the GHI has a DNI component, it can be reflected and focused to a particular place through the use of mirrors, glasses, reflective materials, raindrops and other materials which can cause light dispersion.

GHI values are measured using a pyranometer, which can be of two types: thermopile and silicon and photo-electric pyranometers (Figure 8). Thermopile pyranometers are more accurate than silicon pyranometers, but their cost is usually higher. A classification ISO (9060:1990) separates the thermopile pyranometer into 3 classes: secondary standard (best rating with 5 s of response time and 2% of accuracy), first class (medium range with 18 s of response time and less than 5% of accuracy) and second class (low range with 18 s response time and less than 10% of accuracy).



Figure 8. Thermopile and silicon pyranometers

- Latitude tilt irradiation (LTI)

LTI, or also global tilt irradiation (GTI) is a representation of the maximum amount of radiation that can be absorbed at the optimum angle from a particular location. The optimum angle varies with the latitude of the earth, i.e. the distance of the site from the equator. For example, at Durban, the LTI corresponds to the value measured at an angle of  $30^\circ$ , which is same degree than the latitude of the city. At the equator, GHI values are equal to the LTI values as no angular adjustments are required. Pyranometers are used for LTI measurements.

### *2.1.1.3 Solar resource assessment*

Before installation of a solar system, an assessment has to be performed in order to evaluate the amount of solar irradiation received by a site. For this, the characteristics of the location that are susceptible to have an effect on the solar irradiance received, must be determined: landscape, topography, vegetation, latitude, longitude, elevation above the sea level, among other. In the same way, the characteristics of the technology to implement must be defined.

A solar resource assessment will enable to determine the expected amount of solar energy available and the seasonal variations. It constitutes then an important decision tool before the implementation of any solar technology, which enables to determine the feasibility of a project and the design parameters, such as the required land, as well as to predict the performance of the plant.

### *2.1.1.4 Solar map*

A solar map shows how solar irradiance is distributed in a region. Solar maps are developed from the data collected by meteorological or radiometric stations, or satellite. The most sophisticated versions combine both type of terrestrial and satellite data.

Different types of solar maps can be found as a function of the type of radiation, namely GHI, DNI, DIFF or LTI. It is important to note that the information provided by the maps usually differs as a function of the type of radiation. For example, Figure 9 compares the GHI and DNI solar maps in the African continent from the south to the equator. Both GHI and DNI decrease as moving towards the equator, however this trend is considerably stronger in the case of DNI: while the GHI values diminish by about 20% from southern to central Africa, the decrease is about 65% for the DNI.

The solar maps can be used for the solar assessment and can drive decision-making. For example, according to Figure 9, the implementation of solar technologies based on solar energy concentration are generally less suitable in central Africa compared to the south, as they require high DNI values. In contrast, the location for the implementation of technologies based on solar energy collection (e.g. solar water

heater and PV panels) does not make a great difference, as they rely on GHI values which do not change considerably between the different regions.

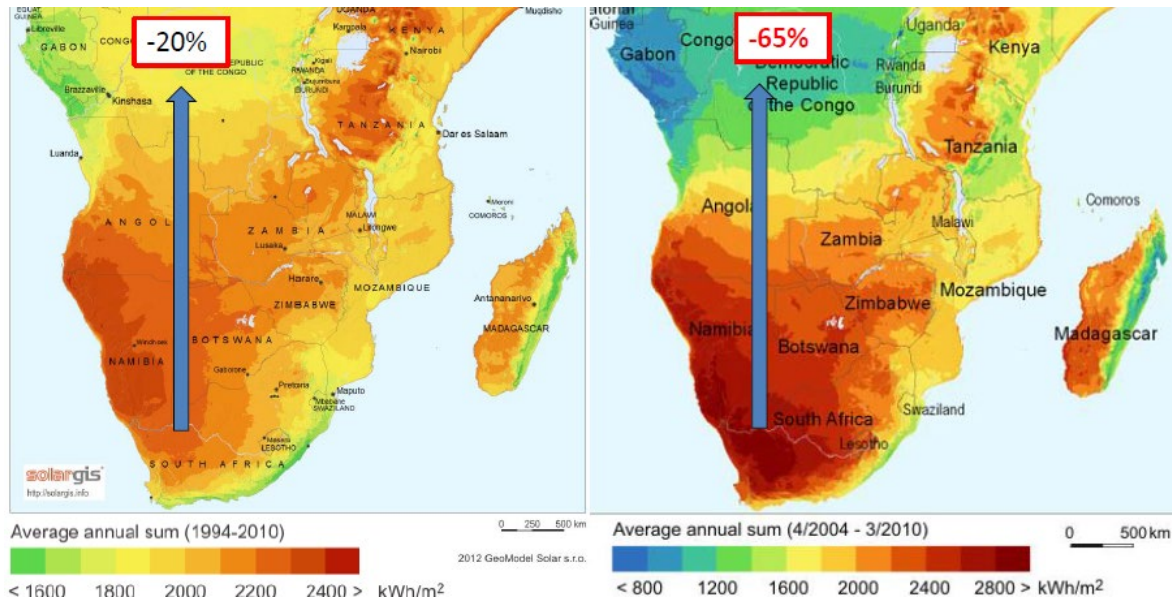


Figure 9. Solar map of Africa from the south to the equator, based on GHI (left) and DNI (right) values (source: Solargis)

### 2.1.2 Use of solar energy in the sanitation field

Usually the regions with unimproved sanitation are poor areas that also lack of other basic services as electricity and water, which makes more difficult the access to improved sanitation. Solar energy could be then a solution to tackle simultaneously the lack of sanitation and energy in these areas.

If we compare the GHI solar map in the world (Figure 10) to the map showing the proportion of people using improved sanitation (Figure 11), areas with a high deficit in sanitation coverage have an abundant solar energy source, as many countries in the Sub-Saharan Africa and the Indian subcontinent. Globally, the countries with the least access to improved sanitation (50% or less) are located in the “Sun Belt”, where the solar irradiance is higher than the average in the planet.

## GLOBAL HORIZONTAL IRRADIATION

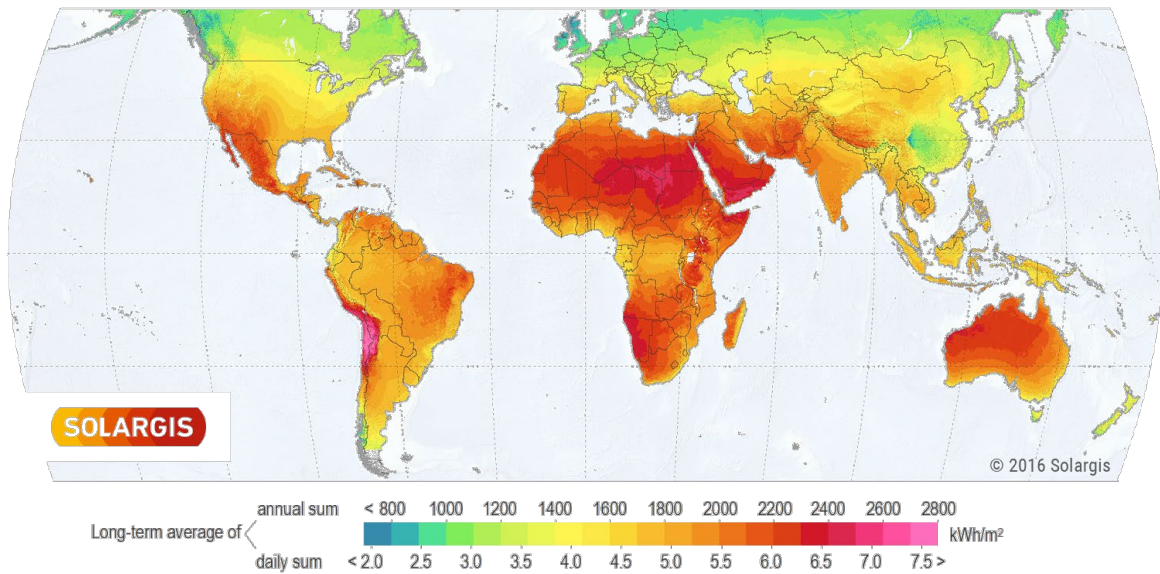


Figure 10. Distribution of GHI in the world in 2016 (source: Solargis)

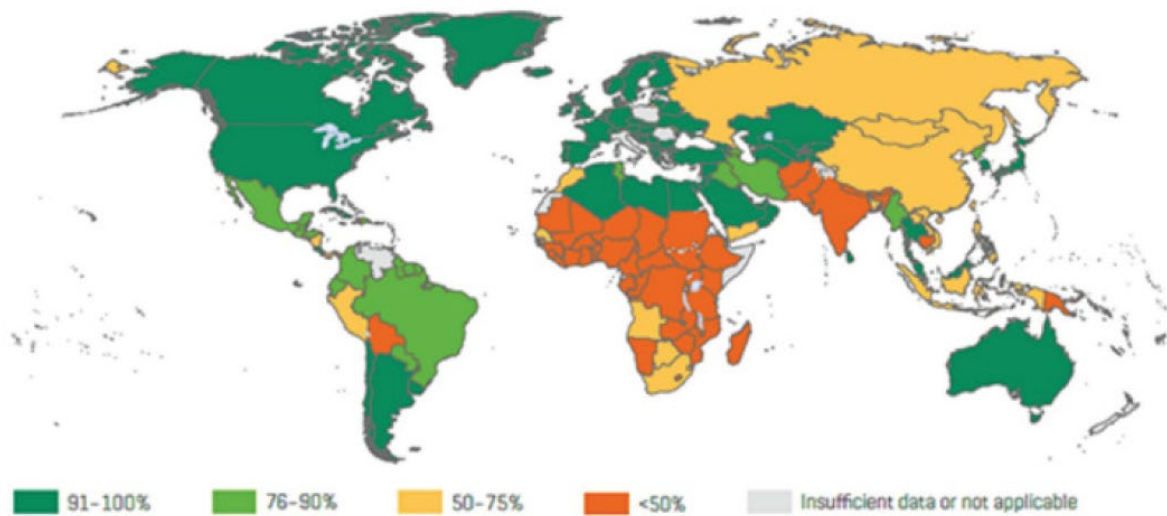


Figure 11. Proportion of the global population using improved sanitation (source: World Health Organization)

By taking a closer view to the solar irradiance map in the African continent (Figure 12), it can be seen that a major part of the countries with severe lacks of sanitation have very high solar irradiance ( $> 2200 \text{ kWh/m}^2$ ). The most remarkable examples are Namibia, Tanzania, Kenya, Ethiopia, Eritrea, Soudan and Chad.

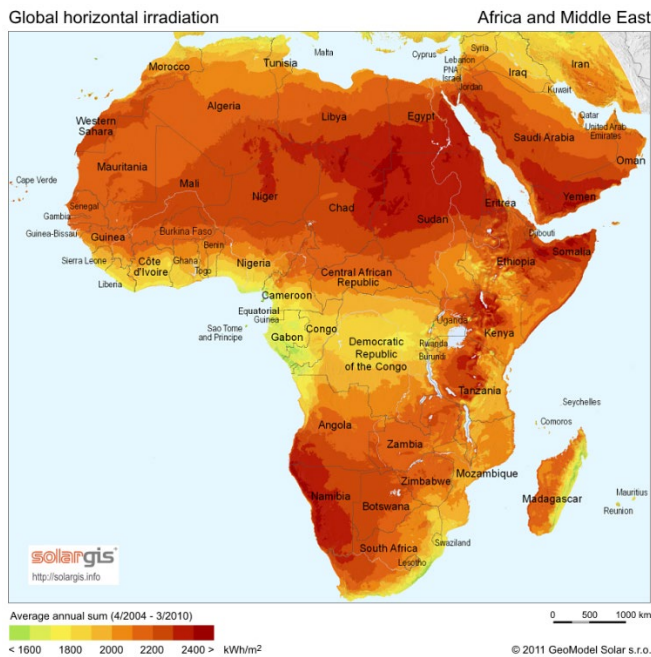


Figure 12. Distribution of GHI in Africa in 2016 (source: Solargis)

Solar energy can tackle simultaneously the lack of proper sanitation and electricity provision in the underdeveloped regions of the world, including a major part of African countries. Solar energy can bring a sustainable solution for the treatment of faecal sludge, in order to go towards an improved sanitation management where the treated waste could be valorised in different ways. At the same time, electrical and fuel could be provided to the communities for their basic needs, through the direct conversion of solar energy into electricity (for example, through PV systems) or the conversion of the excreta into biofuel after solar treatment (for example, use of dried faecal sludge as briquettes).

## 2.2 DRYING OF FAECAL SLUDGE

### 2.2.1 Concepts of drying process

Drying is defined as the removal of water or any other solute from a moist solid. This process is a chemical engineering unit operation that is commonly applied in diverse applications in chemical, agricultural, biotechnology, food, polymer, ceramics, pharmaceutical, pulp and paper, mineral and wood processing industries (Mujumdar, 2006).

### 2.2.1.1 Thermodynamics aspects

Drying is driven by the difference of thermodynamic activity between water as vapour in the air and water as moisture in the wet solid. Therefore, drying occurs when the thermodynamic activity of the moisture in the solid is higher than that of the vapour water in the air, and it stops at the thermodynamic equilibrium, i.e. when the water activities are equal. In the opposite, the solid can gain moisture if the activity of the vapour water in the air is higher than the activity of the moisture, for materials defined as hygroscopic. In contrast, non-hygroscopic material cannot be rehydrated after losing its moisture.

The moisture content of a solid in thermodynamic equilibrium with the humidity of the surrounding air is termed as equilibrium moisture content. For a hygroscopic solid, the relationship between equilibrium moisture content and air humidity at a given temperature can be expressed by the sorption isotherm curves, which include a desorption (dehydration) and adsorption (rehydration) component, as shown in Figure 13. The pattern of the sorption isotherm curves depend on the temperature and surface properties of the solid. Note that the sorption isotherm presents a hysteresis, which demonstrates that the way in which the solid is dehydrated and rehydrated differs.

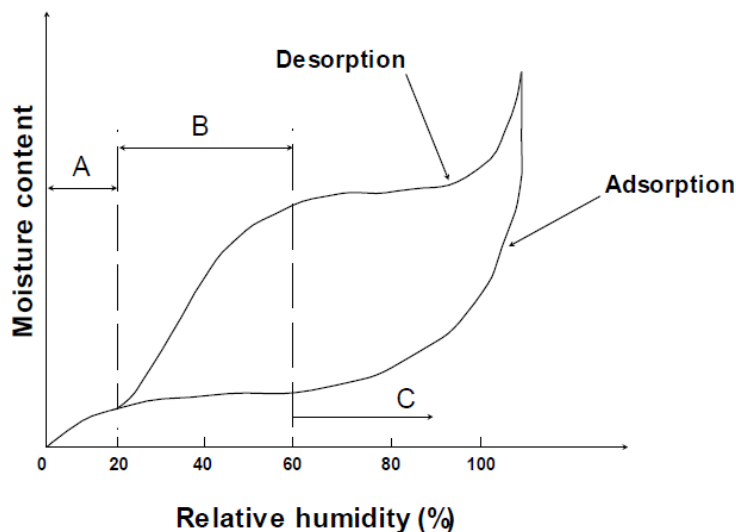


Figure 13. Sorption isotherms (Mujumdar and Devahastin, 2000)

As the equilibrium moisture content depends on the temperature and the relative humidity of the air, it is then very important to know the thermodynamic properties of the surrounding air. An important tool for this is the psychrometric chart (Figure 14), which shows the thermodynamic properties of an air-vapour mixture at constant pressure, often equated at sea level. The most relevant psychrometric parameters for drying are:

- Absolute humidity, defined as the mass of water vapour per mass of dry air;
- Relative humidity (%), defined as the partial pressure of water vapour in air divided by the vapour pressure of water at a given temperature;
- Wet-bulb temperature, corresponding to the temperature of a parcel of air cooled by the evaporation of water into it until achieving saturation, after supplying the latent heat for this;
- Dry bulb temperature, corresponding to the temperature of the air-vapour mixture.

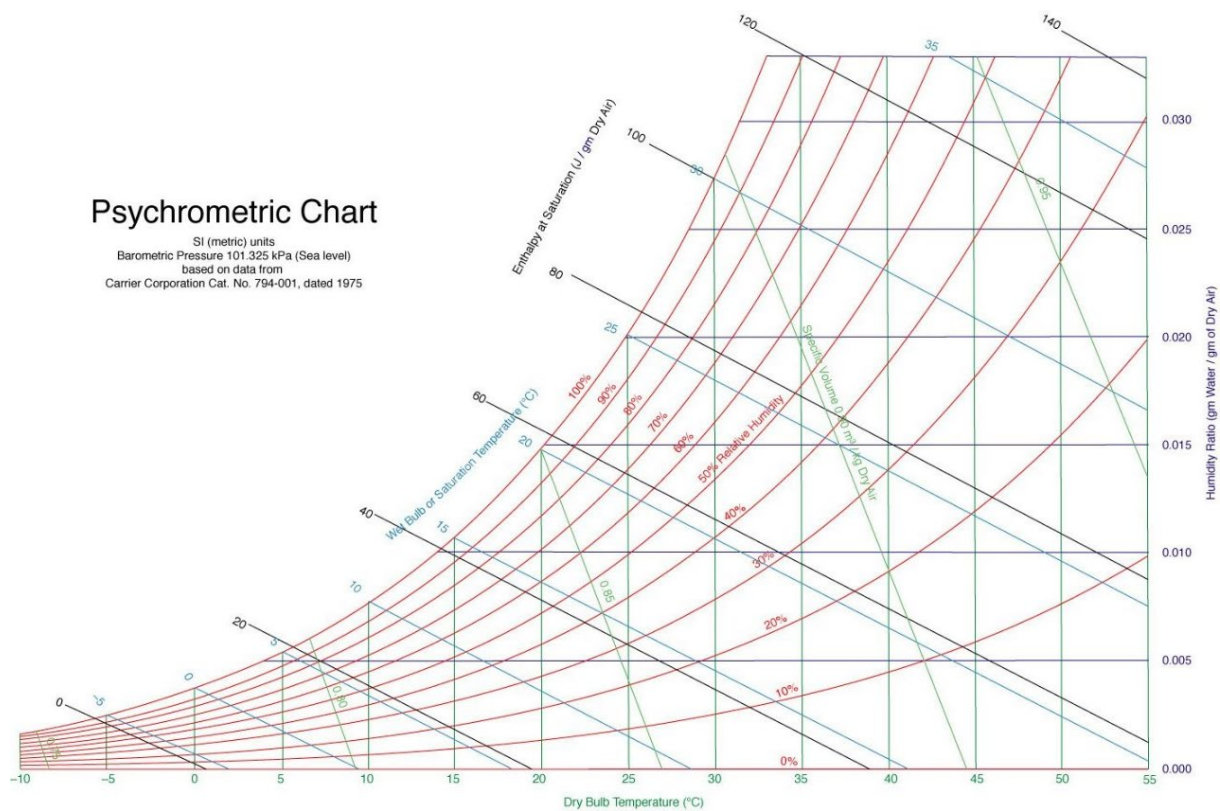


Figure 14. Psychrometric chart of vapour water – air mixture (source: Carrier Corporation)

Air is saturated in humidity when its relative humidity is equal to 100%. Under these conditions, air loses its ability to hold further vapour water and consequently drying cannot progress.

### 2.2.1.2 Types of moisture

The bounding of moisture with the solid matrix determines how drying will proceed. The two major types of moisture are:

- Bound moisture, which is linked to the solid matrix biologically, chemically or physically, and exerts a vapour pressure lower than that of water at the same temperature;
- Unbound moisture, which exerts an equilibrium vapour pressure equal to that of the pure liquid at the same temperature, so it behaves as water and can be removed relatively more easily in comparison to bound moisture.

Free moisture is defined as the amount of moisture in excess with respect to the equilibrium moisture content at particular air temperature and humidity. It can be either bounded and / or unbounded.

The different types of moisture of sludge are represented in Figure 15.

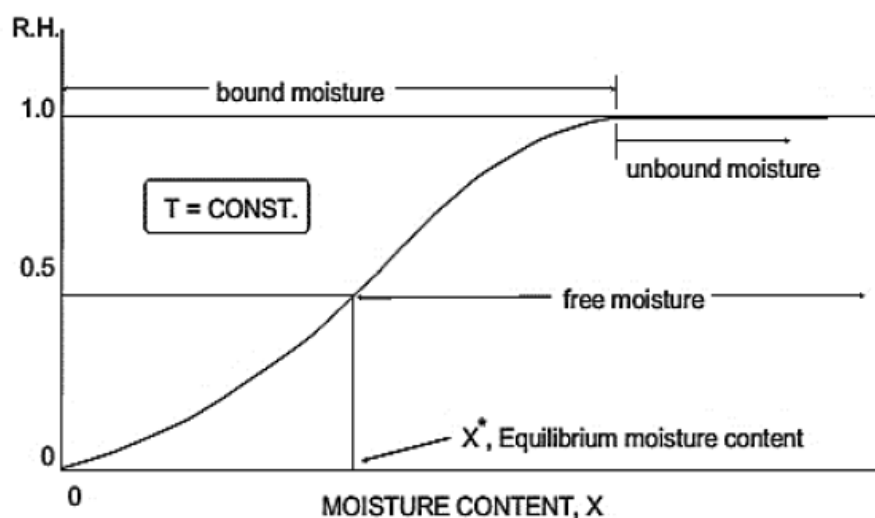


Figure 15. Different types of moisture (Mujumdar and Devahastin, 2000)

The sorption isotherm gives an indication on the binding mechanism of moisture in sludge. In the example from Figure 13, the region A corresponds to moisture with tight bounds, whereas the moisture from region C is loosely held in the solid matrix. The region B is intermediary between A and C.

#### *2.2.1.3 Drying mechanisms*

Drying is a process that includes simultaneously heat, mass and momentum transfer. The heat provided during thermal drying is distributed within the solid, increases the temperature of the material and supplies the latent heat for moisture vaporization. At the same time, the evaporated moisture is transferred from the solid to the surrounding air. The transfer of the moisture at the surface of the solid occurs through convection or molecular diffusion. The moisture migration from the interior towards the surface is done by different mechanisms, such as:

- Liquid diffusion if the moisture is in a liquid state;
- Vapor diffusion if the liquid has been evaporated within the solid;
- Capillary moisture movement, occurring due to capillary suction from the large capillaries to the small ones, driven by a capillary pressure gradient;
- Hydrostatic pressure difference, driven by the build-up of pressure within the solid after moisture evaporation.

#### *2.2.1.4 Drying kinetics*

The moisture content decrease during drying can be expressed by a curve from which the kinetics of the process can be studied, which is known as drying curve. In an ideal case, the drying curve is divided into three distinct stages: the constant rate period, the first falling rate period and the second falling rate period. Figure 16 represents a typical drying curve obtained under steady conditions.

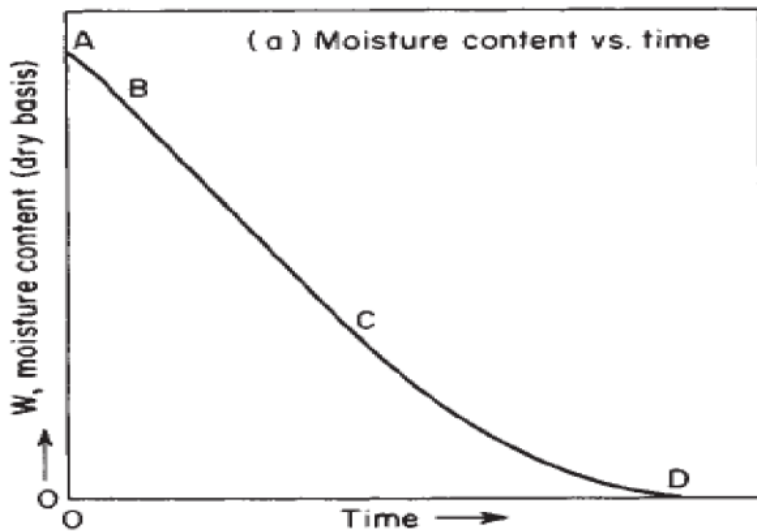


Figure 16. Typical drying curve (Moyers and Baldwin, 1997)

Preceded by the segment AB, representing a stage in transitory conditions, the segment BC corresponds to the constant rate period. In this stage, the entire surface of the material is saturated with moisture, which is replaced immediately after leaving the solid by moisture from inside the particle. Indeed, the internal and external mass transfer are in a dynamic equilibrium, and drying will proceed in a steady continuous manner. The temperature of the material during this stage is fairly constant, approximating the wet-bulb temperature value. A boundary layer of moisture is always available at the evaporating surface, and the heat provided to the solid is utilized for the evaporation of the water at the surface. Thus, the drying kinetics are controlled exclusively by the external heat and mass transfer.

The point C corresponds to the critical moisture content, from where the drying rate starts to decrease. The portion CD is known as the falling rate period and is divided into two parts: the first falling rate period and the second falling rate period. During the first falling period, the surface of the wet solid cannot be anymore maintained saturated in moisture. In fact, the moisture at the surface evaporates at a faster rate than it can be replaced from inside the particle. The temperature of the sludge will start to increase from the wet bulb temperature to the final temperature. During this stage, the drying rate is influenced by both internal and external transfer. In the second falling rate period, it can be considered that the surface is completely dry and an evaporation front

progress towards the center of the solid. The kinetics from this stage is dependent only on the moisture internal mass transfer.

Note that in a real case, the drying curve can deviate from the ideal case and does not necessarily present all the kinetic stages described above.

#### *2.2.1.5 Factors affecting drying*

The rate at which drying occurs, depends on the power supplied by the heating source, type of moisture and the conditions influencing the transfer rates, such as the characteristics of the solid (geometry, size, porosity) and the external conditions (air temperature, velocity and humidity).

As drying progresses, the removal of moisture leads to the chemical and mechanical re-arrangement of the dry bone of the solid. The changes undergone by the solid during drying can have an influence on the internal transport of the moisture and then affect the drying rate.

Temperature plays an important role in the quality of the product. Some products are temperature sensitive as their biological, chemical and / or physical properties can change if a limit of temperature is exceeded. For this type of product, drying should not be conducted at temperature higher than that from which its quality is compromised.

### **2.2.2 Drying technologies**

Drying technologies are classified according to the method of how heat is supplied to the wet material and how the evaporated moisture is evaporated. Dryers, that expose the solid to a hot gas stream, are known as direct or adiabatic. Dryers heated by conduction or radiation are called indirect or non- adiabatic. The most conventional drying technologies categories are as following:

- Convective hot air dryers (direct dryer) where heat is supplied by convection from a hot air stream, and the evaporated moisture is taken away in the air stream. This drying method is by far the most common in despite of the relatively low thermal efficiency, which is due to the lack of cost-effective

method to recover the latent heat of vaporization from the exhaust. This type of drying requires the handling of large volumes of gas, so usually convective drying plants presents a large footprint and gas cleaning constraints.

- Contact dryers (indirect dryer) where heat is supplied by contact with a hot wall, and so conduction is the main heat transfer driving force. Moisture is evacuated from the drying chamber by a vacuum or a moderate gas flow, in order to avoid humidity saturation of the air which can stop drying.
- Radiative dryers (indirect dryer) where heat is supplied by infrared radiation, microwave or radio dielectric frequency. Infrared radiation has relative low penetration within the materials and then heats mostly the surface of the wet solid. In contrast, microwave and radio dielectric frequency waves can penetrate deep within the solid, and so the heating of the material is done at the bulk volume without the need of conduction. Gentle convection or vacuum are usually applied for the removal of the evaporated moisture. Microwave drying has limited applications up to date, due to high capital and operating costs, while infrared drying has found important applications in niche markets, such as the drying of coatings and paintings, and radio frequency in the drying of thick lumber and coated papers (Mujumdar, 2000).
- Solar dryers where the heat is provided from solar energy (more details in the next section).

It is possible to combine the heat transfer modes in the dryers, e.g. conduction or radiation with convection, with the intention to gain performance. Alternative methods to thermal drying also exists in the industry, as for example freeze drying, where the moisture is sublimed at low pressure after previously freezing the solid. This method is not commonly employed in the industry because of its high costs, except for highly heat-sensitive materials, such as some biotechnological, pharmaceutical or food material with high flavour content.

Among each drying method, several technologies have been developed and the innovations carry on. Among the innovation with a promising future, we can find:

- Convective drying using superheated steam which has shown to yield higher efficiency and often higher product quality (Mujumdar, 2000);

- Fry-drying where the wet material is immersed in a hot oil with temperatures above the water boiling point;
- Use of acoustic waves or vibrations during drying in order to increase the heat and mass transfer rate, and at the same time to promote solid-liquid separation;
- Use of explosion puffing where a pressurised wet solid is heated until reaching a certain pressure, followed by a sudden decompression that leads to an explosion due to the brutal moisture evaporation, which increases the porous network;
- Foam-mat drying where a liquid is turned into a porous foam for faster drying.

### **2.2.3 Peculiarities of faecal sludge drying**

#### *2.2.3.1 Reasons for drying*

Drying is an important step for the treatment of bio-solids such as faecal sludge or sewage sludge. The use of sludge in its raw form represents a hazard due to its high pathogen content. Sludge dewatering cannot neutralize its pathogen content into a safe level. The primary goal of drying is then the pasteurization of the sludge by killing the pathogenic organisms present on it, by the effect of moisture reduction and high temperatures. The development of most bacteria is inhibited below a water activity of 0.91 (Mujumdar and Devahastin, 2000), including pathogens such as Escherichia Coli, Salmonella, Shigella and Vibrio Cholerae. This means that most of pathogenic bacteria in the sludge can be deactivated if drying achieves a moisture content corresponding to a water activity lower than 0.91. The high temperatures during thermal drying can lead to the irreversible damage of the structure of the pathogen organisms, causing its eventual destruction. Aitken et al. (2005) and Popat et al. (2010) reported that the deactivation of Ascaris eggs was greater than two log reduction after 2 h of treatment at 50°C. Thomas et al. (2015) found a complete destruction of Ascaris eggs using a conical-augur device operated at 70°C and 6 s of residence time.

Moreover, the reduction of mass and volume during drying reduces diverse costs related to handling, such as storage, transportation, packing and retail. In addition, drying increases the lower calorific value through moisture reduction, consequently

turning the sludge into a suitable biofuel for incineration or co-incineration. Drying also allows to eliminate the fetid odours from sludge and thus it lowers the levels of discomfort related to the handling of the material.

### 2.2.3.2 Moisture in sludge

In order to better understand faecal sludge drying, it is important to know how moisture is present in the material. Faecal sludge can be considered as a slurry with colloidal material, particles and polymers forming a network where moisture is integrated in different ways. Figure 17 depicts the distribution of moisture in a typical sludge into different types.

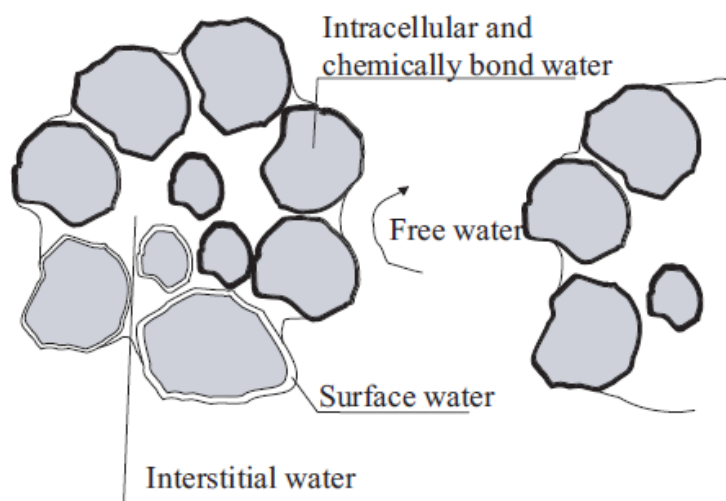


Figure 17. Different types of moisture in the sludge (Chen et al., 2002)

Free moisture is not attached to the sludge particles and it is subordinated to gravity force, so it can be removed from the sludge by gravity-based processes such as settling. Interstitial moisture is found trapped within clusters of sludge flocs and within capillaries, and can be removed by strong mechanical forces. Surface moisture or vicinal moisture (Mowla et al., 2013) is physically bounded to the surface of the flocs by adsorption and adhesive forces, and can hardly be removed mechanically. Chemically bounded moisture or hydration moisture (Mowla et al., 2013), is attached to the solid by chemical interaction, and its removal requires thermal drying.

Intracellular moisture is contained inside the cells and can be removed only by breaking the cell wall structure, which can be done by heating, freezing or electro-induced forces.

In general terms, the moisture that can be removed by dewatering means is termed as “free moisture” (different term than the truly free moisture described above), which contrast with the term of “bound moisture” designating the moisture that can only be removed by thermal drying. Free moisture from the latest definition includes the truly free moisture, interstitial moisture and a part of the surface moisture. Bound moisture encompasses the chemically bound water, the intracellular water and the part of the surface moisture that could not be removed by dewatering. Note that the limit between free and bound moisture content, according to the previous definitions, can change following the involved dewatering methods. For example, the addition of polymers can break some chemical or physical bonds so that chemically bounded moisture or surface moisture can be partially removed by mechanical dewatering.

### *2.2.3.3 Physical changes of faecal sludge during drying*

The removal of moisture content from the sludge induces mechanical stresses and a re-arrangement of the dry bone structure, which are reflected by perceivable physical changes. These have to be taken into consideration for a full comprehension of drying. Nevertheless, in the best of our knowledge, no such investigations have been carried for faecal sludge, on the contrary of sewage sludge where extensive investigations exist. According to these studies, the major changes undergone by sludge during drying are summarized as follow:

- Change of phase from a liquid to solid state, which has important implications on the sludge rheological properties and then on the convey of sludge in the drier. During this transformation, the sludge passes through an intermediary stage of plastic / sticky behaviour. Stickiness can cause fouling in the drier and consequently a drop of its performance (Kudra, 2003), particularly in the case of contact dryers. The different phases during drying are illustrated in Figure 18.

- Shrinkage of the sludge, which can lead to a reduction in volume between 50 to 70% and occurs mainly during the constant rate period (Léonard et al., 2004, 2003a, 2003b, 2002; Tao et al., 2005).
- Formation of crust or skin at the surface (Tao et al., 2006), which can constitute a barrier for mass and heat transfer, and is more likely to occur in cases of fast drying ;
- Cracking of the surface, which occurs mainly in the falling rate period, and can occupy 30 to more than 50% of the volume (Léonard et al., 2004, 2003a, 2003b, 2002; Tao et al., 2005). Cracking can enhance the diffusion of evaporated moisture out of the particle, increasing the drying rate.

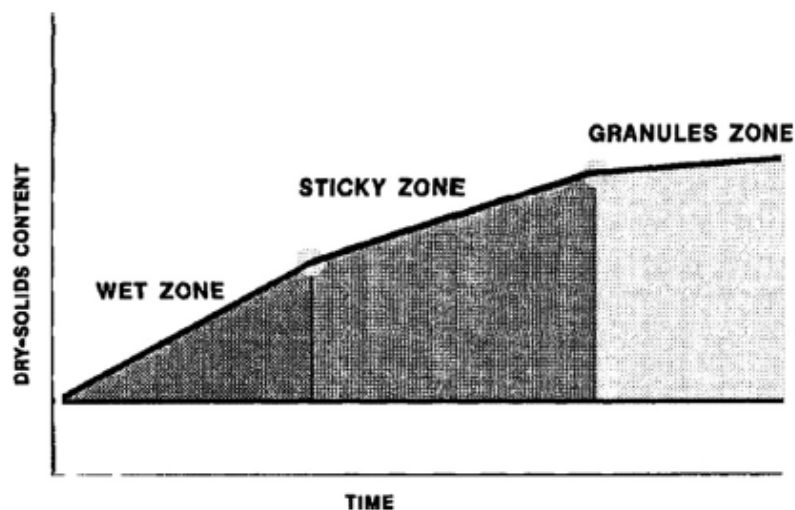


Figure 18. Different phases of the sludge during conductive drying (Lowe, 1995)

#### 2.2.3.4 Technologies for faecal sludge drying

In the faecal sludge field, drying is typically performed in drying beds. However, this practice is unable to lead to low moisture content and the drying times are usually long. With the emergence of new technologies in the last decade, thermal drying has gained a great interest.

Drying is an expensive process as moisture evaporation is energy intensive due to the high water vaporization latent heat. In order to reduce the energy consumption, a dewatering step should precede drying in the case of sludge with high moisture

content. It is important to improve the existing dewatering technologies, in order to increase the amount of moisture that can be dewatered, which will reduce the need of thermal drying.

Table 1 shows some of the faecal sludge drying technologies that are currently available or being developed. It can be seen that most of these technologies rely on convective and contact drying, with only a few based on infrared, microwave and solar drying. The possibility to use alternative type of drying, such as superheated steam drying and fry-drying, have not been explored by the moment, even if they have shown a great potential for sewage sludge (Bennamoun et al., 2013).

As a relatively recent technology in the faecal sludge sector, drying presents considerably wide areas of exploration to carry on. Lessons and good practices can be obtained from the experience in other sectors where drying is in a more mature stage, particularly for similar material as sewage sludge. However, the drying technologies used in sewage sludge can be hardly transposed to faecal sludge. The technologies applied for faecal sludge must be specific to the material characteristics and context. In particular, the technologies must be as cost-effective as possible, due to the low budget available for faecal sludge management in developing countries, which makes difficult the implementation of high-tech equipment from the sewage sludge sector, requiring a high investment.

An interesting option to explore would be the development of in-situ drying systems where the faecal sludge will be dried at proximity of the generation point. This would lead to a significant reduction of the transportation costs, as considerable less water in the sludge will have to be transported to the treatment plant or the location of reuse.

The source of energy employed for drying is an important parameter. As seen in Table 1, heat from combustion can be recovered for drying when faecal sludge is used as a combustible. However, when faecal sludge is not combusted, an external source of energy has to be employed. This implies the necessity to supply continuously energy to the drying process, as electricity or fuel. Solar thermal energy could be then a suitable solution to bring free energy to the process, leading to the decrease of the operating costs. It could also be used as an extra source of energy in the combustion process, in order to guarantee an enough low moisture content of the solid to combust and lead to a more positive energy recovery.

Table 1. List of faecal sludge drying technologies

Type of drying	Technology	Application	Place in the treatment process	Energy source	Source
Convective drying	Belt dryer	Faecal sludge treatment plant from Tide Technocrats	Drying before a pyrolysis unit for biochar production	Heat from the combustion of the pyrolysis fumes	(Tide-Technocrats, 2016)
	Vertical multi-tray dryer	Reinvented “Firelight” Toilet from Janicki Industries	Drying before a combustion system	Heat from faecal sludge combustion	(SuSana, 2015)
	Rotary dryer	Faecal sludge treatment plant from Pivot	Final treatment (reuse of the product as biofuel)	Combustion of paperboards	(Pivot, 2016)
Contact drying	Hot surface wall screw conveyer	Faecal sludge treatment plant, “Omniprocessor”, operated from Janicki Industries	Drying before a combustion system	Heat from faecal sludge combustion	(Villarreal, 2015)
	Heated rotary plate	Reinvented “A Better Toilet” from Research Triangle Institute	Drying before a combustion system	Heat from faecal sludge combustion	(RTI, 2013)

<b>Convective, contact, radiative drying</b>	Drying in the top of a fixed bed with a smouldering front at the bottom	Reinvented “Sanitation NoW” from Toronto University	Drying before a smouldering system	Heat from faecal sludge smouldering	(Yermán, 2016)
<b>Convective and radiative</b>	LaDePa machine (convective pre-drying stage, followed by an infrared belt dryer stage)	Treatment of faecal sludge from VIP latrines in eThekweni municipality	Final treatment (reuse of the product in agriculture)	Diesel generator providing the hot air and electricity	(Harrison and Wilson, 2012; Mirara, 2017)
<b>Radiative</b>	Microwave dryer	Treatment of faecal sludge in emergency cases	Final treatment	Microwave radiation generated using electricity	(Mawioo et al., 2017)
<b>Solar</b>	Greenhouse dryer	Faecal sludge treatment plant from Pivot	Pre-drying before the rotary dryer (see above)	Solar energy	(Pivot, 2016)

A faecal sludge drying flow diagram is proposed in Figure 19.

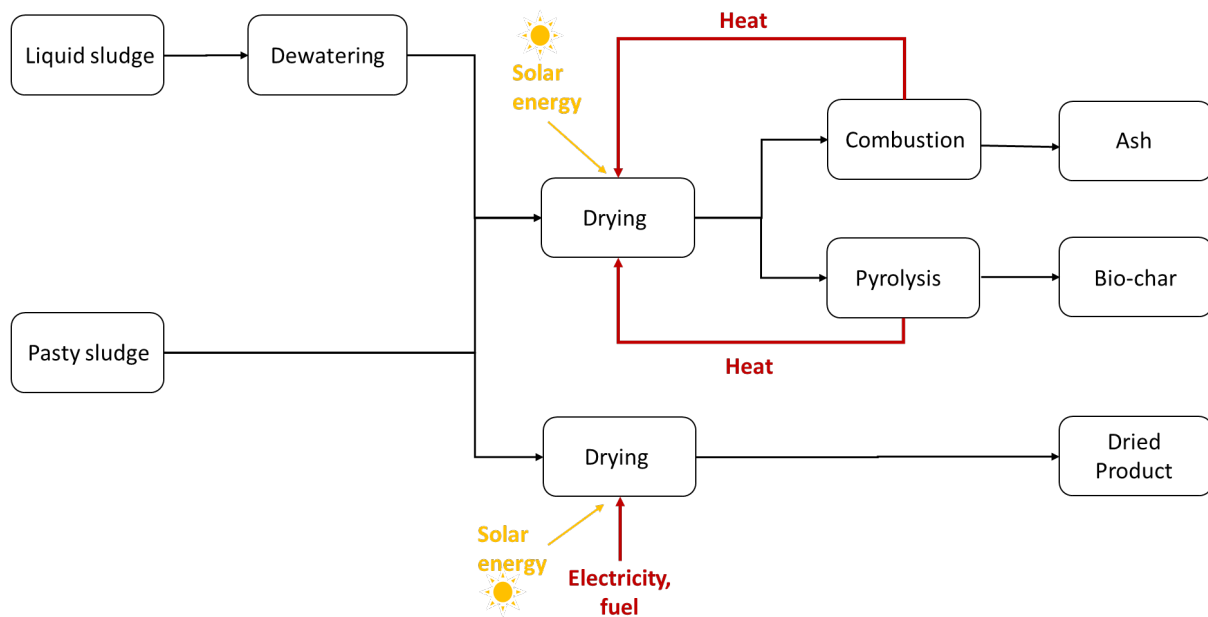


Figure 19. Faecal sludge drying flow diagram

## 2.3 SOLAR DRYING

### 2.3.1 Solar thermal systems

Solar thermal energy systems convert solar energy into heat and have different applications, for example power generation, water heating, cooking and drying. Solar thermal energy can be harnessed by two methods: solar thermal collection or solar thermal concentration. Solar collection is used rather for heating application, while solar concentration is mostly used for power generation through a conventional combined cycle.

In solar thermal collection systems, the major component is the solar absorber, which converts the incoming solar radiation into heat and then transfer it to a fluid flowing (usually air, water, or oil). Solar thermal concentration systems use reflectors and mirrors to focus solar irradiation onto the absorber in order to increase the power density from solar radiation. The solar absorber should be made of a material with high absorbance and should be enclosed in a structure with transparent windows to allow

solar radiation penetration. The material of the window can be glass or a transparent polymer, such as polycarbonate or acrylic. The containment of the solar collector into an enclosure will prevent from heat losses to the environment, and the window will create a greenhouse effect, by trapping the radiation emitted by the solar absorber. Thermal insulation of the equipment and piping is very important to achieve high thermal efficiencies.

During periods of overproduction, the heat collected from the solar irradiance can be stored in liquids, phase changing media (such as molten salts), ceramics, and concrete, among other. The stored heat can be utilized during periods where the solar radiation received is not sufficient to cover the demand (for example in nights and overcast days). An auxiliary source of energy could be also used for assistance of the solar thermal system.

### **2.3.2 Solar drying technologies**

Solar drying is an ancient practice used during the history of humankind. Solar energy has been employed since prehistoric times as a source energy to dry food for its preservation in winter time, soils bricks for construction and animal skins for dressing. The first known solar drying installation, found in South of France, dates from 8000 B.C. Various other installations, dating from 7000 to 3000 B.C., have been additionally discovered. With the beginning of the use of biomass and wood as a heating source, construction material as bricks started to be dried in primitive furnaces. Nonetheless, solar drying continued as the preferred method for food and crops preservation for centuries until the industrial area, where the conventional drying systems started to develop. In the modern era, solar energy is still being used for drying purposes at rather small scale, but it is gaining importance due to the actual energetic and environment constraints in terms of the use of fossil fuel. Solar drying is becoming an attractive option to replace conventional drying systems, which usually requires of a carbon energy source to run. Besides, in many rural places in developing countries, the access to energy is unavailable or too expensive, making of solar drying an attractive commercial proposition (Mekhilef et al., 2011; Zhang et al., 2012).

The traditional practices of using solar energy to dry were used to be done at the open-air. Nevertheless, these present several inconvenients, such as: high labour costs,

large area and long-time requirements, inability to control the drying process, degradation of the product due to biochemical reactions or insects, among others. The use of a solar thermal system for drying is an attractive option to increase efficiency, to yield to a higher quality product and to operate in controlled conditions, compared to the traditional open-air drying methods (Jain and Tiwari, 2003). These systems usually require a higher investment and skilled labour than open-air drying installations, but these drawbacks can be rapidly overcome by their advantages.

The classification of solar dryers is summarized in Figure 20. Appendix A presents an overview of the main solar drying technologies. Solar dryers are classified into two major groups (Belessiotis and Delyannis, 2011):

- Passive solar natural dryers (conventionally termed natural-circulation solar drying systems) where the air flows by natural convection, as a result of difference in buoyancy forces as it is heated and / or pressure difference with respect to the wind;
- Active solar-energy drying systems (most types of which are often termed hybrid solar dryers), where the airflow is forced by external means, such as fans or compressors.

Each of these categories is broken down into three subdivisions:

- Direct drying, where the material to dry is exposed directly to sun radiation;
- Indirect drying, where only an air stream is heated by solar thermal energy before contact with the material to dry;
- Mixed drying, which is a combination of direct and indirect dryers.

Direct dryers are globally simpler and cheaper than the indirect-type for the same processing capacity. Nevertheless, the quality of the product can be degraded by solar radiation and the moisture condensation on the transparent window could reduce its transmissivity. Indirect dryers offer a better drying control and are recommended for photo-sensitive materials. The mixed mode combines the feature of direct and indirect solar drying: the wet material can be heated by the dual action of solar irradiance and convection from an air stream pre-heated in a solar collector. This can lead to higher temperature, so higher drying performances.

The use of solar concentration for drying has been poorly studied in literature. However, the application of this type of technology has a great potential as it could lead to considerably higher temperatures than conventional solar drying systems. The drying times could then be significantly shorten, as shown by Wagner et al. (1979) during the drying of fruits using a parabolic reflector. This would have positive implications in the design of solar drying plants, as this would enable to dry higher throughput of material at a lower land footprint. Nevertheless, the use of solar concentration will not be suitable for thermos-sensitive material.

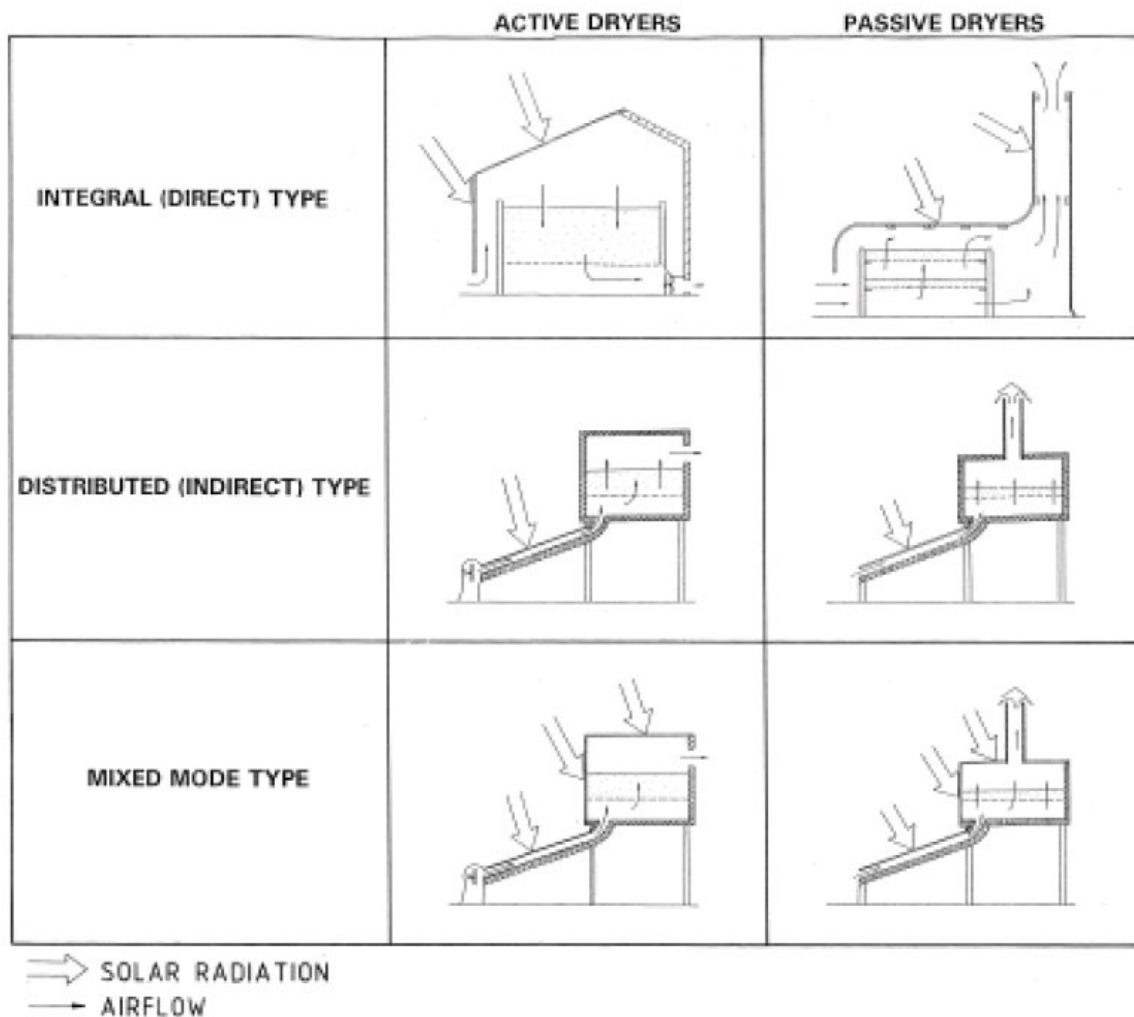


Figure 20. Typical solar dryer classification (Ekechukwu, 1999)

### **2.3.3 Solar drying of sewage sludge**

#### *2.3.3.1 Overview*

The treatment of wastewater generates high amounts of sludge that needs to be disposed in order to limit its negative impact on the environment. Solar drying has been opted as an alternative to treat sewage sludge for its safe disposal in different locations worldwide. Apart from open-air drying, sewage sludge solar drying has been mostly done in greenhouse-type solar dryer. Salihoglu et al. (2007) shown that better results can be obtained when drying is covered in a greenhouse compared to when it is uncovered (open-air drying), in terms of moisture loss, drying rate and pathogen removal.

By 2006, an estimated number of 70 solar drying plants in operation could be find in some European countries, the United States and Australia (Seginer and Bux, 2006). No more recent figures could be obtained from literature, but it can be supposed that the number of solar drying plants have increased since 2003. The use of solar drying to solve the problem of sewage sludge disposal is gaining interest in further countries, such as Greece, Turkey, Algeria, Morocco and China, where studies and testing have been undertaken.

#### *2.3.3.2 Greenhouse description*

In the greenhouse, the sludge is spread in a thick layer above the ground and is regularly mixed, by manual or mechanized means, in order to homogenize the distribution of the dried sludge and avoid crust formation. The sludge absorbs part of the solar radiation that passes through the transparent walls of the greenhouse and this absorbed heat leads to moisture evaporation. Note that a small fraction of the radiation is loss by reflectance and absorbance on the transparent wall, and reflectance on the sludge. The greenhouses usually include a ventilation system in order to evacuate the evaporated moisture, and mixing fans to create turbulence in order to lead to higher drying rates by enhancing the mass transfer. Examples of commercial available technologies for sewage sludge solar drying are those developed by Thermo-System® (Bux et al., 2002) and Hubert® (Dellbrügge et al., 2015). Figure 21 illustrates the transfer phenomena during solar drying in a

greenhouse. Figure 22 illustrates a typical greenhouse solar dryer. Appendix B presents photographs of large-scale greenhouses.

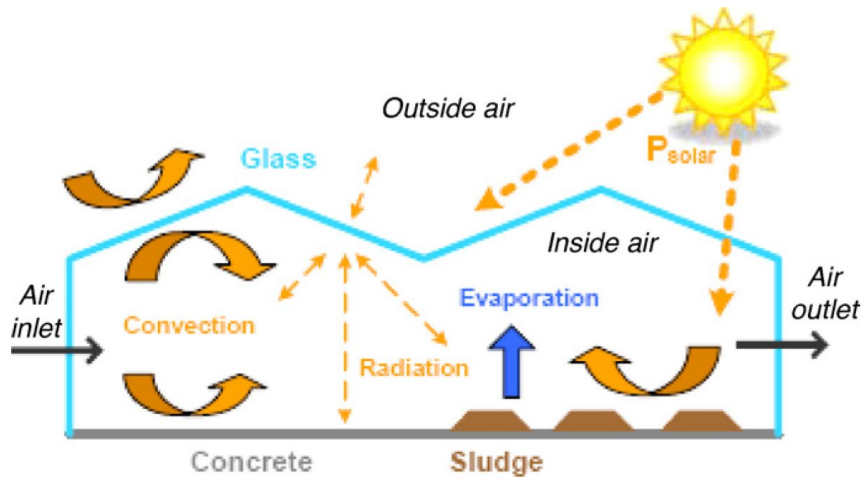


Figure 21. Schematic representation of the transfer phenomena during sewage sludge solar drying in a greenhouse (Roux et al., 2010)

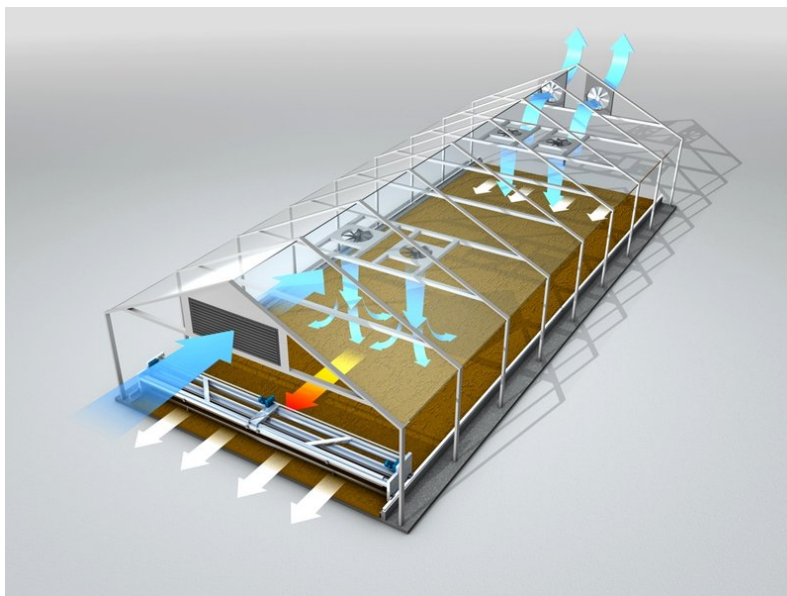
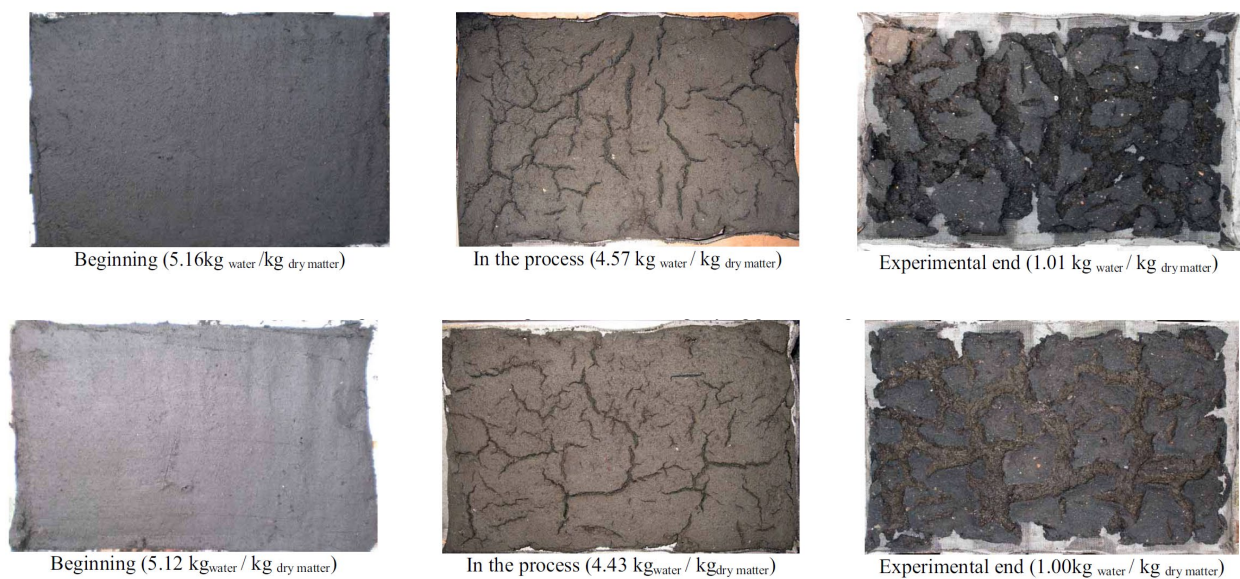


Figure 22. Typical greenhouse solar dryer (Huber, 2007)

The main factors of greenhouse design are based on the drying rate, the sludge production rate and the final dryness of the product (Seginer et al., 2007; Seginer and Bux, 2006). The drying rate depends on the environmental conditions (solar irradiance,

air temperature and humidity), operating condition (ventilation and mixing fan rates, mixing, thickness of the bed) and the type of sludge (particularly on the initial total solids content). Authors have observed that the drying rate tends to accelerate during the process (Bux et al., 2002; Mathioudakis et al., 2013), which is an unexpected behaviour with respect to the drying kinetic theory. The increase of the drying rate was attributed to the increase of the surface area after granulation of the sludge. The apparition of cracks during drying leads to the increase of the surface area, as displayed in Figure 23, which could contribute to the increase of the drying rate.



*Figure 23. Photographs of the sludge aspect at different moisture content during solar drying (Zhao et al., 2009)*

As the solar irradiance depends on the season and the weather conditions, the performance of a greenhouse drops during the cold days in winter or during very cloudy days. Besides, no drying occurs by night, as no sun radiation is available. In order to offset these limitations, different measures have been developed, including: heating of the floor from solar water heaters (Krawczyk and Badyda, 2011; Salihoglu et al., 2007); use of an auxiliary heating source such as infrared lamps (Krawczyk and Badyda, 2011) or waste heat from an external process (Bux, 2010); thermal energy storage (Salihoglu et al., 2007); use of heat pumps to pre-heat the drying air and for floor heating (Slim et al., 2008); addition of lime (Salihoglu et al., 2007) or flocculants

(Bux et al., 2002). A solar drying plant can become off-grid in terms of electricity by the installation of photovoltaic panels, as suggested by Kurt et al. (2015). The elements added in the solar plant increase the investment, so a comprehensive financial study must be undertaken in order to verify that the gain of performance is worth and leads to operating costs savings in the long term.

#### *2.3.3.3 Drying performance*

Table 2 presents the characteristics and performance of greenhouse for sewage sludge solar drying from large applications to bench-scale trials. The solar plant located in Mallorca is the largest plant in the world, while the one installed in Managua is the largest in the American continent. The plants in Oldenburg, Renquishausen and Fathiye are in continuous operation, whereas those in Kavala and Brisbane are pilots in trials. The greenhouse from Tongji University is a laboratory-scale prototype. It can be seen that solar drying can increase the sludge dry matter content (or total solid content) up to 80-90%, leading to a product with a moisture content lower than 20%. The energy consumption only includes the electricity to run the equipment of the greenhouse, as the thermal energy for drying is provided by solar radiation. Its value, varying between 20 to 60 kWh/t, is considerably lower than the typical electricity consumption of conventional drying ranging from 70 to 110 kWh/t. By considering the thermal energy input in a conventional drying process, the total energy requirement drastically rises up to 800-1000 kWh/t, leading to considerably large difference with respect to a solar dryer where the thermal energy is “free”. This demonstrates the considerable operation cost savings that solar drying can achieve.

Table 2. Characteristics and performance of greenhouses for sewage sludge solar drying

Location	Surface (m <sup>2</sup> )	Capacity (tonnes sludge per year)	Dry material content (%)		Drying time (days)	Drying rate (tonnes evaporated moisture per year per m <sup>2</sup> )	Energy consumption (kWh per tonnes evaporated moisture)	Reference
			Initial	Final				
Mallorca (Spain)	17,260	30,000	20-30	60-80	-	1-1.7 (year average)	55-60	(Socias, 2011)
Oldenburg (Germany)	6,500	30,000	20-25	60-70	-	-	-	(Thermo-System, n.d.)
Managua (Nicaragua)	8,760	26,000	28	70	21	4.3	20	(Meyer-Scharenberg and Pöppke, 2010)
Renquishausen (Germany)	700	500	3	93	83 (without flocculent)-64 (with flocculent)	-	28 (without flocculent)-2 (with flocculent)	(Bux et al., 2002)

Location	Surface (m <sup>2</sup> )	Capacity (tonnes sludge per year)	Dry material content (%)		Drying time (days)	Drying rate (tonnes evaporated moisture per year per m <sup>2</sup> )	Energy consumption (kWh per tonnes evaporated moisture)	Reference
			Initial	Final				
Fathiye (Turkey)	2,000	-	-	-	2 to 2.5 (summer)-3.5 (winter)	-	-	(Kurt, 2014)
Brisbane (Australia)	340	820	12	70-90	15-35	1-2.5	30-45	(Horn et al., 2008)
Kavala (Greece)	66	-	10-20	85-95	8 (summer)-31 (winter)	4.2 (summer)-1.5 (winter)	-	(Mathioudakis et al., 2013)
Tongji University (China)	0.08	-	16	56	5.2	1 (summer)-0.2 (winter)	-	(Zhao et al., 2009)

#### *2.3.3.4 Disinfection performance*

In terms of disinfection, the quality of the sludge differs from one study to another in literature. Authors usually agree that solar drying leads to a significant decrease of the bacteria population by a few order of magnitudes, e.g. *Escherichia coli* and faecal coliforms (Bux et al., 2001; Horn et al., 2008; Mathioudakis et al., 2013; Salihoglu et al., 2007; Sypuła et al., 2013). Concerning salmonella, there is no a general consensus about the effect of solar drying: while Shanahan et al. (2010) claim that salmonella is not detected in the final product, Sypula et al. (2013) observed that the salmonella population was not considerably affected during drying up to 50% of moisture content. Otherwise, Shanahan et al. (2010) noted that viruses are completely eliminated during the process. In contrast, solar drying only has a weak influence on the deactivation of *Ascaris* eggs (Sypuła et al., 2013).

The relative low temperatures in the greenhouse may be the reason that avoids the total elimination of bacteria, which can even regrowth for sludge rich in nutrients (Goldstein et al., 1988). Sypula et al. (2013) estimated that, according to their data, the deactivation of *Escherichia Coli* and *Salmonella* require of 72 and 196 days respectively. In the case of *Ascaris* eggs, the conditions in a greenhouse may be insufficient for their deactivation, as they are very resistant to external factors and can subsist in improperly sanitized material for several years (Carrington et al., 1991; Strauch, 1991).

According to some cases, the bacterial pathogen reduction after solar drying can be enough for the sludge to meet the regulations of reuse with restrictions (Mathioudakis et al., 2013; Salihoglu et al., 2007), and even without restrictions under favourable climatic conditions with high irradiances (Mathioudakis et al., 2013). However, as disinfection to a safe level cannot be guaranteed in all the cases, it is recommended further processing after solar drying, for example composting or the addition of a chemical. Lime addition has been employed with success to lead to a product possible to reuse without restrictions (Bux et al., 2001; Salihoglu et al., 2007). The use of external source of energy, floor heating or drying at night from stored thermal energy can increase pathogen reduction (Kurt, 2014).

#### *2.3.3.5 Summary*

Solar drying is an attractive option for sewage sludge disposal in countries with temperate weather by the installation of small and medium scale plants, and in countries with warm climate by the installation large sized plants (Seginer and Bux, 2006). It represents a good alternative with respect to conventional dryers, with usually lower capital and operational costs (Kurt, 2014), and lower greenhouse gas emission (Bux, 2010). In counterpart, it presents a higher footprint and lower treatment rate. Post-processing is recommended to ensure full disinfection of the product, in particular for reuse in agriculture.

#### **2.3.4 Potential use of solar drying for faecal sludge**

Solar drying offers a good opportunity to meet with the specifications of faecal sludge drying. Solar energy, which is usually abundant in developing countries, could be employed for drying applications, leading to a cost-effective solution with low operating costs. Besides, solar energy could be the perfect source of energy to power an eventual in-situ drying system, particularly in places with restraint access to electricity or fuels at affordable prize.

## **3 METHODOLOGY**

---

This chapter describes the feedstock (faecal sludge from ventilated improved pit latrines), the apparatus (solar drying rig) and the analysis performed in the sample (physical, thermal and chemical analysis), and it provides the experimental planning.

### **3.1 FEEDSTOCK: FAECAL SLUDGE FROM VIP LATRINES**

The feedstock selected for the experiments was faecal sludge from ventilated improved pit (VIP) latrines. The sample was taken during pit emptying in the eThekweni municipality. In the laboratory, the faecal sludge was stored in a cold room at 4°C in order to stop any biological degradation and preserve its properties in the extent of possible. Prior to the experiments, the sludge was screened in order to remove the trash as textile, plastic and metal detritus.

An ethical clearance was obtained from the UKZN Biomedical School in order to be allowed to experiment with faecal sludge, which is considered as a Human tissue and then its use for research purposes requires ethical approval. The ethical clearance is attached in Appendix C.

### **3.2 SOLAR DRYING RIG**

One of the objectives of this project was to design and construct of an experimental rig for the characterization of solar drying. This apparatus consists essentially in a thermobalance, installed at the roof of the Chemical Engineering building (latitude: 29°52'08.1" S; longitude: 30°58'46.6"E) at the UKZN, Durban, South Africa. The solar assessment of the experimental site can be seen in Appendix D. The sample was exposed to the solar radiation inside a transparent box and it was placed on a crucible linked to a balance so as to measure the loss of weigh during drying and determine the kinetics of the process. An airflow stream was introduced in the drying chamber, in order to remove the evaporated moisture and enhance the drying process. The air stream could be optionally heated before introduction into the drying chamber. The humidity, temperature and flowrate of the air stream were measured at different points.

The temperature of the sample was also monitored. The data was continuously logged and recorded in a computer. The drying rig was stored in a shed when it was not used for protection against bad weather and thefts.

The diagram and a photograph of the drying rig are depicted in Figure 24 and Figure 25 respectively.

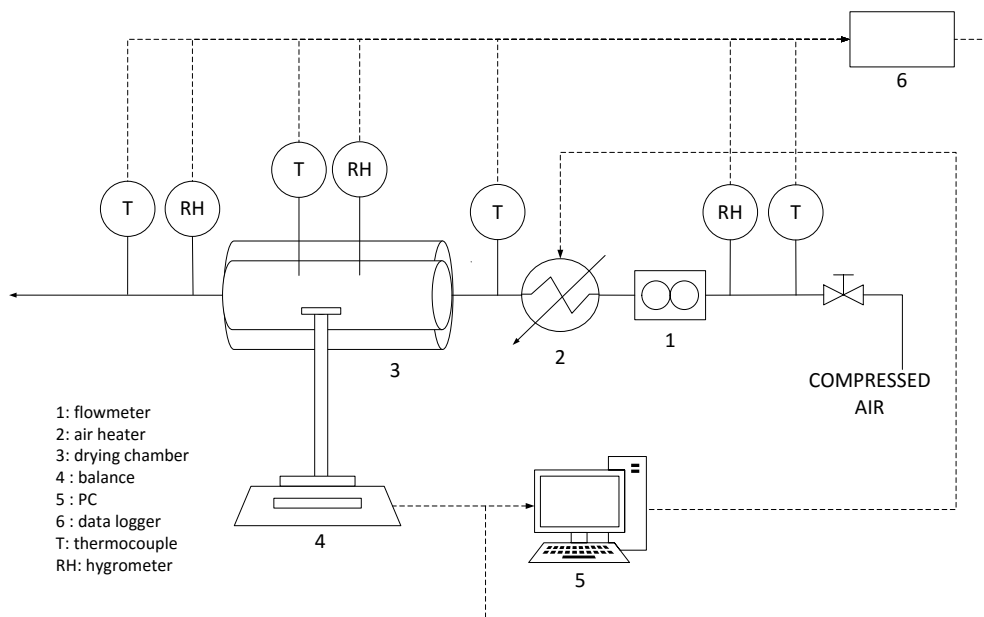


Figure 24. Solar drying rig diagram



Figure 25. Solar drying rig setup

### 3.2.1 Drying chamber

The drying chamber is a double-walled cylinder made of acrylic, with a vacuum between the inner and outer wall for thermal insulation. The drying chamber was 150 mm of inner diameter and 400 mm of length. The outer tube was 200 mm diameter and 500 mm length. The transmittance with respect to the solar irradiance is estimated to approximately 80%. The sample is placed on a crucible that stands in a support linked to the mass balance. Figure 26 shows a photograph of the drying chamber with the sample support.

The reasons for the selection of acrylic as the material of the drying chamber can be found in Appendix E. The construction plans of the drying chamber can be consulted in Appendix F.

The drying chamber and the sample weighing system were contained inside a box to protect the mass reading from external perturbations, in particular wind, and to avoid overheating from the exposure to solar radiation. The drying chamber inside the protection box is displayed in Figure 27.



Figure 26. Setup of the sample support in the solar drying rig



Figure 27. Drying chamber inside the protection box

### 3.2.2 Air stream

The air stream in the drying chamber was supplied by the compressed air line from the Chemical Engineering building. The compressed air supply is enough to achieve the desired air velocities (0.1 to 1 m/s). The air stream was introduced in the drying chamber by a multi-entries inlet that enables an even distribution of the air velocity along the cross-section, according to CFD simulations (Appendix G). The flowrate was controlled by a buoyancy flowmeter, model *PS-31/6300* from *Tecfluid*.

Before introduction into the drying chamber, the air stream could be heated in a costume-designed electric air heater. The air heater and its interior can be seen in Figure 28 and Figure 29 respectively.



Figure 28. Air heater



Figure 29. Interior of the air heater

### 3.2.3 Measurement of temperature and relative humidity

Type-k thermocouples of 0.3 mm diameter were employed to measure the temperature at different locations: within the sample, inside the drying chamber, in the environment. The length of the thermocouples wire is covered by glass fibre in order to avoid heat losses that can lead to an inaccurate temperature reading.

Temperature sensors pt100 were used to measure the temperature of the air stream at the inlet and outlet of the drying chamber.

The air humidity was measured at the inlet and outlet of the drying chamber, and inside the drying zone, using humidity probes model *HPP809A031* from *TE Connectivity* and *HP474ACR* from *Delta Ohm*.

### 3.2.4 Measurement of solar irradiance

The solar irradiation was measured on-site by a second-class pyranometer, model *CMP3* from *Kipp & Zonen*.

### 3.2.5 Interface and data logging

The interface between the measuring instruments and the computer enables to visualize the mass, temperature, relative humidity and solar irradiance measurements

during experiments and log the data into a computer. In the interface setup, the mass balance was connected directly to the computer, while the thermocouples, temperature sensors pt100, humidity meters and the pyranometer transferred the measurements to the computer via data loggers.

Figure 30 shows the data acquisition box where the data loggers, power supply and the controls for the air heater have been installed. A screenshot of the software used to log the data is displayed in Figure 31.



Figure 30. Data acquisition box

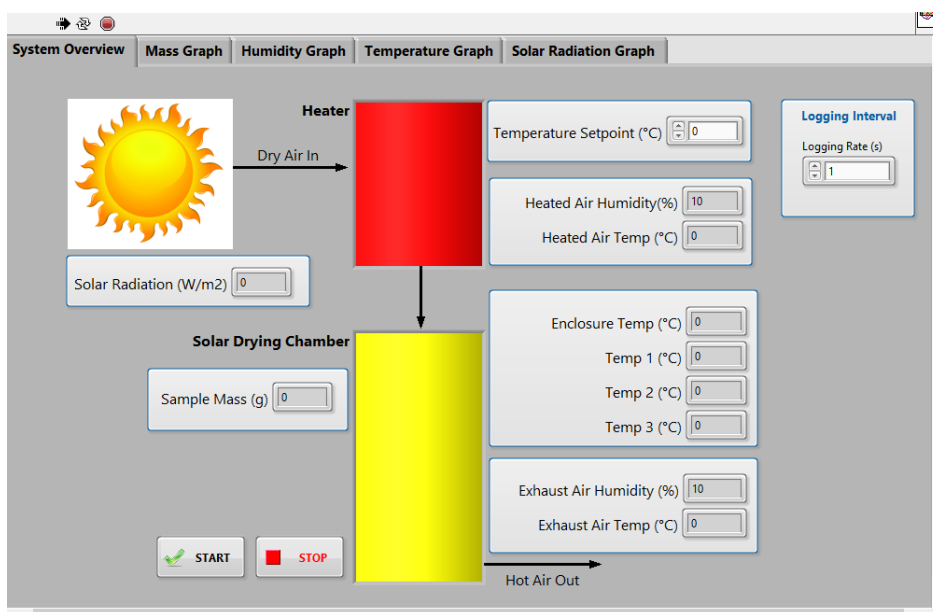


Figure 31. Software to log the data from the solar drying rig

## **3.3 EXPERIMENTAL PLAN**

### **3.3.1 Experiments in the solar drying rig**

The experimental campaign in the solar drying rig was performed from the beginning of October to the beginning of December 2017. The experimental rig was carefully positioned at an emplacement where the surrounding objects and walls did not cause shade at any moment of the day. Prior to the experiments, the faecal sludge was spread as a thin layer on a circular crucible, which was then placed at the top of the weighing system. A second identical sample, placed at the open-air nearby the drying chamber, played the role of a control. Its mass was monitored by manual weighing each 30 minutes in a scale. The experiments started at 10 AM and finalized at 4 PM. The effect of the parameters considered as the most influent was studied, which are:

- The weather conditions (sunny, partially cloudy, overcast);
- The flowrate of the air stream (0, 0.5 and 1 m<sup>3</sup>/min, corresponding to an air velocity of 0, 0.5 and 1 m/s, respectively);
- The temperature of the air stream (ambient temperature, 30 and 60°C);
- The size of the sample (5 and 10 mm thickness, 60 and 120 mm diameter).

The initial mass of the sample was comprised between 15 to 60 g, depending on its size. From the mass readings by the balance, the drying curve was plotted as the mass normalized with respect to its initial value versus time. The reference conditions were: sunny weather, air velocity of 0.5 m/s, no air heating, sample of 5 mm thickness and 60 mm diameter. During the experiments, only one parameter was varied individually from the reference conditions. Experiments at the same conditions were done in duplicates.

Preliminary tests were done in order to verify the functionality of the apparatus, after its commissioning, as describe in Appendix H.

### **3.3.2 Characterization of the dried product**

Several analyses were undertaken in the samples before and after the solar drying experiments. Moisture content and ash analysis were performed in order to determine the amount of moisture removed during the process and to detect organic matter

degradation, respectively. The morphological changes in the sludge were characterized, among which the shrinkage, cracking and crust formation, which enables to have a deeper insight of the process. The calorific value, thermal properties (thermal conductivity, heat capacity) and nutrient analysis were measured for the evaluation of the dried sludge as biofuel and fertilizer. In previous investigations, these properties have been determined for faecal sludge convective and infrared drying (Makununika, 2016; Mirara, 2017). This research will allow to confirm whether or not the same findings are obtained with solar drying.

Most of these analyses were based on the Standard Operating Procedure from the Pollution Research Group (PRG, 2014). These methods have been already employed in previous investigations (Makununika, 2016; Mirara, 2017; Zuma et al., 2015).

#### *3.3.2.1 Moisture content and ash analysis*

The moisture and ash content were measured for the raw faecal sludge and the dried product. The moisture content was determined by measuring the sample mass before and after drying in an oven at 104°C for 24 hours. The ash content was determined by measuring the mass before and after calcination in a muffle furnace at 550°C for 2 hours.

#### *3.3.2.2 Calorific value*

The calorific value was measured in an oxygen bomb calorimeter model *Parr 6200*. This device is able to measure the heat of combustion of the sample after introduction of pure oxygen.

#### *3.3.2.3 Thermal analysis*

The thermal conductivity, heat capacity and thermal diffusivity of the samples were measured using a *C-Therm TCi* thermal analyser. In this device, the sample was placed on a sensor which was heated over a short time. Through the thermal transient response of the system to the heat input, the thermal properties were determined.

#### *3.3.2.4 Nutrient analysis*

The content of phosphorus (P), potassium (K), calcium (Ca) and magnesium (Mg) was determined after digestion of the samples and analysis in a Microwave Plasma-Atomic Emission Spectrometer (MP-AES) model *Agilent 4100*. The digestion was performed by adding nitric acid to the sample and then placing the solution in a microwave digester model Ethos 1 – Milestone, heated to 130°C for 1 hour. The content of carbon (C) and nitrogen (N) was measured in a CN analyser model LECO TrueMac. The content of molecular compounds, such as ammonium (NH<sub>4</sub><sup>+</sup>), nitrates (NO<sub>3</sub><sup>-</sup>), nitrites (NO<sub>2</sub><sup>-</sup>) phosphates (PO<sub>4</sub><sup>-3</sup>), was analysed using the spectroquant Nova 60-Merck. The sample was prepared by blending the sample with water, centrifugation, recovering the liquid fraction and adding the commercial test kit specific to each compound for the coloration of the solution.

#### *3.3.2.5 Morphological characteristics*

The dimensions of the sample were measured before and after solar drying, enabling to determine the variation of volume along the process. From this information, the shrinkage of the sample could be evaluated. Similarly, by also taking into consideration the sample weight before and after experiment, the change of density could be estimated. Nevertheless, because the measurement of the dried sludge dimensions was challenging due to its irregular shape and the low precision of the measurement device (a ruler), the shrinkage and density variation results could be only considered as rough estimations.

#### *3.3.2.6 Qualitative observations*

Visual observations in the samples were performed in order to identify further morphological changes occurring drying, such as cracks apparition and crust formation. Attention was also paid to the changes of colour and odour of the sludge after drying, based on the appreciation of the experimenter.

### **3.3.3 Solar air heating chimney**

In addition to the solar drying rig, a solar air heating chimney was constructed as a part of an undergraduate student project. The concept of this device is to heat an air stream using solar thermal energy and use the heated air for drying purposes. Several modifications have been done since the original design and the effect of each modification has been tested. After optimization of the solar chimney, it will be linked to the solar drying rig, which will allow studying solar drying in a mixed and indirect mode. In the mixed mode configuration, the sample to dry will be simultaneously exposed to solar radiation and the hot air stream flowing from the solar chimney. In the indirect mode configuration, an opaque cover will block the penetration of solar radiation into the drying chamber and thus the sample will be only dried by convection from the air heated by the solar chimney.

Appendix I describes the solar chimney setup, the modifications performed and results obtained so far (investigation not concluded).

## 4 RESULTS AND DISCUSSION

---

This chapter presents and discusses the results obtained during the faecal sludge solar drying experiments, which includes the mass loss along time and temperature measured in the samples. It also presents the chemical, physical and morphological variations of the sludge during solar drying.

### 4.1 SOLAR DRYING

#### 4.1.1 Effect of the weather conditions

This section describes the results obtained in the experimental drying rig during different weather conditions: sunny, cloudy and overcast. For these experiments, the air stream was set at velocity of 0.5 m/s in the drying chamber and was not heated. The tests were conducted by using a sample of 5 mm thickness and 60 mm diameter.

##### 4.1.1.1 Irradiance

The irradiance is an indicator of the available thermal energy for drying from the solar radiation. Figure 32 compares the solar irradiance measured during 5 hours of experiments in a sunny, cloudy and overcast day. The average values were 1000, 600 and 350 W/m<sup>2</sup>, during a sunny, cloudy and overcast day, respectively. As expected, the irradiance depended on the weather conditions: it was the highest during sunny days, whereas it is the lowest in an overcast weather. During cloudy conditions, moments of low and high irradiance were alternating, leading to an intermediate value compared to sunny and overcast conditions. These fluctuations could be explained by the alternation between clouds and sunshine.

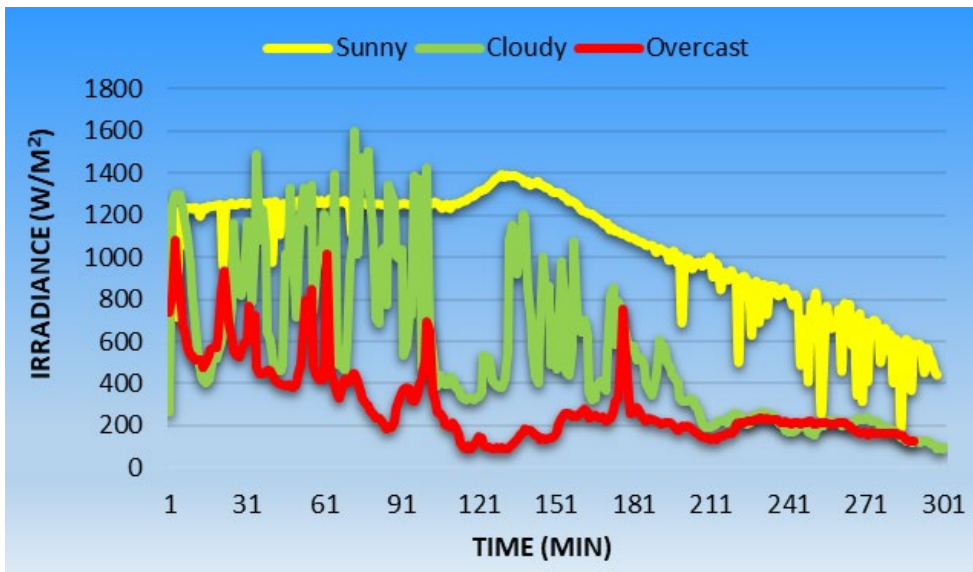


Figure 32. Irradiance measured during solar drying in a sunny, cloudy and overcast days

The irradiances from the rest of the experiments are displayed in Appendix K. In general, irradiances were the highest at the beginning of the experiment and diminished with the progression of time. This trend can be explained from the normal course of a day where the higher sunshine occurs in the morning and declines in the afternoon. Nonetheless, the patterns of the irradiance curves were never the same and not all the experimental cases followed the aforementioned trend. Therefore, due to the variability of the irradiance during the solar drying experiments, the duplicates from the same experiment could never been done in identical conditions. This corresponds to the main challenge to conduct experiments with solar energy, where the conditions from one day to another can have similitudes but are unique.

#### 4.1.1.2 Temperature of the sludge

Figure 33 displays the evolution of temperature with time, measured at the core and surface of the sludge, during a sunny, cloudy and overcast day. The highest temperatures were obtained during a sunny day, with peak values between 30 and 50°C. Overcast and cloudy conditions presented lower temperatures that varied mostly between 10 to 20°C, with a peak at 35°C for one of the experiments performed in cloudy conditions. At the different weather conditions, the temperature of the sludge

at the surface and the core were not significantly different during the process, so drying could be considered as isothermal.

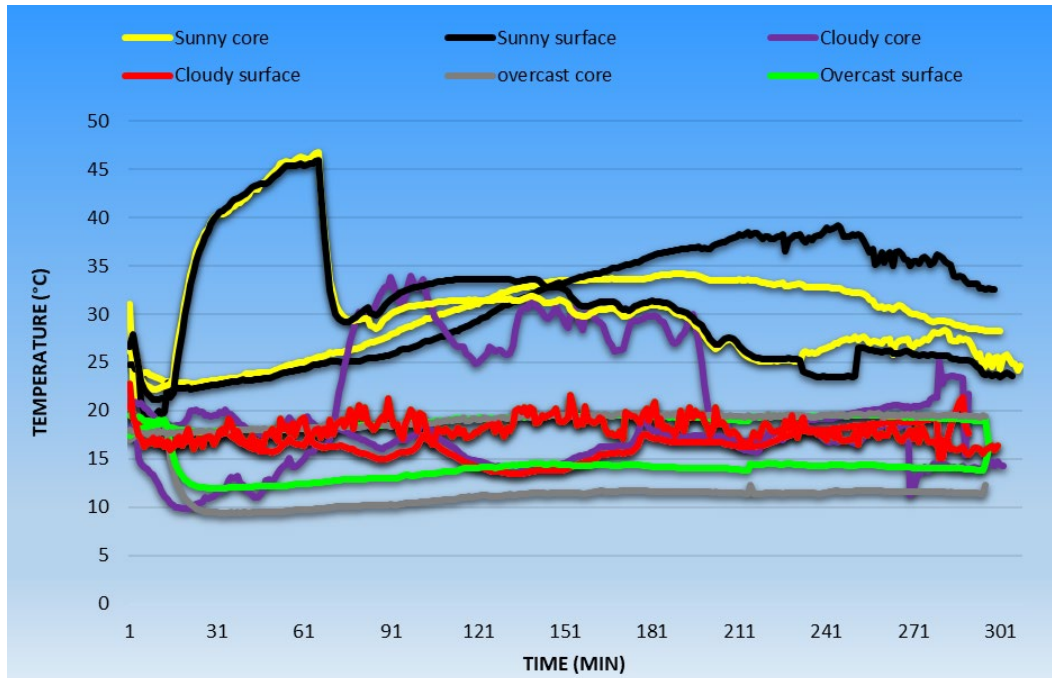


Figure 33. Temperature measured at the core and surface of the sludge during solar drying in a sunny, cloudy and overcast day

The overall of the temperature measurements from the ambient air and the air stream inside the drying chamber is presented in Appendix L. During sunny conditions, the temperature of the sludge could exceed the ambient temperature (25-30°C), and was approximately the same than that of the airflow in the drying chamber (25-45°C). The sludge can be then considered in thermal equilibrium with respect to its environment. In contrast, during a cloudy and overcast weather, the temperature of the sludge was lower than the ambient temperature (20-25°C) and that of the air inside the drying chamber (20-45°C). The lower temperature of the sludge under these conditions could be explained by the cooling effect induced by moisture evaporation and the lower solar irradiance that could not counteract this.

Note that, the temperature of the air stream inside the drying rate was generally higher than the ambient temperature. The air inside the drying chamber was probably heated by contact with the material of the solar drying rig that absorbed a fraction of the solar

irradiance. This rise of temperature was effective even in cloudy and overcast conditions.

It can be noticed that the temperature of the ambient air and the air in the drying chamber was fairly constant along time during the experiments. In contrast, the sludge temperature for two replicates of the same experiment usually varied within a same range but followed a considerable different pattern. The sources of pattern variations from one experiment to another could not be identified.

#### 4.1.1.3 Drying rates

- Comparison between sunny, cloudy and overcast conditions

Figure 34 displays the graph of the mass ratio (defined as the ratio of the mass of the sample at a given moment to the initial mass) versus time during experiments in sunny, cloudy and overcast conditions. The results for each experimental case are shown in duplicates.

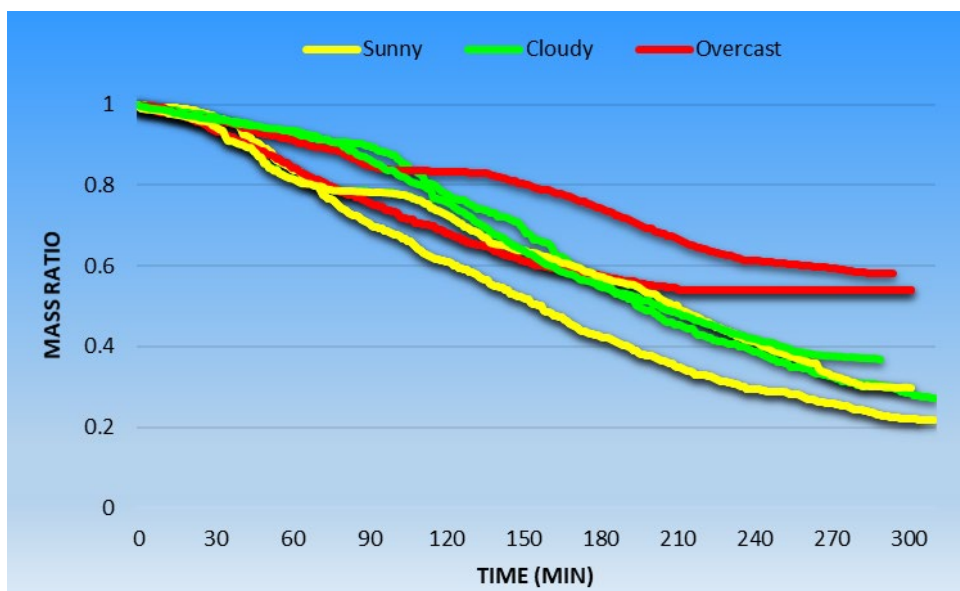


Figure 34. Mass ratio evolution as a function of time during solar drying in a sunny, cloudy and overcast day

In the early stage of drying, the mass loss was similar between the different cases. It was only after 90 minutes when the differences of mass loss rate started to appear and they were accentuated as drying proceeded. The sample mass loss was the fastest during sunny conditions, followed closely by the results obtained in cloudy conditions. The final mass ratio depended on the weather conditions: 20-30% in a sunny weather, 40-30% in cloudy conditions and 50-60% in overcast weather. It can be noted that the final mass ratio attained was close between the experiments in sunny and cloudy conditions, whereas it was considerably higher in the case of overcast conditions, which means that the mass loss in the latter case was considerably lower. In addition to this, the mass loss in overcast conditions stabilized at the end of the experiment, which was not the case during drying in sunny and cloudy conditions.

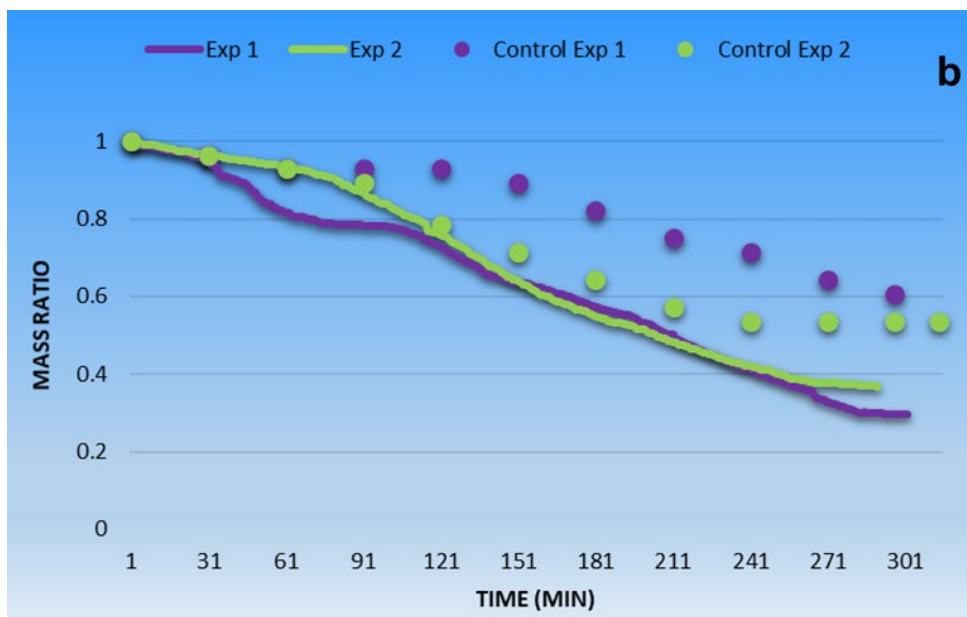
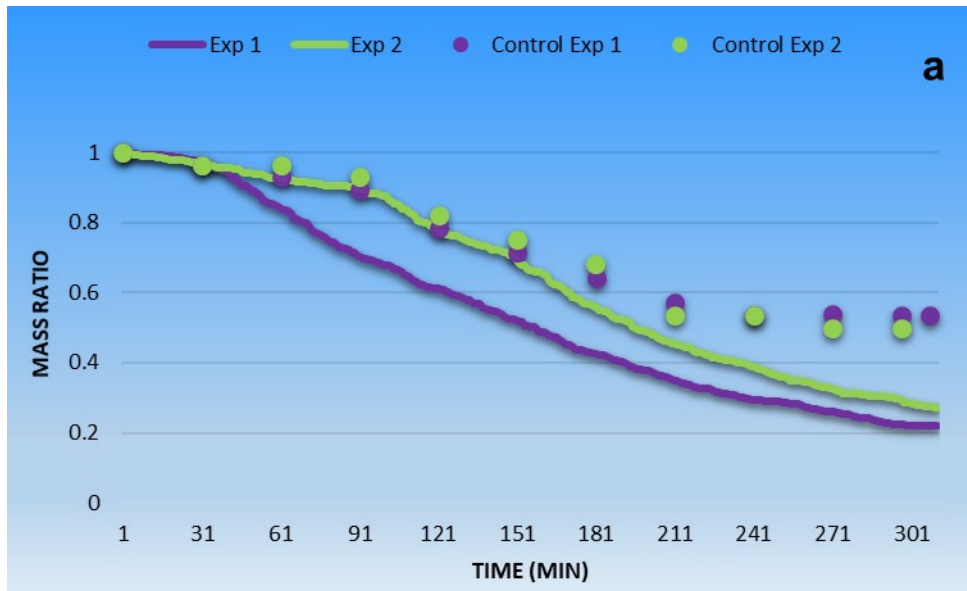
As it could be foreseen, sunny conditions led to faster drying rates, probably due to the higher irradiance and sludge temperature (refer to section 4.1.1.1 and 4.1.1.2). Although the difference with respect to cloudy conditions was low, the results differed in overcast conditions where the drying rate was considerably lower. This should be related to the low irradiance under these conditions (refer to section 4.1.1.1). Another relevant difference to note was the mass loss reached at the end of the experiment: whereas the sample mass was reduced up to 60 to 80% in sunny and cloudy conditions and looked as it would be able to carry on if the experiment time was longer, the mass loss stabilized at 50% in overcast conditions.

- Comparison between the enclosed and open air samples

Figure 35 compares the mass ratio evolution between the sample enclosed inside the drying chamber from the solar drying rig and the sample exposed to the open air (the control sample). This comparison was conducted for sunny, cloudy and overcast conditions. Note that the plots of the open-air samples are constituted of less points than the enclosed samples, as the mass measurements in the former case were done by 30 minutes of interval while the mass in the latter case was recorded each minute.

The solar drying of the enclosed and open-air samples behaved differently. During the drying of the enclosed sample in sunny and cloudy conditions, the mass loss was higher and globally occurred at faster rate. After 300 minutes, the mass loss was

approximately 50% for the open-air sample whereas it reached 60-80% for the enclosed sample. This difference was even more drastic in overcast conditions, where almost no mass loss was measured for the open-air sample.



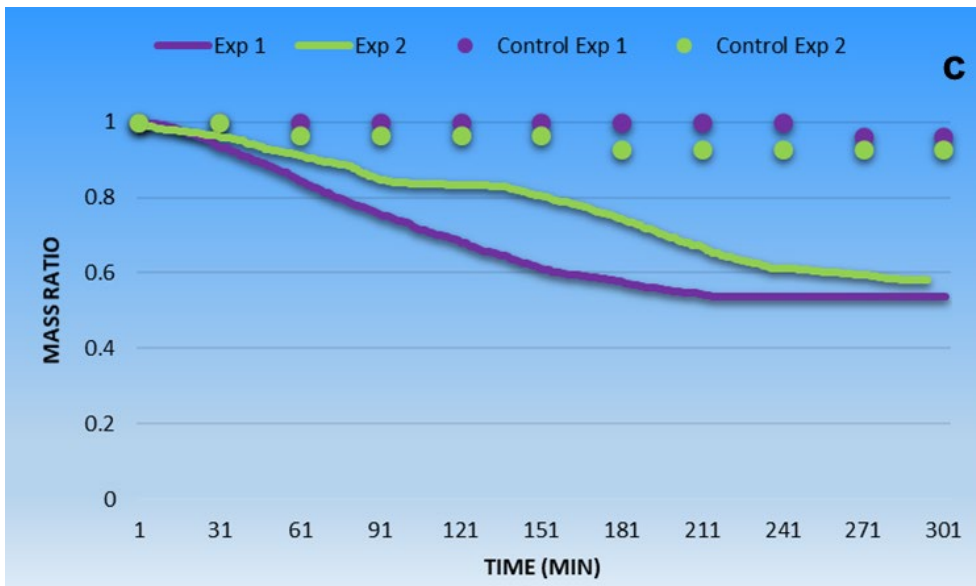


Figure 35. Mass ratio evolution as a function of time during solar drying of the enclosed sample (Exp 1 and Exp 2) and open-air sample (Control Exp 1 and Control Exp 2), in a sunny (a), cloudy (b) and overcast (c) day

These results demonstrate the benefits of solar drying inside an enclosed transparent volume, such as drying in greenhouses, in comparison to drying at open air, as done in the drying beds. Drying in an enclosed volume leads to a faster process and enables to dry the sludge at a lower moisture content. Indeed, transparent enclosure prevents heat losses to the environment by protecting the material against environmental factors, such as the wind that can cool the surface of the sludge. Moreover, transparent materials are usually opaque to long wave infrared radiation, which is the type of radiation emitted by most of the bodies heated by solar radiation. Therefore, the long wave infrared is trapped in the enclosure, leading to a greenhouse effect and a subsequent increase of temperature. The benefits of solar drying in an enclosed volume are evident in the case of overcast conditions where drying is possible in despite of the unfavourable meteorological conditions, whereas this not the case for the sample at the open-air.

Another reason that could have an influence on the difference between the open-air and enclosed sample is the surrounding air humidity: the environment air in Durban has a high humidity averaging between 70 to 80%, whereas the compressed air line humidity is much lower as it is dried before being compressed. A lower humidity in the air allows drying at a lower moisture content and at a higher rate.

## 4.1.2 Effect of size

### 4.1.2.1 Diameter

Figure 36 displays the mass evolution during the solar drying of samples with 6 and 12 mm diameter and 5 mm thickness in sunny conditions, with an air velocity of 0.5 m/s inside the drying chamber. Figure 37 shows the temperatures measured at the core and surface of the samples during the experiments.

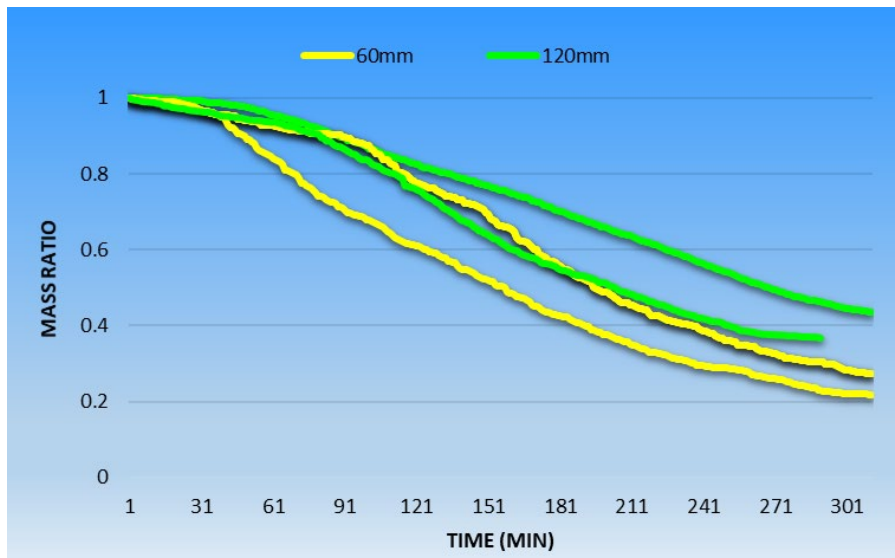


Figure 36. Mass ratio evolution as a function of time during solar drying of the 60 and 120 mm diameter sample

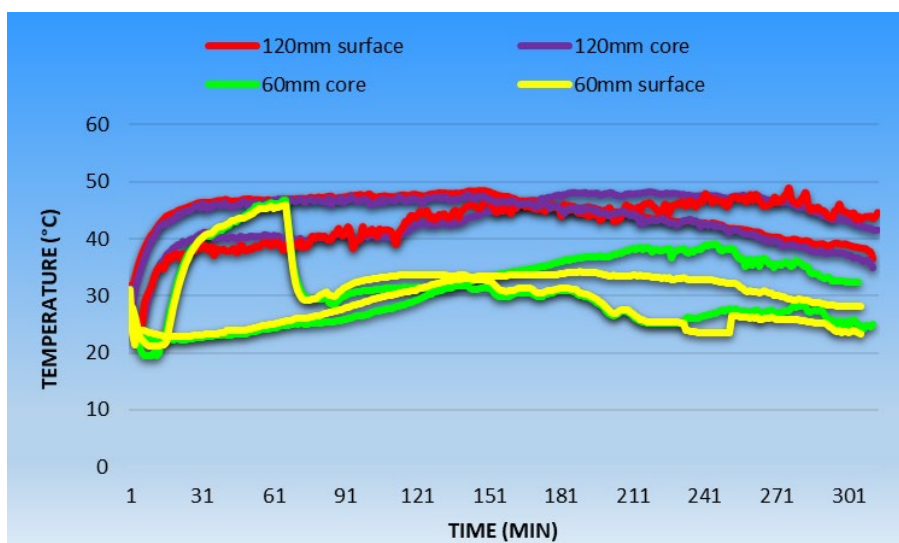


Figure 37. Temperature measured at the core and surface during solar drying of the 60 and 120 mm diameter samples

There was no any significant difference between the results obtained for the 60 and 120 mm samples, in terms of mass and temperature. Therefore, the difference of the diameter size of the samples did not lead to any significant drying difference. The mass loss ranged between 60-80% for all the experimental cases. The transformation was isothermal for any of the samples, with an equal temperature at the core and surface. The maximum temperature reached during solar drying was comprised between 30 to 50°C. Note that the temperature of the 120 mm sample was slightly higher than that of 60 mm, but this difference was not reflected in a significant difference in terms of mass loss. This suggest that a difference of a few degrees do not considerable influence the drying rate.

By increasing the diameter of sample from 60 to 120 mm, the mass of sample was quadrupled but also the surface area. The amount of mass to dry per area unit remained then unchanged. Assuming that the sample is uniform, the drying rate in each surface unit should be the same, so the addition of supplementary surface units must not affect the overall drying rate.

#### *4.1.2.2 Thickness*

The mass and temperature evolution during solar drying of samples with 5 and 10 mm thickness and 60 mm diameter, are shown in respectively Figure 38 and Figure 39. The experiments were conducted during a sunny air and the air velocity in the drying chamber was set at 0.5 m/s.

The sample with 5 mm thickness exhibited a faster mass decrease than the sample of 10 mm thickness, as well as a higher mass reduction at the end of the experiments (70 to 80% versus 40 to 60% for the 10 mm sample). No significant difference was observed in terms of temperature, with both samples being isothermal during the process. The maximum temperature attained by the samples ranged mostly between 30 to 50°C.

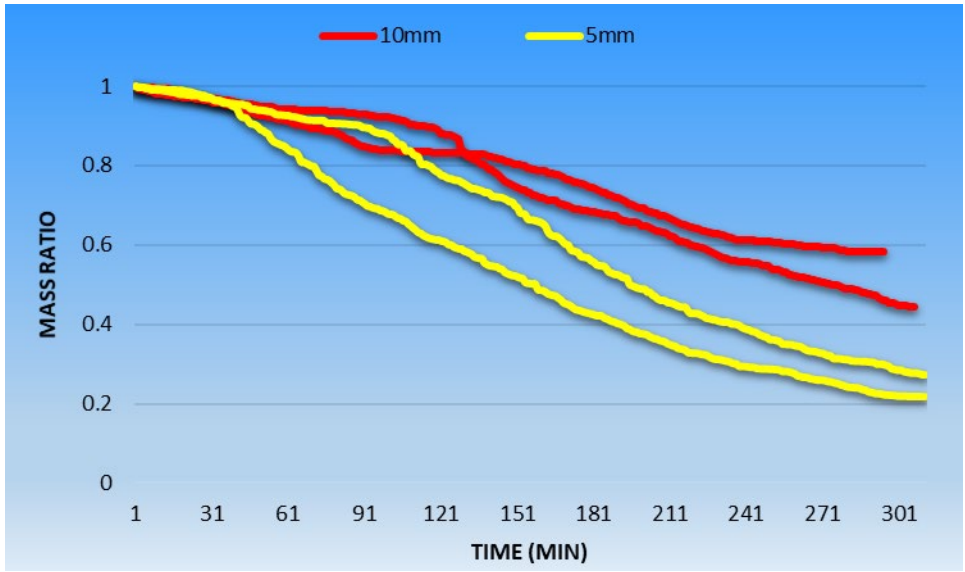


Figure 38. Mass ratio evolution as a function of time during solar drying of the 5 and 10 mm thickness sample

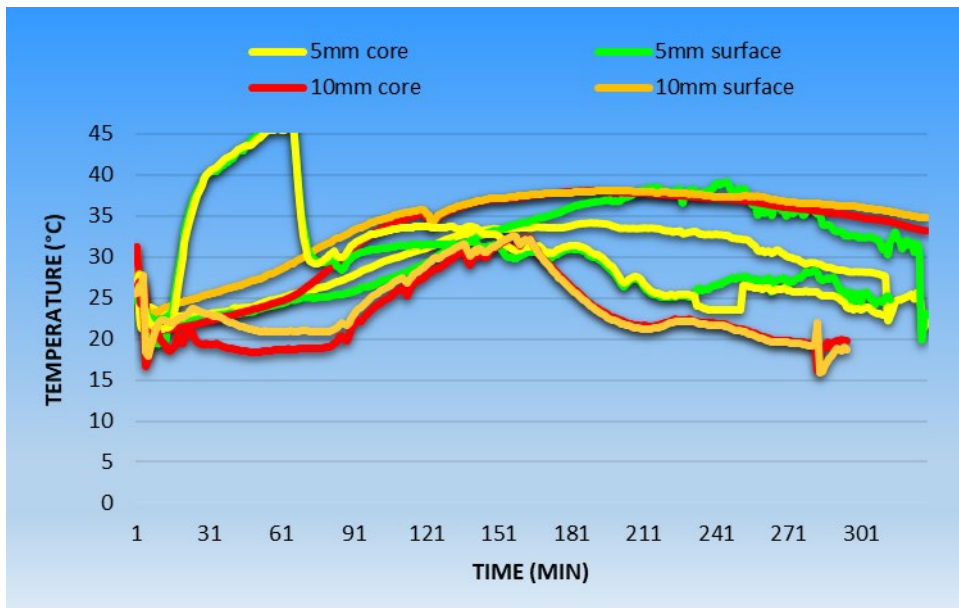


Figure 39. Temperature measured at the core and surface during solar drying of the 5 and 10 mm thickness samples

Considering that the remaining mass after drying with respect to the initial value was about 25 and 50% for the 5 and 10 mm sample respectively, it can be seen that the 5 mm sample dried two times faster than the 10 mm. The same factor applied for the difference of initial mass between the 5 and 10 mm samples: by keeping constant the sample diameter, so the surface area, the increase of thickness by a factor two implied

to double the mass load. The difference of drying rate between the 5 and 10 mm samples was then related to their difference of initial mass, and not to mass transfer limitations. Moreover, the increase of thickness did not either affect the heat transfer by limiting the heat penetration within the material, as suggested by the temperature of the samples varying in the same range.

### **4.1.3 Effect of air stream**

#### *4.1.3.1 Air velocity*

Figure 40 and Figure 41 show the graphs of sample mass and temperature versus time, respectively, during solar drying experiments at different air velocities inside the drying chamber (so different flowrates). The experiments were performed in a sunny day, for the sample with 60 mm diameter and 5 mm thickness. Natural convection refers to the case when no airflow was introduced in the chamber, i.e. flow velocity equal to 0 m/s. In this case, a natural convection flow is assumed to occur inside the drying chamber and be driven by the gradient of temperature from the heating of the drying chamber by the solar radiation. The air flowrate from natural convection was not quantified, and it was supposed to be much lower than when airflow is introduced (forced convection). As a proof of this, the relative humidity in the drying chamber was higher when no airflow was introduced (30-40%), in comparison to the relative humidity measured in the cases with airflow introduction (10%). This result reveals that the natural convection flow was not enough important to sweep away all the vapour from moisture evaporation, on the opposite to the cases with forced convection.

No significant difference was observed between the experiments without airflow introduction and the experiments with an airflow velocity of 0.5 m/s. The sample mass decreased more slowly in the case of the experiments with an airflow of 1 m/s and the loss of mass was lower (40% in this case versus 60-80% for the former two cases). No particular trend was seen for the temperature of the different experimental cases, which reached a peak value ranging between 35 and 50°C, similarly to the previous studied cases.

The decrease of the drying rate by increasing the air velocity is a surprising result which differs from the theory. Typically, increasing the air velocity increases the external mass transfer rate, leading to a faster transfer of moisture from sludge to the environment. In contrast, during drying using radiation as a heat source (as in the case of solar drying), the air velocity increase can take away part of the heat absorbed from the radiative heating and can cause the reduction of the material temperature, which has a negative effect on the drying rate. In our case, no cooling effect was observed by increasing the air flowrate, as the sample temperature remained in the same range (Figure 41). After discarding the cooling effect as a possible reason to explain the lower drying rate at higher air velocity, crust formation could explain this unexpected result. Indeed, high air velocities could lead to a faster depletion of moisture at the surface of the sludge, leading to a faster crust formation. This should create a considerable mass transfer resistance for moisture evaporation into the environment, causing a drop of the overall drying rate. Crust formation is discussed with more detail in section 4.2.

It is important to notice that the drying rate during experiments without airflow introduction could be higher than what was observed, if it was not by the relative humidity in the surrounding air that was higher than the normal (30% versus 10%).

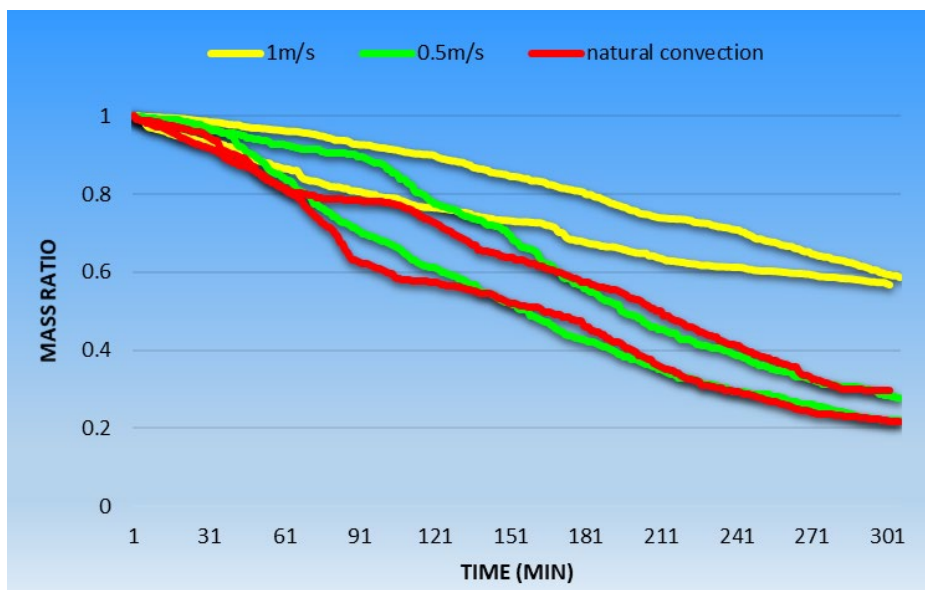


Figure 40. Mass ratio evolution as a function of time during solar drying at different airflow velocities inside the drying chamber (“natural convection” refers to the case without airflow introduction)

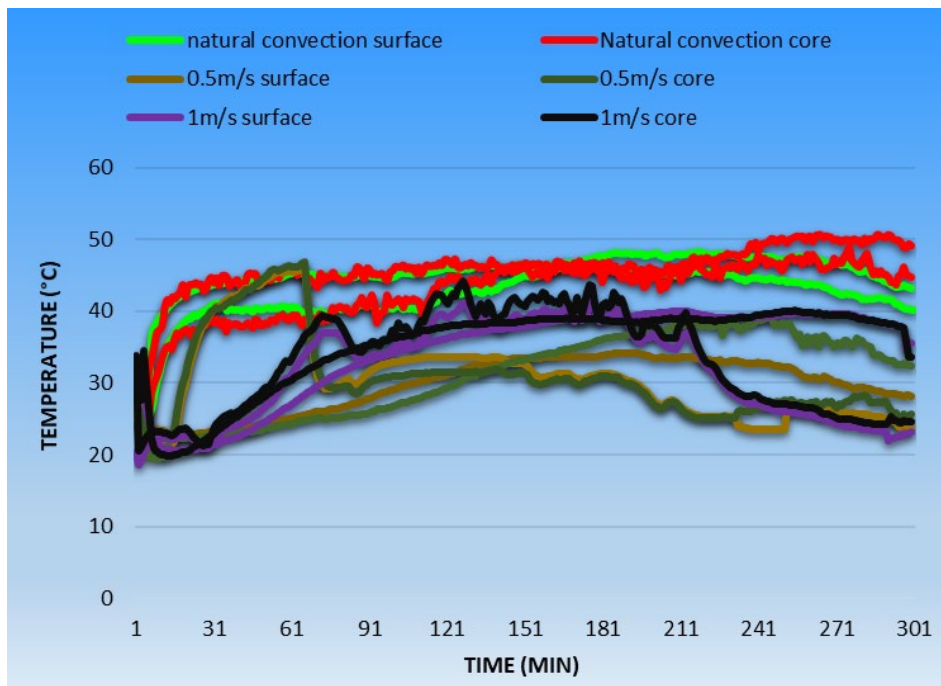


Figure 41. Temperature measured at the core and the surface during solar drying at different airflow velocities inside the drying chamber (“natural convection” refers to the case without airflow introduction)

#### 4.1.3.2 Air temperature

Figure 42 presents the mass evolution during solar drying experiments by varying the temperature of the air stream flowing in the drying chamber, at a constant air velocity of 0.5 m/s. This includes air without heating, and air heated at 30 and 60°C. The temperature measured at the surface and core of the samples can be seen in Figure 43. The experiments were carried out in a sunny day, with the sample of 60 mm diameter and 5 mm thickness.

It was difficult to appreciate any significant difference of drying rate between the different experimental cases, due to the scattering of the results. The only clear difference was the final mass achieved after solar drying: during the experiments with air at 60°C, the mass stabilized after removing 50 to 60%, whereas the mass was reduced up to 70 to 80% without air heating and with air at 30°C. Concerning the temperature measurements, the samples shown again to be isothermal during the process. As it could be anticipated, the temperature of the air heated at 60°C was the highest with values attaining up to 70°C after stabilization. It was then followed by the

air heated at 30°C and air without pre-heating with peak temperatures varying between 35 to 50°C.

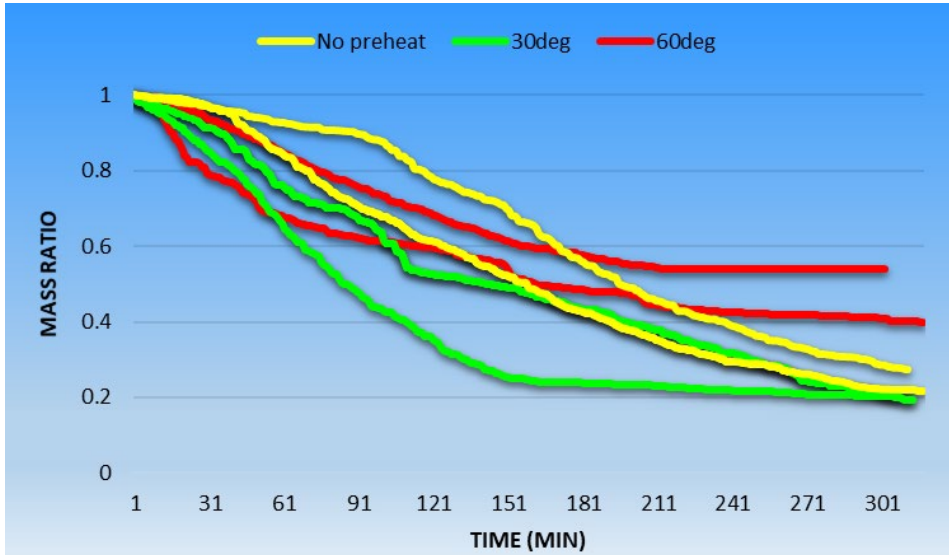


Figure 42. Mass ratio evolution as a function of time during solar drying with the airflow inside the drying chamber preheated at different temperatures (“No preheat” refers to the case without air preheating)

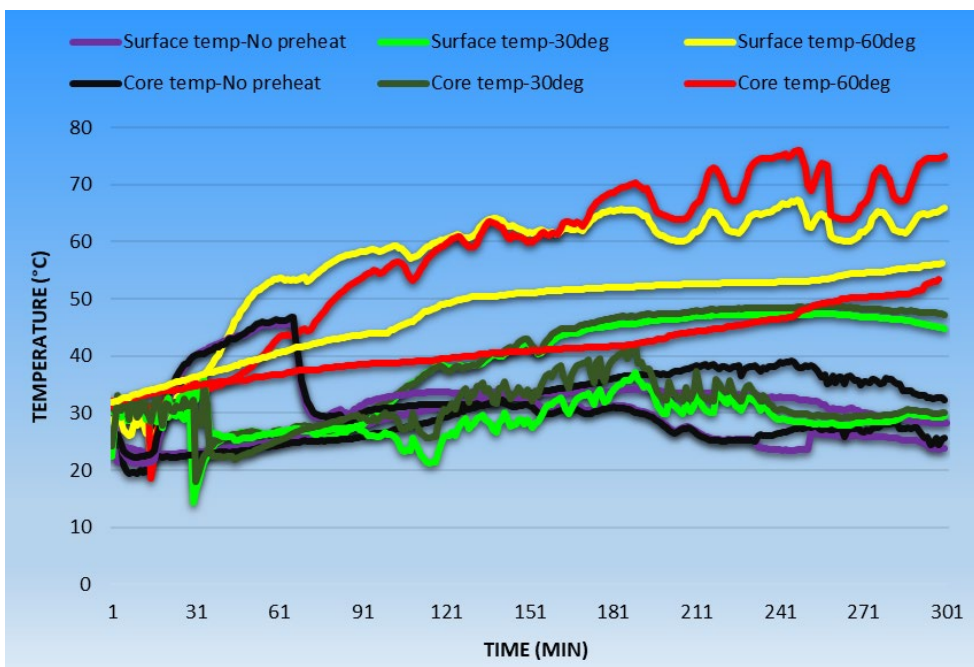


Figure 43. Temperature measured at the core and the surface during solar drying with the airflow inside the drying chamber preheated at different temperatures (“No preheat” refers to the case without air preheating)

The drying behaviour of the sludge did not significantly differ by heating the air at 30°C, which could be expected as the ambient temperature was close to 30°C during these experiments. Unexpectedly, heating the air at 60°C led to a lower moisture removal. Besides, this result is opposite to the theory, which stipulates that an increase of temperature should lead to faster heat and mass transfer, as well as to an increase of the energy available for moisture evaporation, increasing the overall drying rate, which was not observed in our results. To explain these surprise results, it was assumed that drying with air 60°C induced a crust formation, due to the rapid depletion of moisture at the surface of the sludge, affecting negatively moisture removal. This is discussed with more detail in section 4.2.

## 4.2 CHARACTERIZATION OF THE SAMPLES

This section presents the physical and morphological variations of the sludge during solar drying, as well as the thermal and chemical analysis of the dried sludge. Table 3 displays the label of the different samples that is used in the discussion of the experimental results in the following sub-sections.

*Table 3. Label of the samples*

<b><u>Label</u></b>	<b><u>Description of sample</u></b>				
	Type of sample	Weather conditions	Sample thickness	Air velocity	Air preheating
1	Initial faecal sludge	N.A.	N.A.	N.A.	N.A.
2	Sludge dried at open-air	Sunny	5 mm	N.A.	N.A.
3	Sludge dried at open-air	Cloudy	5 mm	N.A.	N.A.
4	Sludge dried at open-air	Overcast	5 mm	N.A.	N.A.

<u>Label</u>	<u>Description of sample</u>				
	Type of sample	Weather conditions	Sample thickness	Air velocity	Air preheating
5	Sludge dried within the drying chamber	Sunny	5 mm	0.5 m/s	No preheating
6	Sludge dried within the drying chamber	Cloudy	5 mm	0.5 m/s	No preheating
7	Sludge dried within the drying chamber	Overcast	5 mm	0.5 m/s	No preheating
8	Sludge dried within the drying chamber	Sunny	5 mm	0 m/s	No preheating
9	Sludge dried within the drying chamber	Sunny	5 mm	1 m/s	No preheating
10	Sludge dried within the drying chamber	Sunny	5 mm	0.5 m/s	Preheating at 60°C
11	Sludge dried within the drying chamber	Sunny	10 mm	0.5 m/s	No preheating

#### 4.2.1 Moisture and ash content

Figure 44 visualizes the moisture content measured for different samples, using the method described in section 3.3.2.1. Note that the moisture content can be also estimated from the drying curves in the previous sections, assuming that the mass loss is only due to moisture evaporation. Both methods to determine the moisture content gave similar results, except for the sample 9 where the direct measurement of moisture content underestimated its value with respect to the drying curve. This could be issued from an experimental mistake.

The moisture content of the initial faecal sludge was around 80% (sample 1). The lowest moisture contents were obtained for the 5 mm thickness sample, during sunny and cloudy conditions (sample 5, 6, 8, 9 and 11), where they achieved values under

40% after 5 hours of solar drying. Open-air drying in sunny and cloudy conditions, using a sample of 10 mm thickness and heating the air at 60°C (sample 2, 3, 7 and 10) led to a moisture contents comprised in the range of 40 to 60%. The moisture content of the sample dried at open-air during overcast conditions had a similar moisture content than the initial sludge (sample 4), meaning that drying did not occur in a significant way in this case.

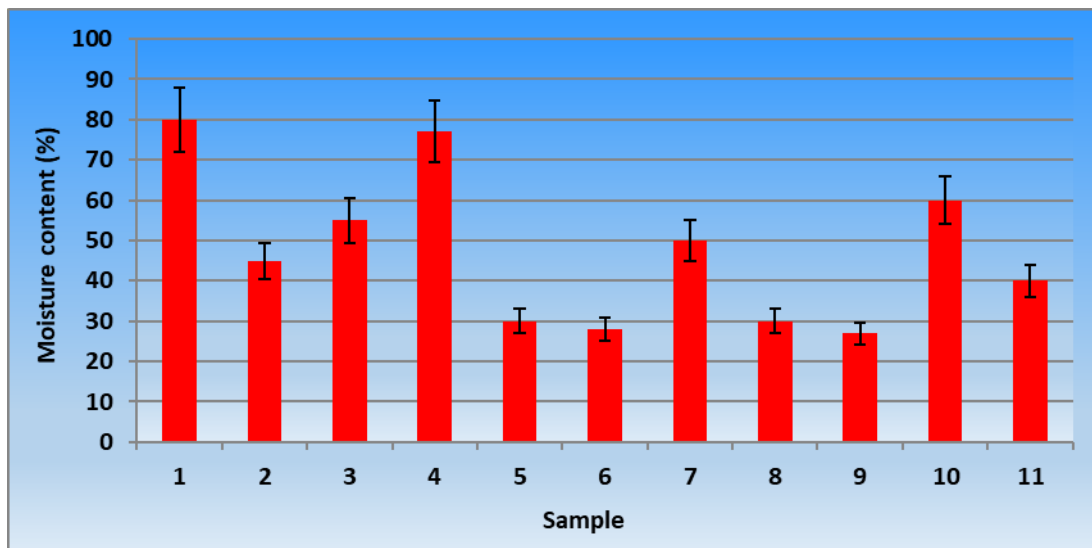


Figure 44. Moisture content of the sludge samples

The measurement of moisture content confirms the results from the drying curves in the previous sections. The better drying performances were obtained in a sunny or cloudy weather, with the lower thickness of sample. The results highlighted the benefits of drying in an enclosed volume (drying chamber) in comparison to open-air drying, particularly in the case of overcast conditions. Heating the air at 60°C led to a poor drying performance, with a relatively high moisture content of the sample (60%), which could be originated from the crust formation, as discussed in section 4.2.5.3.

No difference of ash content was observed between the different samples (Figure 45), which implies that the dry bone of the sludge was not degraded during solar drying. The ash content of the samples was approximately 0.5 g/g dry biomass, which is a relative high value indicating that half of the dry bone was constituted of inorganic material.

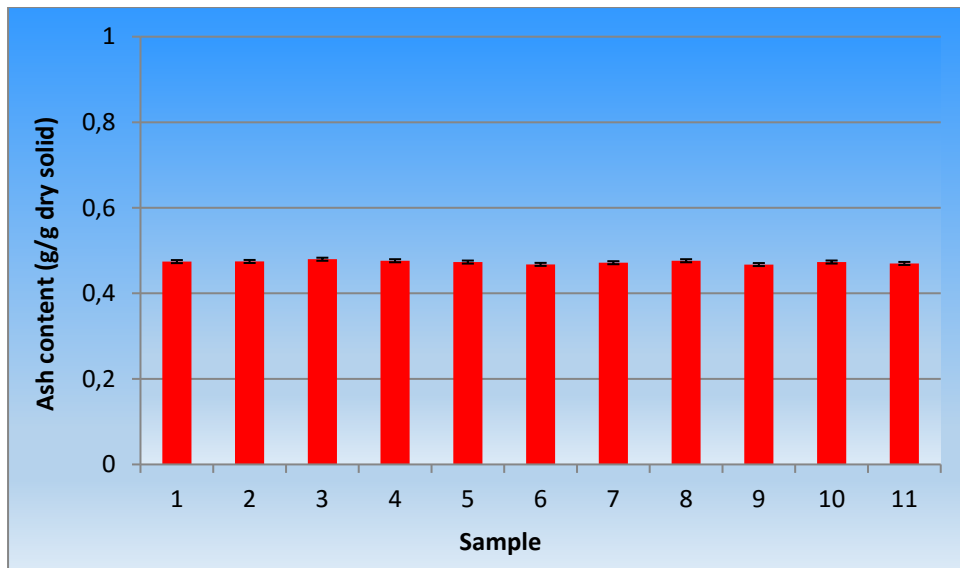


Figure 45. Ash content of the sludge samples

#### 4.2.2 Nutrient analysis

The results from the nutrient analysis can be found in Appendix M. No conclusions could be got due to the high scattering of the results and the inconsistency with respect to the previous investigations (Makununika, 2016; Mirara, 2017). This was presumed to be arisen from the lack of accuracy of the analyses or the too high heterogeneity of the sludge. These analyses should be repeated in the future.

Note that the results from the P, K, Mg and Ca content analysis are pending due to technical problems with the MP-AES analyser.

#### 4.2.3 Calorific value

Figure 46 shows the calorific value of the different samples. The calorific value of most of the samples was comprised between 10 to 15 MJ/kg, which is a range that could be expected for faecal sludge (Makununika, 2016; Muspratt et al., 2014; Zuma et al., 2015). Sample 1, 4 and 10 were the outliers from this range, which was probably originated from an experimental inaccuracy.

In previous studies (Makununika, 2016; Mirara, 2017), it was seen that the calorific value was not modified during drying, which seems to be also the case for solar drying in this study. Moreover, according to the ash analysis (section 4.2.1), no degradation

of the dry-bone of the sludge was observed during the experiments, which supports the assumption that the calorific value was remained the same along the process.

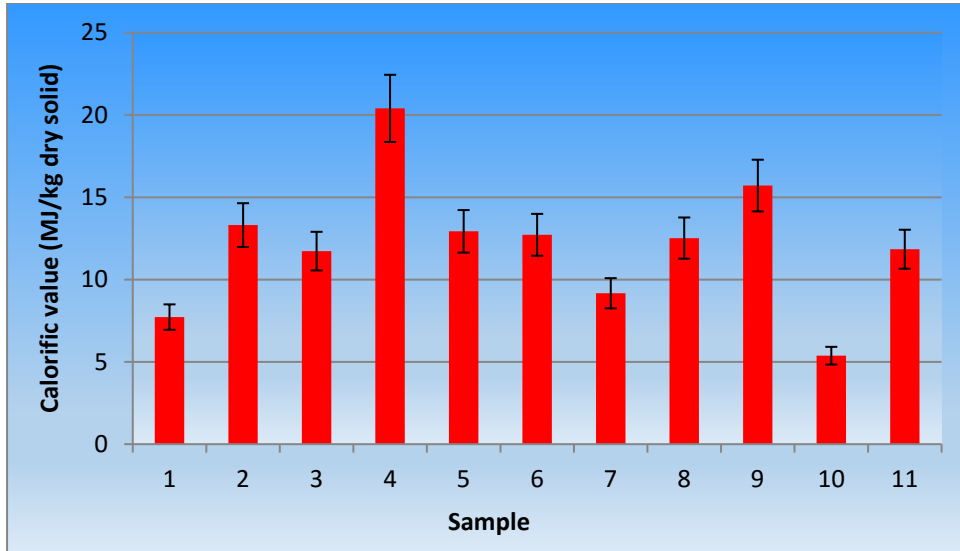


Figure 46. Calorific value of the sludge samples

## 4.2.4 Thermal properties

### 4.2.4.1 Thermal conductivity

The thermal conductivity measured for the different samples are displayed in Figure 47. The thermal conductivity of the initial faecal sludge (sample 1) was about 0.6 W/m/K. The thermal conductivity of the samples after solar drying exhibited lower values, except for sample 3 where an abnormal high value was measured, which was probably related to an experimental error.

The value of thermal conductivity depended on the experimental conditions and was mainly related to the moisture content of the sludge. Indeed, previous investigations (Makununika, 2016; Mirara, 2017) demonstrated that the thermal conductivity of the wet sludge is controlled by its moisture content but this influence is reduced as the solid is dried, which is reflected by a decrease of the thermal conductivity until arriving to a stable value. In our case, the thermal conductivity of the initial faecal sludge, with a value close to that from pure water, suggested that it was highly controlled by the moisture in it. The samples with the lowest moisture content (< 30%) were those with

the lowest thermal conductivity ( $< 0.1$  W/m/K), namely sample 5, 6, 8 and 9. The samples with intermediary moisture content (40 to 60%) shown intermediary thermal conductivity values (0.1 to 0.4 W/m/K), namely sample 7, 10 and 11. These results demonstrated that the corroboration between thermal conductivity and moisture content, found in previous studies, is valid in this investigation.

Note that a couple of inconsistencies were identified in the aforementioned trend: sample 2 and 4 exhibited a lower thermal conductivity than expected with respect of their moisture content. This inconsistency may be attributed to an experimental inaccuracy.

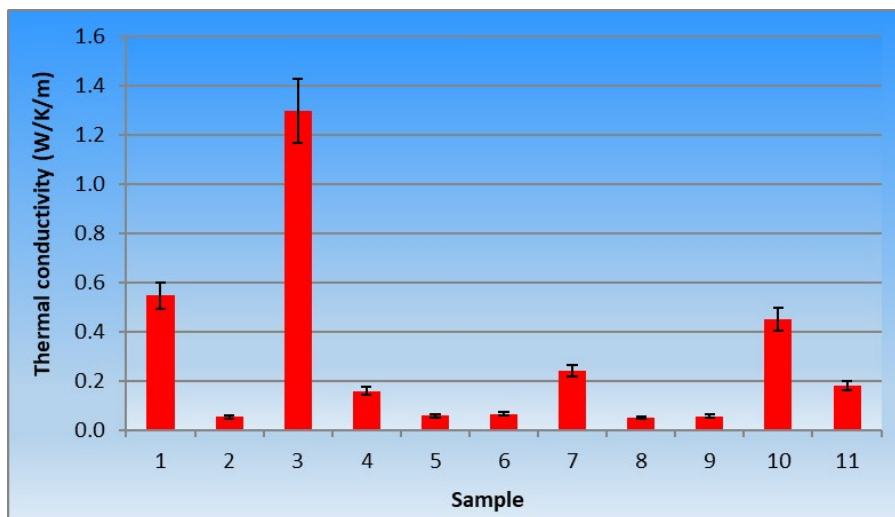


Figure 47. Thermal conductivity of the sludge samples

#### 4.2.4.2 Heat capacity

Figure 48 shows the heat capacity measured for the different samples from the solar drying experiments. In the same way than thermal conductivity, the heat capacity depends on the moisture content of the sludge and decreases as drying progresses (Makununika, 2016; Mirara, 2017). The heat capacity of the faecal sludge (sample 1) initially had a value near to that from water ( $\sim 4200$  J/kg/K) and decreased after solar drying up to values comprised between 300 to 1500 J/kg/K for samples with moisture content around 30% (sample 5, 6, 8 and 9). The heat capacity of the samples with a

moisture between 40 and 60% ranged between 1500 to 3500 J/kg/K (sample 4, 7, 10, 11).

Note that the results from sample 2, 3 and 4 are inconsistent with respect to the trend described in the previous paragraph. This same inconsistency was observed for the thermal conductivity and could be attributed to an experimental error. In fact, both heat capacity and thermal conductivity were measured simultaneously with the same instrument, so if one of the properties is wrong, the second property should also be like this.

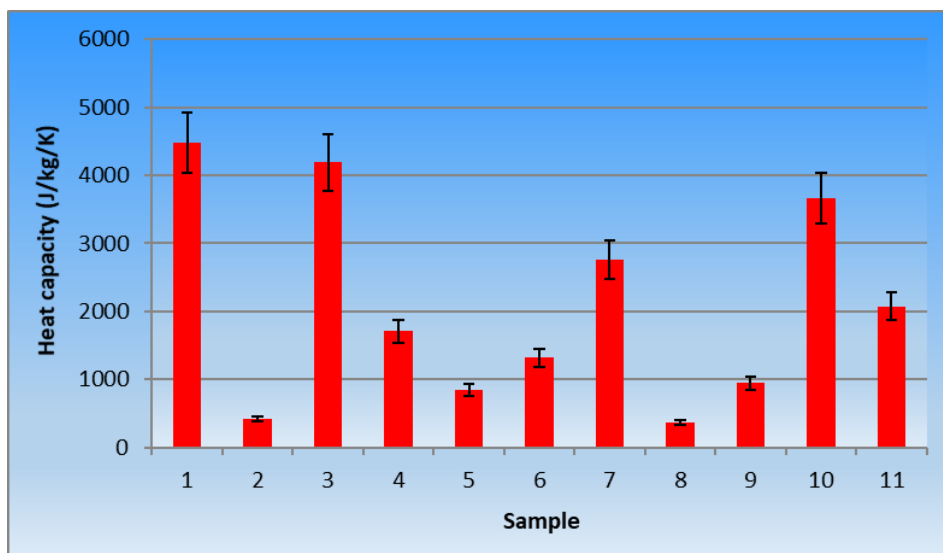


Figure 48. Heat capacity of the sludge samples

## 4.2.5 Morphological characteristics

### 4.2.5.1 Density

The results from the density measurement of the samples are presented in Figure 49. The sludge density varied from 800 to 1100 kg/m<sup>3</sup>. The highest values (1000-1100 kg/m<sup>3</sup>) corresponded to the initial faecal sludge or to the samples with a moisture content higher than 50% (sample 2, 3, 4, 7 and 10). Lower densities (800-900 kg/m<sup>3</sup>) were found for the samples with lower moisture content (< 40%), namely sample 5, 6, 8, 9 and 11. It can then be seen that the density of the sludge decreased as moisture was removed during drying, similarly to the thermal conductivity and heat capacity.

Drying is known to reduce the mass and volume of the material to dry. In our case, the mass reduction seemed more important than the volume reduction, since drying led to a product with lower density.

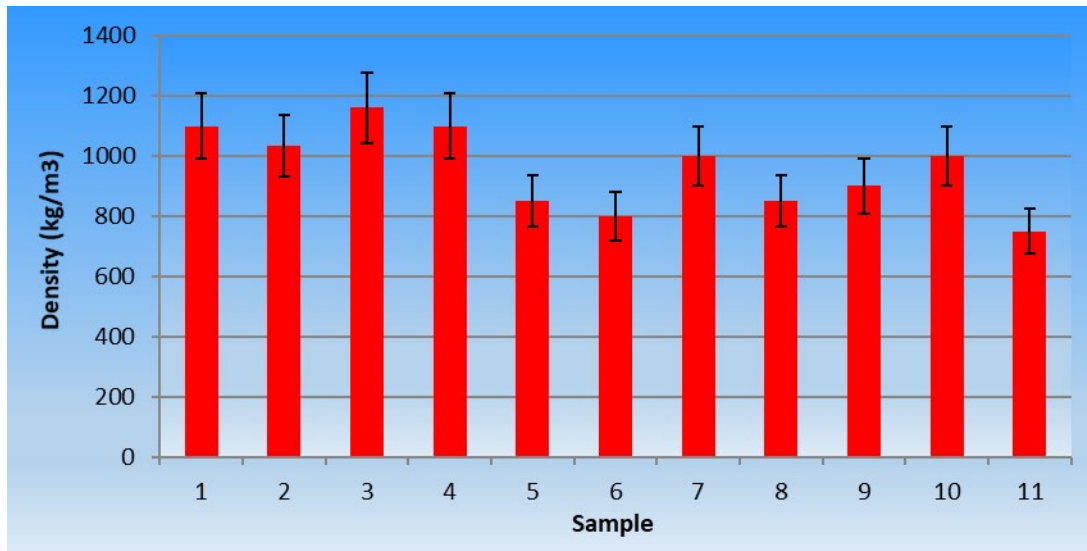


Figure 49. Density of the sludge samples

#### 4.2.5.2 Shrinkage

Figure 50 presents the samples shrinkage results after solar drying. For obvious reasons, sample 1 (the initial faecal sludge) exhibited a null value. No shrinkage was observed for sample 4 as almost no drying occurred in this case. For the other samples, the shrinkage was comprised between 30 and 70%. As it could be expected, the shrinkage was corroborated to the progress of drying, thus to the moisture content of the sample. The samples with a moisture content between 30 to 40% (sample 5, 6, 8, 9 and 11) shrunk about 60 to 70%, whereas the samples with a moisture content between 40 to 60% (sample 2, 3, 7 and 10) experienced a shrinkage between 30 to 50%.

As an explanation of this phenomenon, the loss of moisture in the solid during drying leads to the creation of void spaces that can be eventually occupied by the remaining material, leading to the contraction of the structure and the subsequent shrinkage of the solid. As drying progresses, further void spaces in the material are created, increasing the chances of a more important shrinkage.

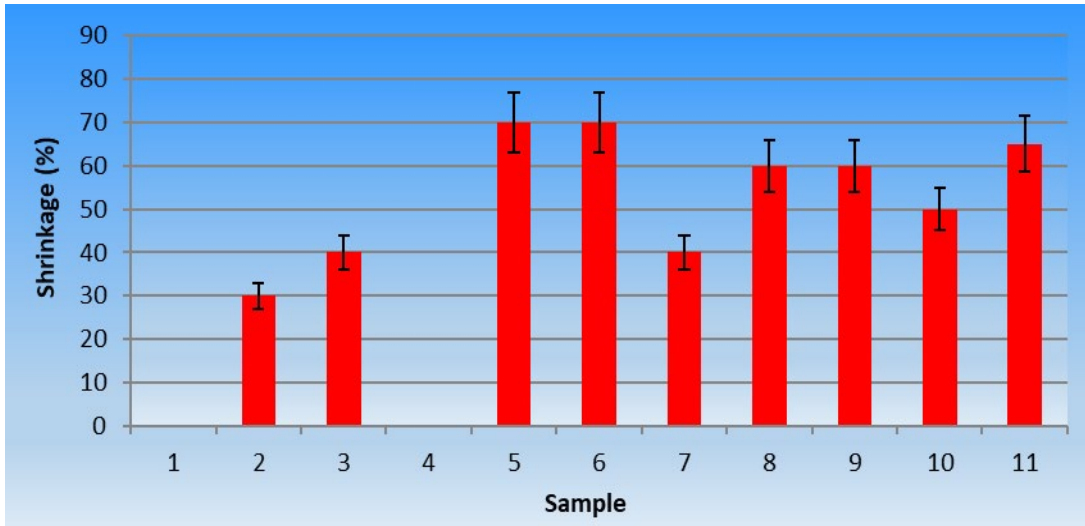


Figure 50. Shrinkage of the sludge sample after solar drying

#### 4.2.5.3 Qualitative observations

Figure 51 compares the aspect of the sludge before and after solar drying in sunny conditions, for the sample of 5 mm thickness and 120 mm diameter. The initial sample presented a shining dark aspect, while the dried sample had the same dark colour but without any brightness. The shining aspect of the untreated faecal sludge could be due to its high water content and may reflect a certain degree of reflectance of solar radiation. After drying, the shining aspect of the sludge disappeared, suggesting that the dried sludge should absorb better the solar thermal energy due to a lower reflectance. Furthermore, the shrinkage of the sludge and the apparition of cracks were perceivable in the dried sample.



Figure 51. Sludge sample before and after solar drying in sunny conditions (left and right photograph, respectively)

Table 4 summarizes the qualitative observations in regards to the modifications of the sludge characteristics after solar drying. These include the colour, the formation of a crust at the top surface, the apparition of cracks and the release of odours. These observations were based on the perceptions of the experimenter, so they only can be considered as indicative.

*Table 4. Qualitative observations*

<b><u>Sample</u></b>	<b><u>Colour variation</u></b>	<b><u>Crust formation</u></b>	<b><u>Crack formation</u></b>	<b><u>Odour</u></b>
<b>2</b>	o	+	o	+
<b>3</b>	o	+	o	o
<b>4</b>	o	o	o	o
<b>5</b>	+	++	+	+
<b>6</b>	o	+	+	o
<b>7</b>	o	o	o	o
<b>8</b>	o	+	o	+
<b>9</b>	+	++	++	+
<b>10</b>	++	+++	+	++
<b>11</b>	o	++	+	+

“o”: no change; “+”: slightly; “++”: important; “+++”: very important

No or a slight change of colour and odour with respect to the initial sample was observed for most of the samples, except when the airflow in the drying chamber was heated to 60°C (sample 10) where the colour of this sample was considerably darker and the odour was stronger. This sample also shown the formation of the hardest crust, and a slight cracking. Solar drying in sunny conditions and with airflow introduction in the drying chamber (samples 5, 9, 11) led to an important crust

formation and some cracking. A thin crust formation and almost no cracking were observed to occur after open-air drying in sunny and cloudy conditions (sample 2 and 3), as well as after drying in the experimental rig during cloudy conditions (sample 5) and without airflow introduction (sample 8). No crust and cracking were detected in overcast conditions.

It can be seen that the formation of crust and cracking were more likely to appear in sunny conditions. According to the observations above, drying at high air temperatures and with an airflow introduction could intensify the phenomenon of crust formation, provoking a negative effect on drying by limiting the mass transfer of the moisture from the core of the sludge to the environment. Indeed, drying under these conditions was assumed to enhance the fast depletion of moisture at the surface of the sludge, which, combined with effect of solar radiation, could have led to favourable conditions for crust formation. The intensity of crust formation should then determine the level of mass transfer limitation. This hypothesis may explain the lower moisture removal observed when the air was not heated or when no airflow was introduced in the drying chamber, as discussed with more detail in section 4.1.3, whereas the opposite trend was expected. No crust was formed in overcast conditions, which reinforces the hypothesis that solar radiation plays a key role in the formation of the crust.

Otherwise, the strong change of colour and odour for sample 10 could be related to the possible structural changes during the formation of its crust, which was the hardest among all the samples. It is also interesting to remark that, according to the experimenter, the levels of odour was the same or higher than the initial faecal sludge. This observation implies that solar drying could not remove the odours from sludge and even intensified them. Probably higher temperature would be required for this.

### **4.3 SUMMARY**

After 5 hours of solar drying, the moisture content was reduced from 77% (3.3 g/g dry solid) up to 20 to 60% (0.3 to 1.5 g/g dry solid), representing a moisture reduction varying between 60 to 95% as a function of the operating conditions. The average rate of moisture removal varied subsequently between 0.5 to 1.0 kg/h/m<sup>2</sup>. The sludge attained temperatures around 35 to 50°C, which was higher than the ambient

temperature. The sludge was isothermal during drying, which implies that no heat transfer limitations were observed under the explored conditions.

The most favourable conditions for solar drying occurred during sunny conditions. Considering the average solar irradiance measured from Figure 32 ( $\sim 1000 \text{ W/m}^2$ ), the maximum moisture removal rate was  $1.6 \text{ kg/h/m}^2$  if all the solar thermal energy was used for drying. As the observed rate was around  $1.0 \text{ kg/h/m}^2$ , the efficiency of the solar drying system could be estimated to 60%. This value was close to the maximum theoretical efficiency considering the unavoidable irradiance losses by reflectance and absorbance from the drying chamber walls ( $\sim 20\%$ ), and reflectance from the sample ( $\sim 10\%$ ). Obviously, the drying time was reduced after increasing the thickness for the sample from 5 to 10 mm, as the double amount of sludge needed to be dried using the same surface area. Nevertheless, the calculated average drying rate was similar for both thicknesses ( $\sim 1 \text{ kg/h/m}^2$ ), suggesting that mass transfer was not rate limiting (as neither the heat transfer). As expected, increasing the surface area of the sample did not affect the drying performance.

The least favourable conditions for drying corresponded to an overcast weather where the moisture removal rate was the lowest ( $0.5 \text{ kg/h/m}^2$ ). Considering an average irradiance at around  $350 \text{ W/m}^2$  calculated from Figure 32, the maximum achievable moisture removal rate would be approximately  $0.60 \text{ kg/h/m}^2$ , leading to an efficiency around 80-90%. This value is higher than the one obtained in sunny conditions, probably because the diffusive radiation during overcast conditions led to a lower reflectance than direct radiation during sunny conditions.

Solar drying in transparent enclosed volume shown a better performance than open-air drying. This difference was particularly appreciable in overcast conditions where almost no drying occurred for the open-air sample. These results highlighted the benefits of solar drying in a transparent enclosed volume compared to open-air practices such as conventional drying beds.

Crust formation, occurring mostly during sunny conditions, was problematic at higher air temperature and velocities, conditions on which it is suspected to cause lower drying than expected. As plausible explanation, the combination of solar radiation with the fast depletion of moisture at the surface at high air temperature or velocity, leads

to the formation of a hard crust that creates a resistance to the transfer of moisture from the sludge to the environment.

As moisture was removed during solar drying, the volume of the sample shrunk, and the density and thermal properties (heat capacity and thermal conductivity) decreased. After the removal of 90% of moisture, the shrinkage factor was about 70%, the density was reduced by 30%, and the thermal properties dropped by approximately a factor of 10. No degradation of the dry-bone structure of the sludge was assumed to occur during solar drying, as the ash content and calorific value in dry basis remained unchanged after the transformation. Interestingly, solar drying did not lead to the removal of odours from the sludge as expected. In the opposite, the odours were stronger in some dried samples.

Considering a moisture content reduction from 80 to 20% at a rate of 0.5 kg/h/m<sup>2</sup>, the area required to treat 1 tonne of faecal sludge per hour (similar capacity to the LaDePa dryer in the eThekweni municipality) would be 1500 m<sup>2</sup>. This is an acceptable footprint since it represents only 1/5 of the area of an official soccer pitch. The area requirements could decrease to 900 m<sup>2</sup> in more optimal conditions with a moisture removal rate of 1 kg/h/m<sup>2</sup>. Assuming 5 to 8 hours of solar drying at rates comprised between 0.5 to 1.0 kg/h/m<sup>2</sup>, the average annual moisture removal rate would be 1 to 2.5 ton/year/m<sup>2</sup>, which is comprised in the range from the existing sewage sludge solar drying plants.

Solar drying has a great potential for its application in the faecal sludge field as a cost-effective option for sludge dehydration compared to conventional drying systems, as already proven for sewage sludge where successful cases of large-scale plants implementation can be found. The main challenges to overcome during solar drying of faecal sludge will be the formation of a crust and the variability of the environmental conditions. Continuous research to improve the process should be undertaken in order to increase the drying performance of the plant and decrease the land footprint at the minimum possible cost.

## 5 GENERAL CONCLUSION FROM THE PROJECT

---

This project, started from April 2016, aims at characterizing faecal sludge solar drying through a fundamental study. This investigation was undertaken with the intention to generate knowledge and data in this area where there is insufficient information in literature, as well as to demonstrate the great potential of faecal sludge solar drying and promote its implementation.

One of the outcomes of this project was the development of a readily functional experimental solar drying rig. The major part of this project was dedicated to the design, commissioning and testing the functionality of this apparatus. The development of the solar drying rig took a longer time than initially planned, due to delays from different sources (construction in the workshop, delivery of material, breakdown of instruments and human reasons). In October 2017, the solar drying rig was finally operational and an experimental campaign was conducted until the beginning of December, where successful results were obtained. The solar drying rig is readily available for future research projects and can be put in the service of sanitation practitioners for faecal sludge solar drying characterization. Some minor modifications will be undertaken for its improvement in a near future. It is important to mention the main challenges to face during solar drying trials, which consist in the heterogeneity of the sludge and the variability of the external conditions from one day to another (weather and sunshine conditions). In order to offset these limitations in the extent of the possible, appropriate sampling methods for heterogeneous material should be applied, which is already done with positive results, and the methods to measure temperature and irradiance employed in our context should be better understood.

The second outcome of the project was the generation of valuable data and knowledge, acquired during the design and construction of the solar drying rig, the literature review, and the experimentation and data analysis phases. Based on the learnt lessons and gained knowledge, section 6 presents initial guidelines for the implementation of solar drying technologies for faecal sludge treatment. This information should be completed and validated with the development of more detailed guidelines in the future.

## 6 GUIDELINES FOR THE DEVELOPMENT OF A SOLAR DRIER FOR FAECAL SLUDGE TREATMENT

---

This project enabled to identify the parameters to take into account during the development and operation of a solar drier for faecal sludge treatment, which are summarized in the below guidelines. This list should not be considered as exhaustive and must be continued to be further developed in the future.

- Potential of faecal sludge solar drying

This work confirmed the great potential of faecal sludge solar drying. Compared to conventional drying beds where the sludge is exposed at the open-air, solar drying has a greater performance. However, this gain in performance requires higher capital costs, so the implementation of a solar drying technology has to be planned with insight in order to make it worth the investment. The advantages that solar drying plant can bring are the drastic reduction of processing time, a better product quality, a better control of the drying conditions, the possibility to treat higher loads of sludge, among others.

- Applicability of faecal sludge solar drying

Moisture removal rate around 1-2 ton/m<sup>2</sup>/year could be expected in locations with similar irradiance than that of Durban in summer, for a solar drier operating in optimal conditions. Based on these figures, drying rates up to 3 ton/m<sup>2</sup>/year could be attained in locations with higher solar irradiance, such as Mumbai (India) and Dakar (Senegal).

Faecal sludge could be applied in different scales, from on-site sanitation facilities to faecal sludge treatment plants. Thereby, large-scale solar driers could be developed for faecal sludge treatment plants, and small and medium size solar driers could be incorporated in on-site sanitation technologies or transfer stations after pit emptying. Drying in a greenhouse could be an interesting possibility where an expertise from sewage sludge is readily available. Nonetheless, in the contrary of the sewage sludge field, solar drying of faecal sludge should not be limited to only greenhouse, and the

development of other type of solar driers is an alternative route that should have to be considered.

- Site selection

A solar assessment is a necessary step for the selection of the most appropriate site for the implementation of a solar drying technology, and provides data for the design, sizing and operation strategies of the process. For this, information should be obtained about the irradiance and meteorological conditions from the location where the solar drying technology could be installed. This information includes, but it is not limited to, the average year irradiance and air temperature, the variations along a year and their evolution through the last years. This data can be obtained from solar maps, local weather or radiometric stations, commercial software and consulting groups.

- Orientation

In order to maximize the solar energy received in average during a year, the solar drier should be aligned in the west-east axis and face the opposite direction of the hemisphere of the planet where it has been installed, i.e. south direction in the north hemisphere, and north direction in the south atmosphere.

At a given season, the solar drier could be tilted at the optimum angle to receive the maximum of solar irradiance, which will depend on the geographical location. An automatic system to track the sun motion in such a way as to receive the maximum solar radiation during the day could also be installed. These options look complicated or unfeasible for large size units. For small size solar driers, tilting seems a reasonable option, on the contrary of tracking that would require of a high investment, complex equipment and a skilled labour able to operate it.

- Enclosure

Solar drying in a transparent enclosure exhibits a better drying performance than open-air drying, such as drying beds. According to the experimental results from this

investigation, the benefits of an enclosure are the most noticeable in overcast conditions, where faecal sludge drying was possible unlike at the open-air. The temperatures inside the enclosure are higher compared to the ambient conditions, due to a greenhouse effect created by the transparent walls. Besides, the enclosure protects the sludge from the wind that can cool it. Higher temperatures are positive for the drying process performance, as they tend to increase the moisture removal rate. Moreover, the enclosure avoids the rehydration of sludge from wet air or rainfalls, enables to operate at controlled conditions, prevents the proliferation of pests developed from the sludge (pathogens microorganisms, insects, etc...), and limits the risks of contamination of the environment.

The enclosure should be in a transparent material in order to allow for the penetration of solar radiation. Different type of materials are possible, such as glass, acrylic, polycarbonate, among others. The transmittance of these materials lies mainly between 70 to 90%. The other factors to take into consideration for the selection of the enclosure material are mechanical strength to bear the environment conditions (rain, wind, hail) and constraints during its maintenance, chemical resistance to eventual compounds released from the sludge decomposition (methane, carbon dioxide, hydrogen sulphide) and resistance to the ultraviolet light. These factors influence the life span of the material. The selection of the most suitable transparent material for the enclosure must consider the applied technology, the environment conditions, the type of sludge and the cost of purchase of the material.

During the experiments in the solar drying rig, it was noted that the external surface of the drying chamber got often dirty, mainly due to the deposition of dust, which obliged the experimenter to clean it with regularity. In a large-scale application, this observation would be transposed into the need of regular cleaning schedules to maintain clear the enclosure walls and like this avoid a drop of its performance. In the case of using detergents for this operation, cleaning should be conducted thoroughly to avoid soap traces in the material that can reduce its transmittance.

- Efficiency of a solar drier

The efficiency to harness the solar thermal energy by a solar dryer could be expected to be comprised between 60 to 90%, for a system with good thermal insulation. Most of the losses would be due to the reflectance and absorbance of solar radiation by the transparent walls of the enclosure and reflectance by the sludge. These losses cannot be avoided, but can be limited by using transparent material with the highest transmittance possible and by adding to the sludge additives to increase its absorbance. Note that the efficiency may vary between a sunny and overcast conditions as the radiation between both cases have different optical properties, leading to a different behaviour of the material after being hit by the radiation.

- Disposition of the sludge

It is important to consider how the sludge will be arranged in the solar drier. In order to increase the performance of the process, the sludge layer thickness should be minimized and the surface area maximized in the extent of the possible. A thinner sludge layer with a higher surface area would decrease the drying time, lead to a more homogeneous drying in the sludge, and limit heat and mass transfer limitations. In contrast, more space would be required to treat the same amount of sludge at a lower thickness, but this can be compensated by the lower residence time required to achieve the moisture content target. Alternatively, stirring and mixing strategies mechanisms can be implemented in order to increase the surface area, enhance the heat and mass transfers and homogenize the sludge.

- Crust formation

A crust can be formed at the surface of the sludge during solar drying and cause the drop of moisture removal. In this study, crust formation was suspected to be induced by solar radiation and intensified under operating conditions leading to a fast depletion of moisture at the surface, such as high air temperatures or velocities. Therefore, the development of means to mitigate crust formation in a solar dryer is critical. Mechanical means, as stirring and mixing, could be employed for this, as well as

chemicals could be added to the sludge to avoid the structural changes provoking the crust formation. If solar radiation is proven as one of the precursors of crust formation, indirect solar drying, where only the air stream for drying will be heated by solar thermal energy, could be applied.

- Ventilation

Ventilation in the drying chamber is necessary in order to evacuate the evaporated moisture and avoid the accumulation of vapour in the air, which can rise its relative humidity and lead to a subsequent drying rate decrease. If the air gets saturated in vapour (relative humidity = 1), drying can stop to occur. Apart from this, the vapour from the air can condense on the walls of the drying chamber, causing the formation of droplets that can reduce the penetration of solar radiation and lead to the risk of rehydration of the sludge.

During the experiments, the increase of the ventilation rate was identified as a cause of crust formation. In addition to this, the introduction of large volumes of air can cool the surface of the temperature of the sludge. Both crust formation and cooling of the sludge have a negative effect on the drying performance, so they have to be avoided. This way, the optimal ventilation rate should be enough high to evacuate the moisture in the drying chamber and avoid a rise of air humidity, but without exceeding levels that can drop the drying performance due to the crust formation or cooling of the sludge.

Pre-heating the air before its introduction into the drying chamber is an option that can theoretically accelerate the drying process, by decreasing the air relative humidity and increasing the moisture evaporation rate. Nonetheless, hot air in the drying chamber can also enhance crust formation during solar drying, as noted during the experiments. Air pre-heating and high ventilation rates could improve significantly the drying performance if the methods to avoid crust formation are applied with success.

- Odour management

An odour management strategy has to be setup in the exhaust air stream from the ventilation system that can carry out olfactory compounds, and in the handling of the dried product where odours may remain after the treatment.

- Variability as function of the seasons and weather conditions

One of the major challenges of solar drying is the variability of solar irradiance, which can lead to an inconstant performance. The solar irradiance changes from one season to another during the year. It tends to increase from winter to summer, and decrease from winter to summer. Within a same season, the weather conditions influences the solar irradiance. As demonstrated in this work, a considerable better performance is obtained during sunny than overcast conditions. The same results could be expected by the comparison of the drying performance in summer with respect to winter.

In order to cope with this variability that can be more and less important according to the geographical location, different measures can be taken into place. For instance, auxiliary heating sources could be utilized as an energy backup, such as solar water heaters, fuel, electricity from the grid or from a renewable source, and heat pumps. Likewise, energy storage systems could be employed in order to store the solar thermal energy during irradiation peak hours and use it in moments with low or null irradiance.

## 7 PERSPECTIVES

---

Experiments in the solar drying rig are planned to be continued by an intern (probably an undergraduate student) and could be the subject of a new master project. Future possible experiments include:

- Experiments to confirm the results obtained in this work;
- Experiments in winter where the irradiance values are the lowest in the year;
- Experiments using thick beds during several days;
- Experiments to study the effect of solar drying in pathogen deactivation;
- Experiments to test the solar air heating chimney for faecal sludge drying, by connecting it to the solar drying rig;
- Experiments using different types of excreta (example: faeces from urine diversion dry toilets).

In addition, one of the possible areas to explore could be the use of solar concentration for faecal sludge drying, which has never been reported in literature. This option is promising as it could lead to fast drying rates if it is controlled adequately (otherwise it the sample could be burnt). This study could be performed in the experimental rig by using magnifying glasses to concentrate the solar thermal energy on the faecal sludge sample.

With this project as starting point, there is the intention to develop solar drying technologies. During 2018, mechanical engineering undergraduate students' final project, with the objective to develop a pilot-scale solar dryer for faecal sludge drying, will be supervised in collaboration with Freddie Inambao (who was also involved in this project as co-supervisor of the Master student).

The development of further solar drying technologies is envisaged for future projects. Here below there is a list with some initial thoughts about possible projects:

- Adaptation and optimization of existing solar drying technologies to the context of faecal sludge, particularly drying in greenhouse or tray cabinet;
- Development of a contact drying system where the walls of the dryer will be heated with solar energy;

- Development of a superheated steam convective drying system where the steam will be generated by solar energy concentration;
- Development of a hot air convective dryer where the air will be heated by a radiator using hot water from a solar thermal collector or molten salts from a solar concentration thermal energy system;
- Development of a transparent auger placed above a parabolic reflector where faecal sludge will be dried during its convey (the auger could be connected to the exit of a toilet);
- Development of a solar collector connected to a pit to provide heat for faecal sludge drying as the pit will be filled;
- Development of a high performance solar collector using perforated steel walls (technology developed by Swansea University), to heat air for faecal sludge drying;
- Development of a parabolic concentrator drier for drying faecal sludge in batch loads (similar principle than conventional solar cookers).

Potential partners have been identified to collaborate in the development of solar drying technologies, which include:

- University of Bath (United Kingdom), where investigations on drying beds are being carried on;
- University of Makerere (Uganda), where there is the great interest for the development of in-situ solar drying equipment;
- University of Cheikh Anta Diop and Polytechnic Institute of Dakar (Senegal), as important activities related to on-site sanitation are in course in Senegal, such as the implementation of the Omni-processor, offering a great opportunity for solar drying development (a collaboration with Senegalese institutions would also strength the connection with West Africa);
- Pan African University Institute of Water and Energy Sciences (Algeria), as faecal sludge solar drying has a great potential for its implementation in Algeria due to the high irradiances found in this country, especially in the Saharan area (a collaboration with this institution would also establish a connexion with North Africa);

- University of Swansea (United Kingdom), where there is the interest to apply their high efficient solar technologies in the sanitation field;
- Solar Thermal Energy Research Group at the University of Stellenbosch (South Africa), where experts in the field of solar thermal energy could give advice and guidance;
- eThekweni municipality, which could facilitate the tests of the developed technologies;
- Eric Noir from Africa Abundance, coordinator of project to develop an ecovillage near Durban, where the developed solar technologies could be potentially tested.

## 8 CAPACITY BUILDING

Table 5 presents the exhaustive list of students that have been involved in the project.

*Table 5. List of students involved in the project*

Name	Gender	Nationality	Race	Academic level	Mission	Duration
Tendayi Mugauri	Male	Zimbabwean	Black	Master in course	Solar drying rig	Since April 2016 up to now
Sumeshini Moodley	Female	South African	Indian	Undergraduate student	Solar drying rig	4 months
Tevin Richards	Male	South African	Indian	Undergraduate student	Solar drying rig	4 months
Thurman Ezikel	Male	South African	Indian	Undergraduate student	Solar air heating chimney	4 months
Malvin Naicker	Male	South African	Indian	Undergraduate student	Solar air heating chimney	4 months
Tureyan Cooppan	Male	South African	Indian	Undergraduate student	Solar air heating chimney	4 months
Ryan Maharaj	Male	South African	Indian	Undergraduate student	Solar air heating chimney	4 months
Ishaaq Lakhi	Male	South African	Indian	Undergraduate student	Solar air heating chimney	2 weeks
Siboniso Zikali	Male	South African	Black	Undergraduate student	Solar air heating chimney	4 weeks
Mthokozisi Zuma	Male	South African	Black	Undergraduate student	Solar air heating chimney	4 weeks
Azhar Ismail	Male	South African	Indian	Undergraduate student	Solar air heating chimney	4 months
Savanna Perumal	Female	South African	Indian	Undergraduate student	Solar air heating chimney	4 months

## 9 TRANSFER OF KNOWLEDGE

---

The data and knowledge generated by this project will be disseminated in the following conferences:

- Presentation of an oral presentation during the UKZN Postgraduate Day, held in Durban, South Africa, during the 26 October 2017;
- Presentation of an oral presentation during the YWP-IWA conference, held in Cape Town, South Africa, during the 10 to 13 December 2017;
- Oral presentation and redaction of a paper during WISA conference, to be held in Cape Town, South Africa, during the 24 to 27 June 2018;
- Oral presentation and redaction of a paper during the 5<sup>th</sup> Southern Africa Solar Energy conference, to be held in Durban, South Africa, during the 27 to 29 June 2018;
- Submission of a paper for the WEDEC international conference, to be held in Nakuru, Kenya, during the 9 to 13<sup>th</sup> July 2018 (waiting results of submission);
- Future submission of a paper for the FSM 5 conference in 2019 (waiting confirmation about details of the conference and call for abstract submission).

One or two papers with the outputs of this project are planned to be submitted in 2018 for publication in a peer-review journal.

The outputs from this project will be included in the project about faecal sludge drying characterization, led by the PRG and funded by the Bill & Melinda Gates through the grant OPP1164143 (to see more details, visit the following website: <http://www.susana.org/en/resources/projects/details/392>). One of the objectives of this project is to organize a webseminar and workshop for knowledge dissemination, which will include the findings from this project.

To finish, the outputs from this project could be part of the redaction of an engineering handbook for faecal sludge drying that is envisaged for the long term.

## 10 REFERENCES

---

- 3P-Technik-Sanitation, 2016. The product – SANI SOLAR [WWW Document]. URL <http://3psanitation.de/the-product-sani-solar/?lang=en> (accessed 3.1.18).
- Aitken, M.D., Sobsey, M.D., Blauth, K.E., Shehee, M., Crunk, P.L., Walters, G.W., 2005. Inactivation of *Ascaris suum* and poliovirus in biosolids under thermophilic anaerobic digestion conditions. *Environ. Sci. Technol.* 39, 5804-5809.
- Belessiotis, V., Delyannis, E., 2011. Solar drying. *Sol. Energy* 85, 1665-1691. doi:<http://dx.doi.org/10.1016/j.solener.2009.10.001>
- Bennamoun, L., Arlabosse, P., Léonard, A., 2013. Review on fundamental aspect of application of drying process to wastewater sludge. *Renew. Sustain. Energy Rev.* 28, 29-43.
- Bux, M., 2010. Solar Drying of Biosolids – Recent Experiences in Large Installations. *Proc. Water Environ. Fed.* 2010, 244-251.
- Bux, M., Baumann, R., Philipp, W., Conrad, T., Mühlbauer, W., 2001. Class-A by solar drying recent experiences in Europe. *Proc. Water Environ. Fed.* 2001, 309-317.
- Bux, M., Baumann, R., Quadt, S., Pinnekamp, J., Mühlbauer, W., 2002. Volume reduction and biological stabilization of sludge in small sewage plants by solar drying. *Dry. Technol.* 20, 829-837.
- Cairncross, S., Hunt, C., Boisson, S., Bostoen, K., Curtis, V., Fung, I.C.H., Schmidt, W.-P., 2010. Water, sanitation and hygiene for the prevention of diarrhoea. *Int. J. Epidemiol.* 39, i193-i205.
- Carrington, E.G., Pike, E.B., Auty, D., Morris, R., 1991. Destruction of faecal bacteria, enteroviruses and ova of parasites in wastewater sludge by aerobic thermophilic and anaerobic mesophilic digestion. *Water Sci. Technol.* 24, 377-380.
- Chen, G., Lock Yue, P., Mujumdar, A.S., 2002. Sludge dewatering and drying. *Dry. Technol.* 20, 883-916.

- Dellbrügge, R., Bauerfeld, K., Dichtl, N., Großer, A., Paris, S., 2015. "Technology transfer-oriented research and development in the wastewater sector – validation at industrial-scale plants"(EXPOVAL) – Subgroup 6: solar sewage sludge drying: first results from investigations with a pilot plant. *Water Pract. Technol.* 10, 371-380.
- Earth-Augur, n.d. Earth Auger [WWW Document]. URL <http://www.earthauger.org/> (accessed 3.1.18).
- Ekechukwu, O.V, 1999. Review of solar-energy drying systems I: an overview of drying principles and theory. *Energy Convers. Manag.* 40, 593-613.
- GCEP, 2006. *An Assessment of Solar Energy Conversion Technologies and Research Opportunities.*
- Goldstein, N., Yanko, W.A., Walker, J.M., Jakubowski, W., 1988. Determining pathogen levels in sludge products. *BioCycle (USA).*
- Habitat, U.N., 2008. *The state of African cities 2008.* United Nations Hum. Settlements Program. Nairobi, Kenya.
- Harrison, J., Wilson, D., 2012. Towards sustainable pit latrine management through LaDePa. *Sustain. Sanit. Pr.* 13, 25-32.
- Horn, S., Barr, K., McLellan, J., Bux, M., 2008. Accelerated air drying of sewage sludge using a climate controlled solar drying hall.
- Huber, 2007. Cold weather cannot stop the HUBER Solar Dryer SRT [WWW Document]. URL <http://www.huber.es/es/global/huber-report/ablage-berichte/newsletter-ext/cold-weather-cannot-stop-the-huber-solar-dryer-srt.html> (accessed 1.10.18).
- Jain, D., Tiwari, G.N., 2003. Thermal aspects of open sun drying of various crops. *Energy* 28, 37-54.
- Jain, N., 2011. *Getting Africa to meet the sanitation MDG: Lessons from Rwanda.*

- Krawczyk, P., Badyda, K., 2011. Modelling of thermal and flow processes in a solar waste-water sludge dryer with supplementary heat supply from external sources. *J. Power Technol.* 91, 37.
- Kudra, T., 2003. Sticky region in drying – Definition and identification. *Dry. Technol.* 21, 1457-1469.
- Kurt, M., 2014. Evaluation of solar sludge drying alternatives on costs and area requirements. Master thesis, Middle East Technical University (Turkey).
- Kurt, M., Aksoy, A., Sanin, F.D., 2015. Evaluation of solar sludge drying alternatives by costs and area requirements. *Water Res.* 82, 47-57.
- Léonard, A., Blacher, S., Marchot, P., Crine, M., 2002. Use of X-ray microtomography to follow the convective heat drying of wastewater sludges. *Dry. Technol.* 20, 1053-1069.
- Léonard, A., Blacher, S., Marchot, P., Pirard, J.-P., Crine, M., 2003a. Image analysis of X-ray microtomograms of soft materials during convective drying. *J. Microsc.* 212, 197-204.
- Léonard, A., Blacher, S., Pirard, R., Marchot, P., Pirard, J.-P., Crine, M., 2003b. Multiscale texture characterization of wastewater sludges dried in a convective rig. *Dry. Technol.* 21, 1507-1526.
- Léonard, A., Blacher, S., Marchot, P., Pirard, J.-P., Crine, M., 2004. Measurement of shrinkage and cracks associated to convective drying of soft materials by X-ray microtomography. *Dry. Technol.* 22, 1695-1708.
- Lewin, S., Norman, R., Nannan, N., Thomas, E., Bradshaw, D., Collaboration, S.A.C.R.A., 2007. Estimating the burden of disease attributable to unsafe water and lack of sanitation and hygiene in South Africa in 2000. *South African Med. J.* 97, 755-762.
- Lowe, P., 1995. Developments in the thermal drying of sewage sludge. *Water Environ. J.* 9, 306-316.

- Makununika, B., 2016. Thermal Drying of Faecal Sludge from VIP latrines and Charcaterisation of Dried Faecal Material. Msc thesis, University of KwaZulu-Natal (South Africa).
- Mathioudakis, V.L., Kapagiannidis, A.G., Athanasoulia, E., Paltzoglou, A.D., Melidis, P., Aivasidis, A., 2013. Sewage sludge solar drying: Experiences from the first pilot-scale application in Greece. *Dry. Technol.* 31, 519-526.
- Mawioo, P.M., Garcia, H.A., Hooijmans, C.M., Velkushanova, K., Simonič, M., Mijatović, I., Brdjanovic, D., 2017. A pilot-scale microwave technology for sludge sanitization and drying. *Sci. Total Environ.* 601, 1437-1448.
- Mekhilef, S., Saidur, R., Safari, A., 2011. A review on solar energy use in industries. *Renew. Sustain. Energy Rev.* 15, 1777-1790.
- Meyer-Scharenberg, U., Pöppke, M., 2010. Large-scale Solar Sludge Drying in Managua/Nicaragua. *Wasser und Abfall* 12, 26.
- Mirara, S., 2017. Drying and Pasteurisation of VIP Faecal Fludge using a bench scale Medium Infrared Machine. Master Thesis, University of KwaZulu-Natal, Durban (South Africa).
- Mowla, D., Tran, H.N., Allen, D.G., 2013. A review of the properties of biosludge and its relevance to enhanced dewatering processes. *Biomass and bioenergy* 58, 365-378.
- Moyers, C.G., Baldwin, G., 1997. Psychrometry, evaporative cooling, and solids drying, in: *Perry's Chemical Engineers' Handbook*.
- Mujumdar, A.S., 2000. Classification and selection of industrial dryers. *Mujumdar's Pract. Guid. to Ind. Dry. Princ. Equip. New Dev. Bross. Canada Exergex Corp.* 23-36.
- Mujumdar, A.S., 2006. *Handbook of industrial drying*. Marcel Dekker, New York, USA.
- Mujumdar, A.S., Devahastin, S., 2000. *Fundamental principles of drying*. Exergex, Bross. Canada.

- Muspratt, A.M., Nakato, T., Niwagaba, C., Dione, H., Kang, J., Stupin, L., Regulinski, J., Mbéguéré, M., Strande, L., 2014. Fuel potential of faecal sludge: calorific value results from Uganda, Ghana and Senegal. *J. Water Sanit. Hyg. Dev.* 4, 223-230.
- NREL, 2014. Concentrating Solar Power Projects [WWW Document]. URL [http://www.nrel.gov/csp/solarpaces/by\\_country\\_detail.cfm/country=ZA](http://www.nrel.gov/csp/solarpaces/by_country_detail.cfm/country=ZA)
- Pivot, 2016. Pivot Works Overview [WWW Document]. URL <http://thesff.com/system/wp-content/uploads/2016/11/2016-Pivot-Works-overview.pdf> (accessed 7.20.08).
- Popat, S.C., Yates, M.V, Deshusses, M.A., 2010. Kinetics of inactivation of indicator pathogens during thermophilic anaerobic digestion. *water Res.* 44, 5965-5972.
- PRG, 2014. Standard Operating Procedures [WWW Document]. URL <http://prg.ukzn.ac.za/laboratory-facilities/standard-operating-procedures> (accessed 1.9.17).
- RaVikas, 2016. RaVikas “MAITRI” Zero Odor / Zero Flush Composter [WWW Document]. URL <http://swachhsolartoilet.com/> (accessed 3.1.18).
- Roux, N., Jung, D., Pannejon, J., Lemoine, C., 2010. Modelling of the solar sludge drying process Solia™. *Comput. Aided Chem. Eng.* 28, 715-720.
- RTI, 2013. A Better Toilet For A Cleaner World [WWW Document]. URL <http://abettertoilet.org/> (accessed 8.1.17).
- Salihoglu, N.K., Pinarli, V., Salihoglu, G., 2007. Solar drying in sludge management in Turkey. *Renew. Energy* 32, 1661-1675.
- Seginer, I., Bux, M., 2006. Modeling solar drying rate of wastewater sludge. *Dry. Technol.* 24, 1353-1363.
- Seginer, I., Ioslovich, I., Bux, M., 2007. Optimal control of solar sludge dryers. *Dry. Technol.* 25, 401-415.
- Shanahan, E.F., Roiko, A., Tindale, N.W., Thomas, M.P., Walpole, R., Kurtböke, D.İ., 2010. Evaluation of pathogen removal in a solar sludge drying facility using microbial indicators. *Int. J. Environ. Res. Public Health* 7, 565-582.

- Slim, R., Zoughaib, A., Clodic, D., 2008. Modeling of a solar and heat pump sludge drying system. *Int. J. Refrig.* 31, 1156-1168.
- Socias, I., 2011. The solar drying plant in mallorca: the drying process in waste management, in: *European Drying Conference*. Palma de Mallorca, Spain.
- Strauch, D., 1991. Survival of pathogenic micro-organisms and parasites in excreta, manure and sewage sludge. *Rev. Sci. Tech.* 10, 813-846.
- SuSana, 2015. Janicki's reinvented Firelight Toilet [WWW Document]. URL <http://www.susana.org/en/resources/projects/details/298> (accessed 8.1.17).
- Sypuła, M., Paluszak, Z., Szala, B., 2013. Effect of Sewage Sludge Solar Drying Technology on Inactivation of Select Indicator Microorganisms. *Polish J. Environ. Stud.* 22.
- Tao, T., Peng, X.F., Lee, D.J., 2005. Thermal drying of wastewater sludge: Change in drying area owing to volume shrinkage and crack development. *Dry. Technol.* 23, 669-682.
- Tao, T., Peng, X.F., Lee, D.J., 2006. Skin layer on thermally dried sludge cake. *Dry. Technol.* 24, 1047-1052.
- Thermo-System, n.d. Case study Oldenburg [WWW Document]. URL <https://www.parkson.com/sites/default/files/documents/document-oldenburg-case-study-1073.pdf> (accessed 1.11.18).
- Thomas, J.E., Podichetty, J.T., Shi, Y., Belcher, D., Dunlap, R., McNamara, K., Reichard, M. V, Smay, J., Johannes, A.J., Foutch, G.L., 2015. Effect of temperature and shear stress on the viability of *Ascaris suum*. *J. Water Sanit. Hyg. Dev.* 5, 402-411.
- Tide-Technocrats, 2016. Community scale fecal sludge and septage processor in an Urban Indian Environment [WWW Document]. URL <http://www.pas.org.in/Portal/document/UrbanSanitation/uploads/Community fecal sludge&septage processor in Urban Indian Environment–Arun Kumar.pdf> (accessed 8.1.17).

- Villarreal, M., 2015. India: clean water and environmental sanitation for the rural population. *African J. Food, Agric. Nutr. Dev.* 15.
- Wagner, C.J., Coleman, R.L., Berry, R.E., 1979. A low cost small scale solar dryer for Florida fruits and vegetables, in: *Proc. Florida State Horticultural Society*. pp. 180-183.
- WHO, 2017. Progress on drinking water, sanitation and hygiene: 2017 update and Sustainable Development Goal baselines. Geneva, Switzerland.
- Yermán, L., 2016. Self-sustaining Smouldering Combustion as a Waste Treatment Process [WWW Document]. *Dev. Combust. Technol.* URL <http://abettertoilet.org/> (accessed 8.24.17).
- Zhang, X., Zhao, X., Smith, S., Xu, J., Yu, X., 2012. Review of R&D progress and practical application of the solar photovoltaic/thermal (PV/T) technologies. *Renew. Sustain. Energy Rev.* 16, 599-617.
- Zhao, L., Chen, D., Xie, J., 2009. Sewage sludge solar drying practise and characteristics study, in: *Power and Energy Engineering Conference, 2009. APPEEC 2009. Asia-Pacific. IEEE*, pp. 1-5.
- Zuma, L., Velkushanova, K., Buckley, C.A., 2015. Chemical and thermal properties of dry VIP latrine sludge. *Water S.A.* 41, 534-540.

# APPENDIX A: SOLAR DRYING TECHNOLOGIES

---

The figures above present a non-exhaustive list of solar drying technologies (Ekechukwu, 1999).

## Passive solar drying systems

- Indirect-type passive solar energy dryers

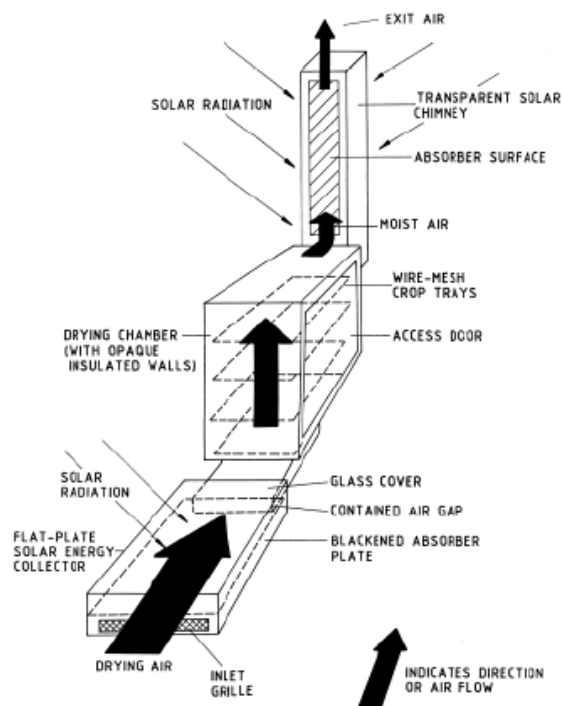


Figure 52. Typical distributed-type natural-circulation solar energy

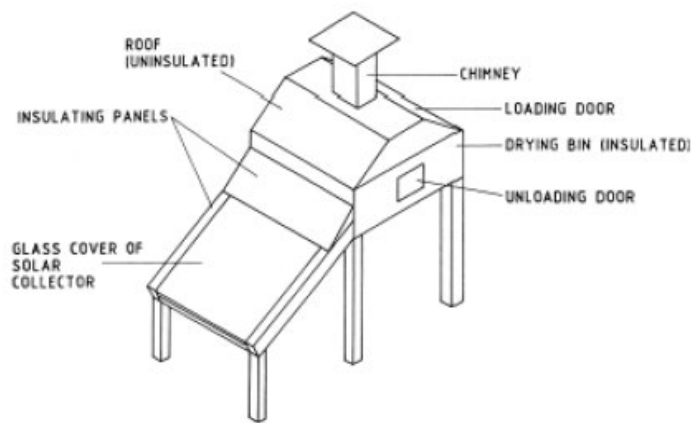


Figure 53. Distributed-type natural-circulation solar dryer

- Indirect-type passive solar energy dryer
  - Solar cabinet dryers

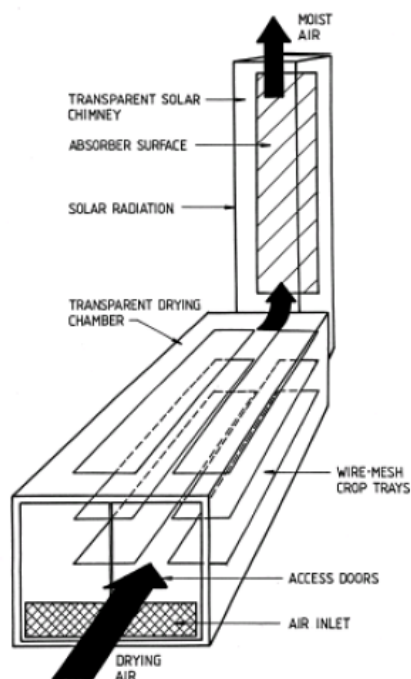


Figure 54. Integral-type (direct) natural-circulation solar energy dryer

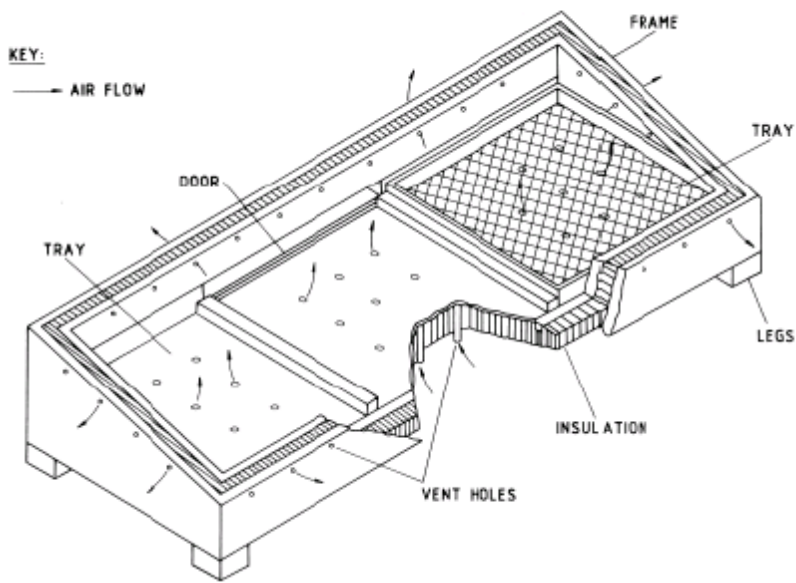


Figure 55. Typical natural circulation solar energy cabinet dryer

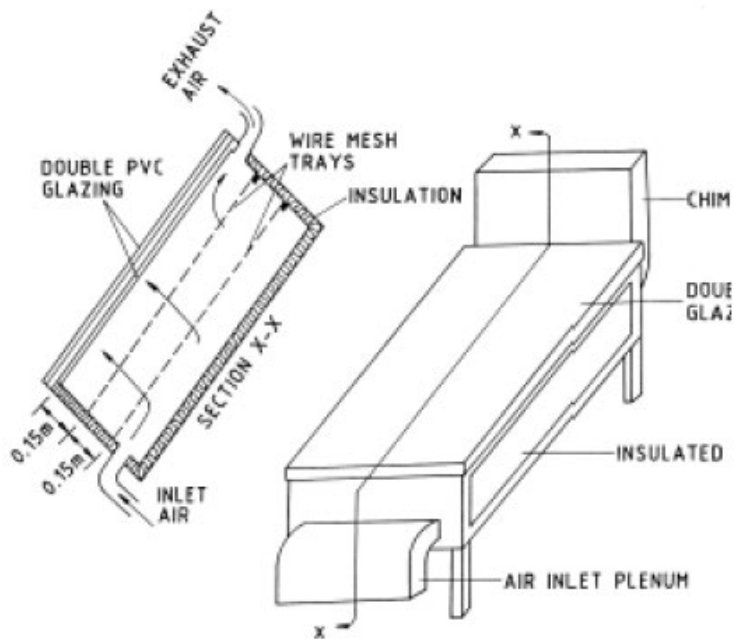


Figure 56. Modified natural circulation solar energy cabinet dryer

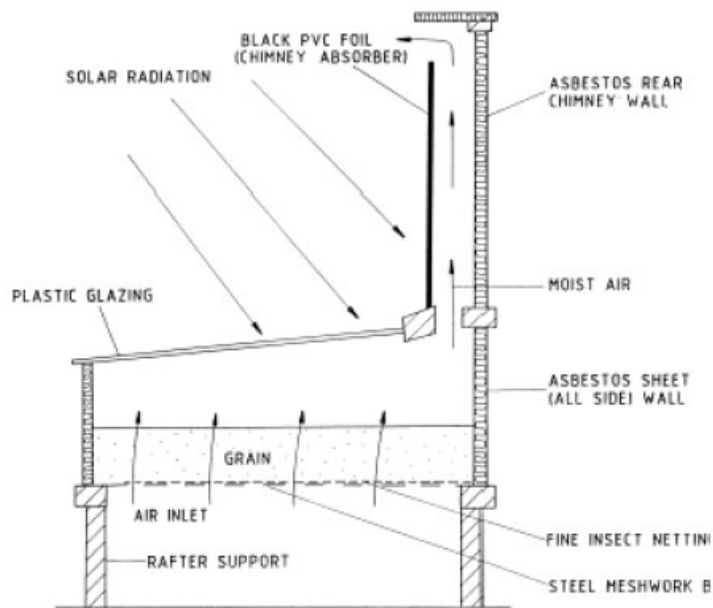


Figure 57. Natural circulation solar energy cabinet dryer with chimney

- Natural circulation greenhouse dryers

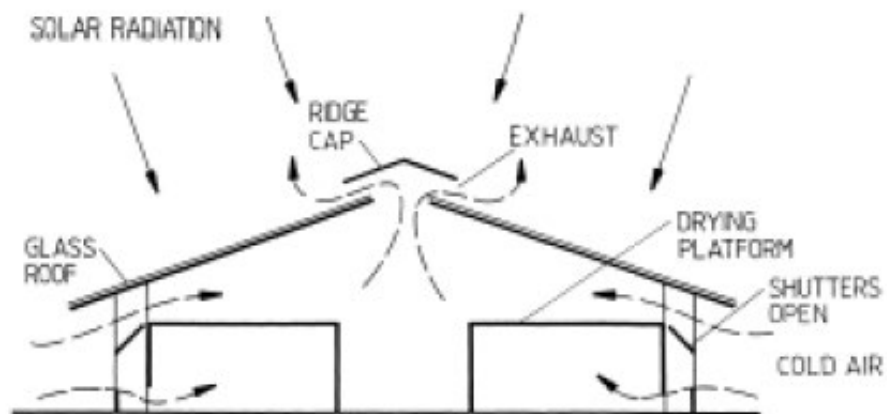


Figure 58. Natural circulation glass roof solar energy dryer

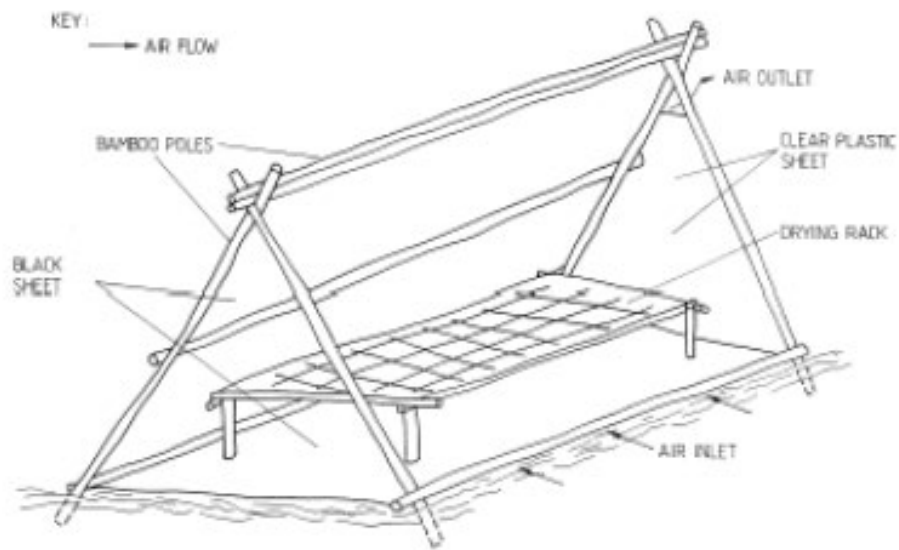


Figure 59. Natural circulation polythene tent dryer

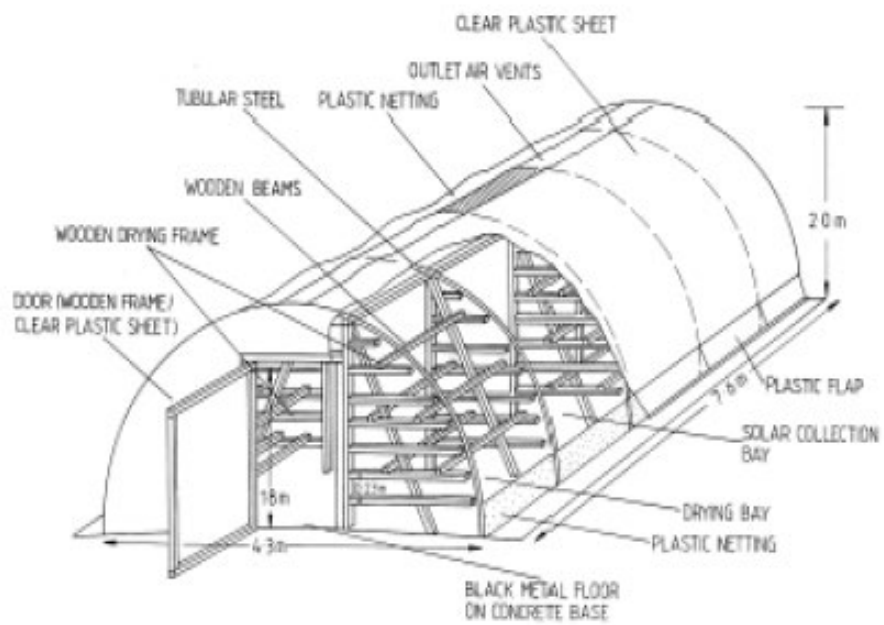


Figure 60. Natural circulation solar dome dryer

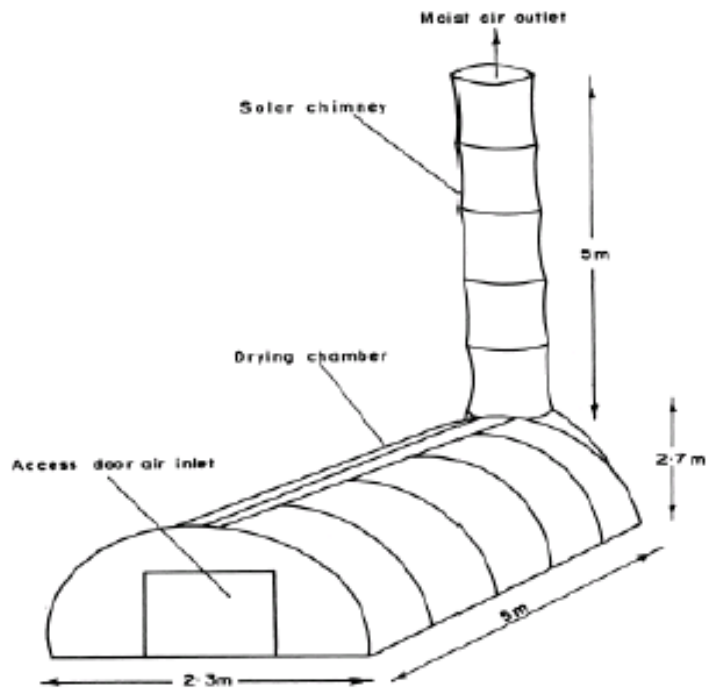


Figure 61. Greenhouse-type natural circulation solar dome dryer

- Mixed mode passive solar energy dryers

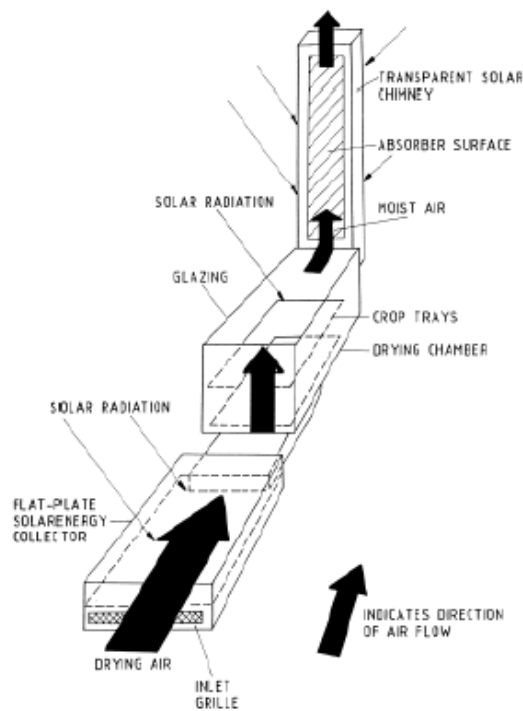


Figure 62. Mixed mode natural circulation solar energy dryer

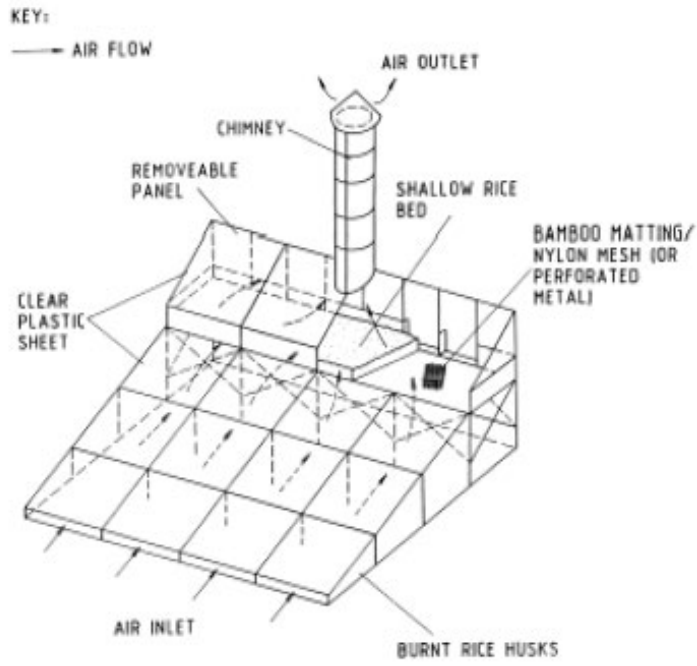


Figure 63. Mixed mode natural circulation solar dryer

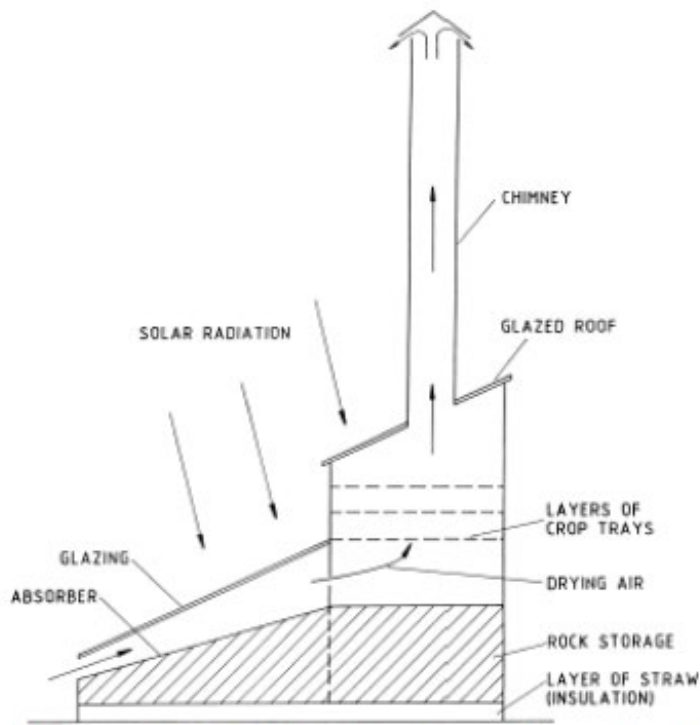


Figure 64. Mixed mode natural circulation solar dryer with thermal storage

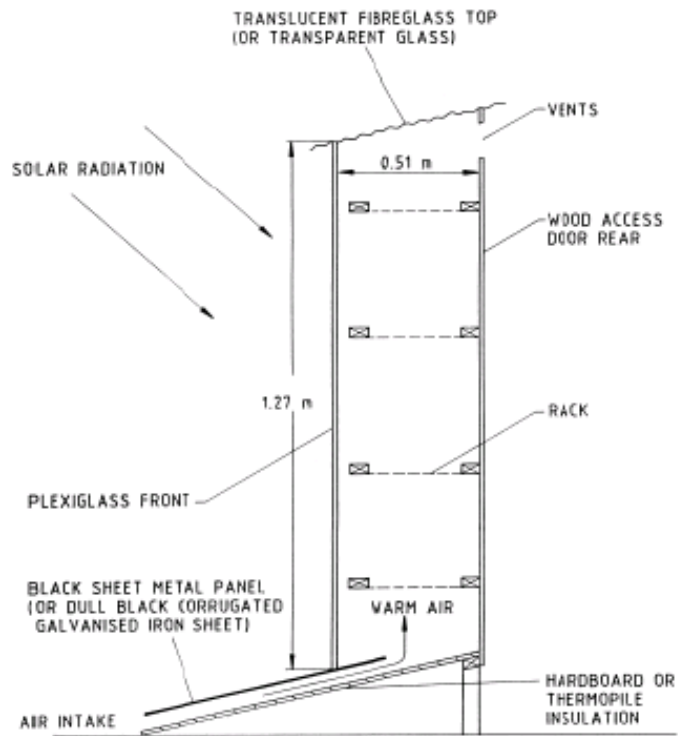


Figure 65. Multi-stacked mixed mode natural circulation solar energy dryer

### Active solar drying systems

- Indirect-type active solar energy dryers

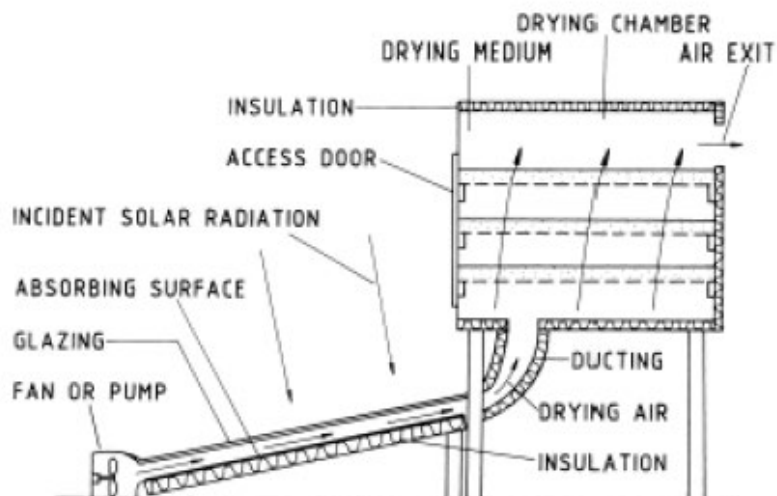


Figure 66. Distributed type active solar energy dryer

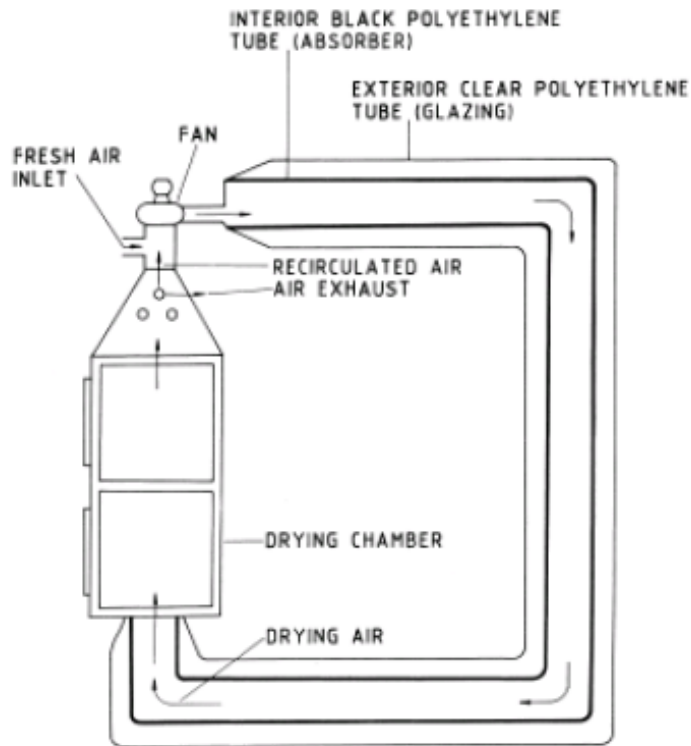


Figure 67. Distributed type active solar dryer with partial air re-circulation

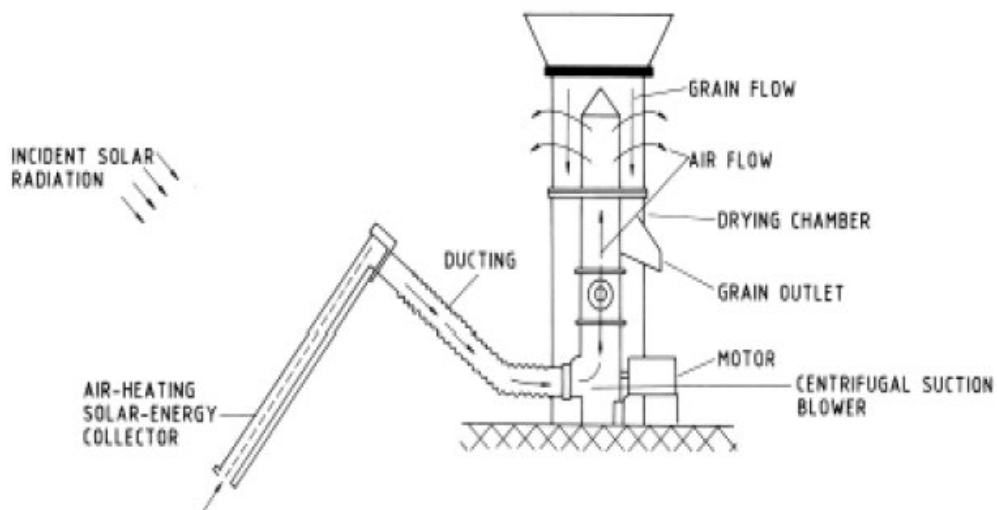


Figure 68. Continuous flow active grain dryer

- Direct-type active solar energy dryers

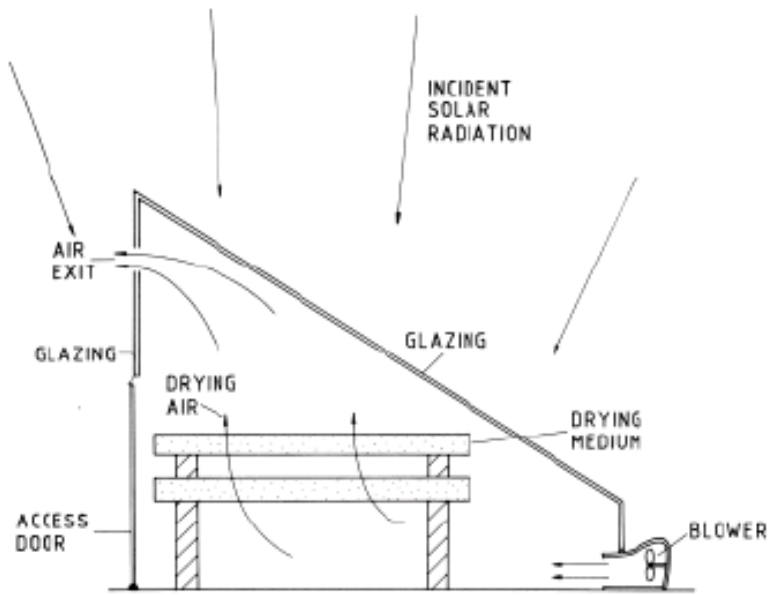


Figure 69. Forced convection greenhouse dryer

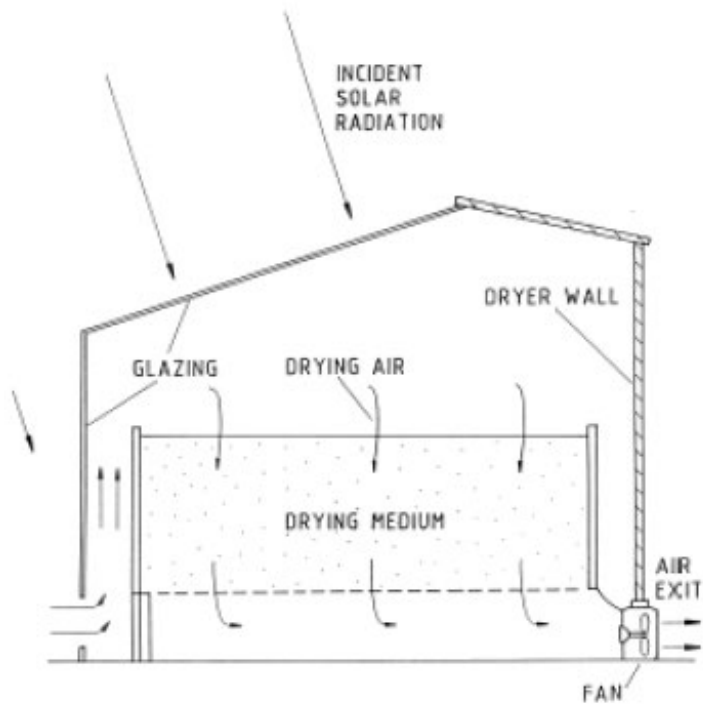


Figure 70. Forced convection transparent roof solar barn

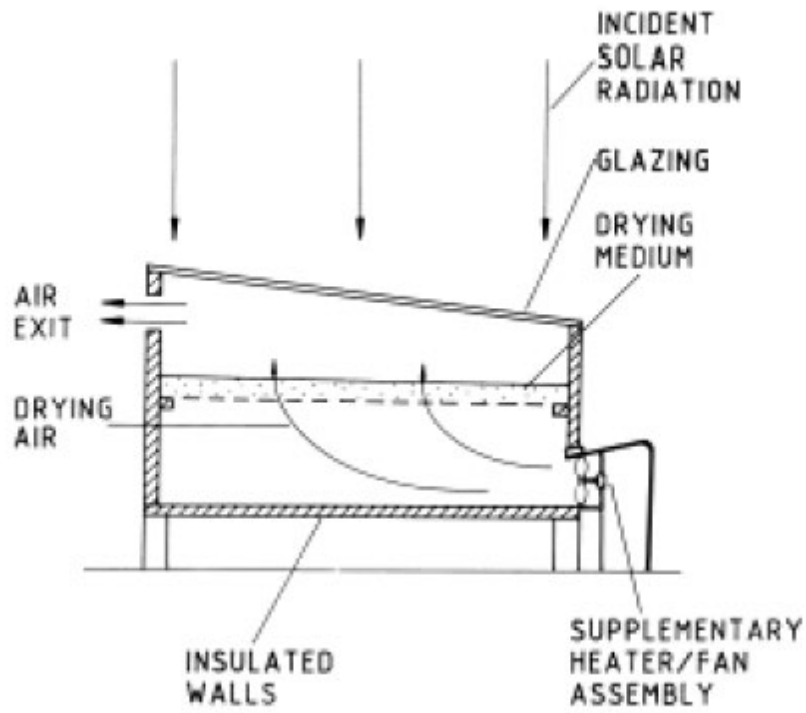


Figure 71. Active solar energy cabinet dryer

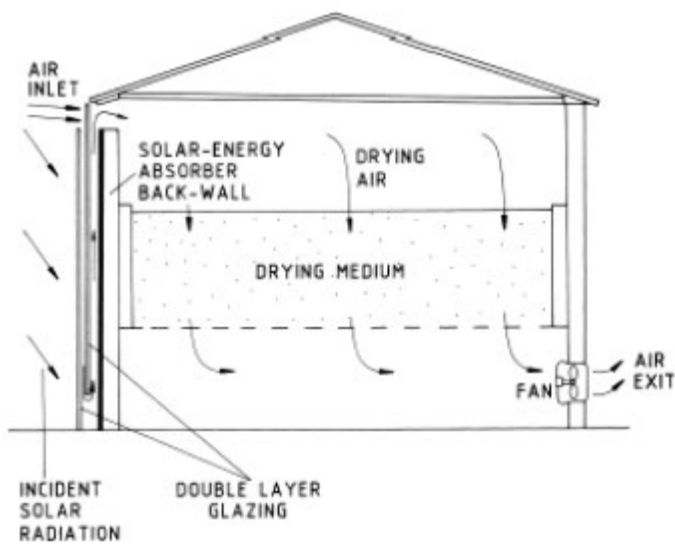


Figure 72. Interior drum absorber greenhouse active solar dryer

- Mixed mode active solar energy dryers

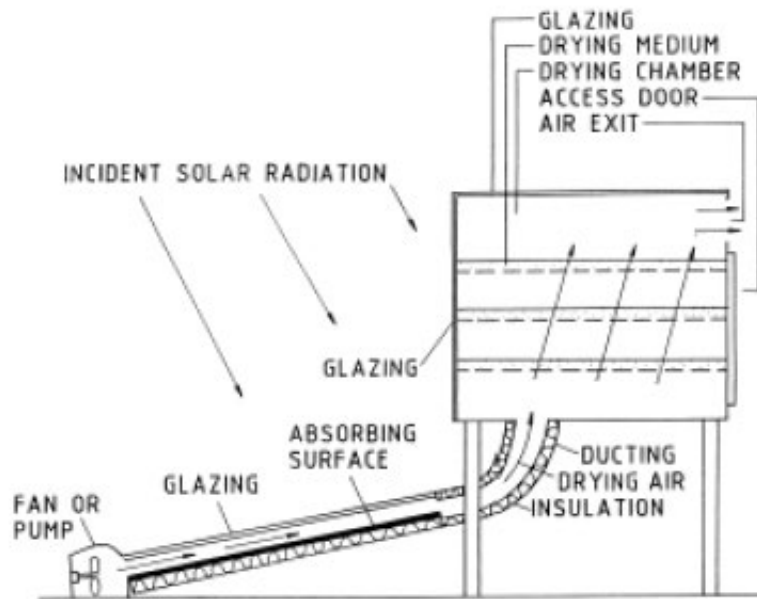


Figure 73. Typical mixed mode active solar energy dryer

- Hybrid-type active solar energy dryers

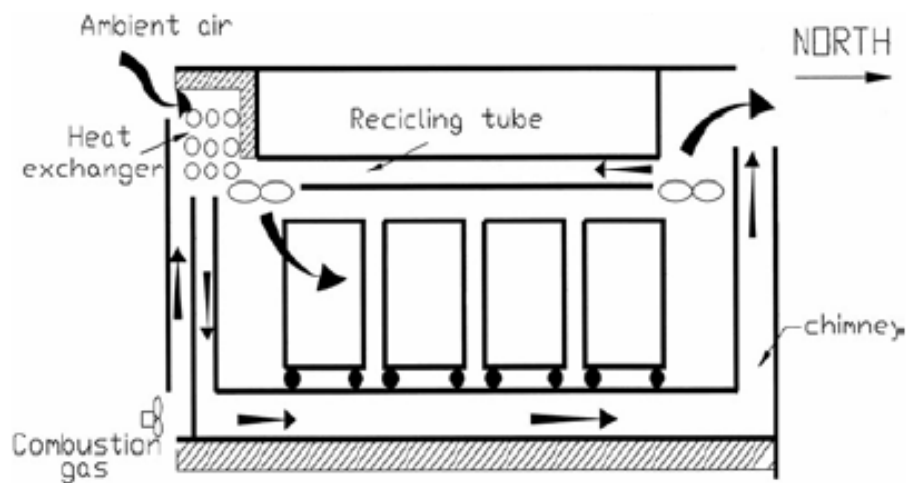


Figure 74. Solar tunnel dryer with an additional auxiliary heating source

## APPENDIX B: GREENHOUSES TO DRY SEWAGE SLUDGE

---

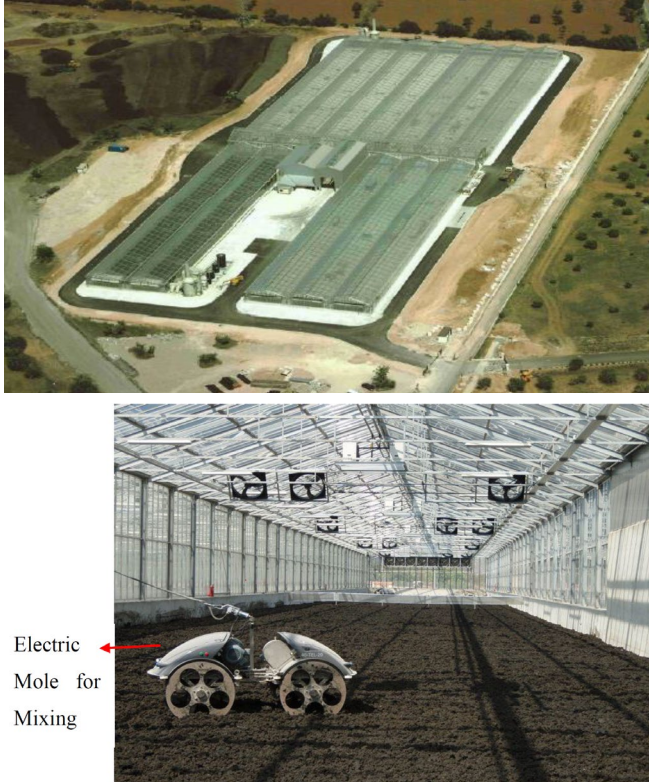


Figure 75. Solar drying plant in Palma de Mallorca, Spain (Bux, 2010)



Figure 76. Solar drying plant in Managua, Nicaragua (Meyer-Scharenberg and Pöppke, 2010)



Figure 77. Solar plant in Oldenburg, Germany (Thermo-System, n.d.)



Figure 78. Solar drying greenhouse in Fethiye wastewater treatment plant, Turkey (Kurt, 2014)

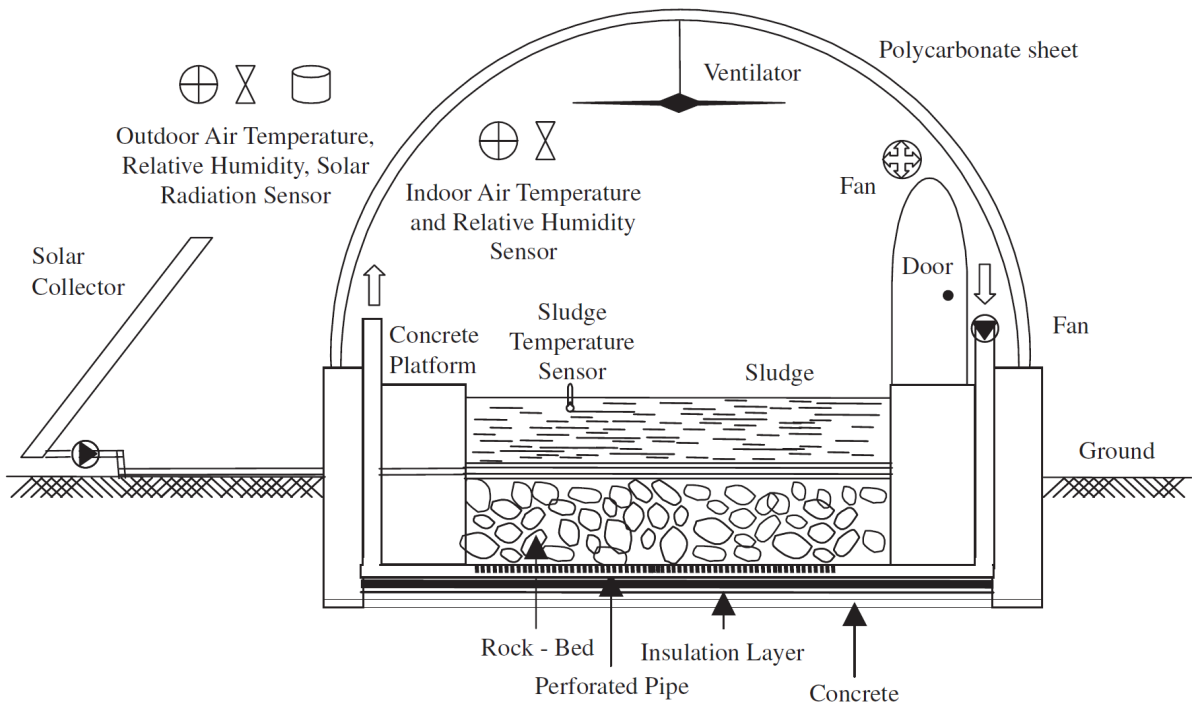


Figure 79. Pilot greenhouse in the East wastewater treatment plant, Turkey (Salihoglu et al., 2007)



Figure 80. Pilot greenhouse in the Kavala wastewater treatment plant, Greece (Mathioudakis et al., 2013)

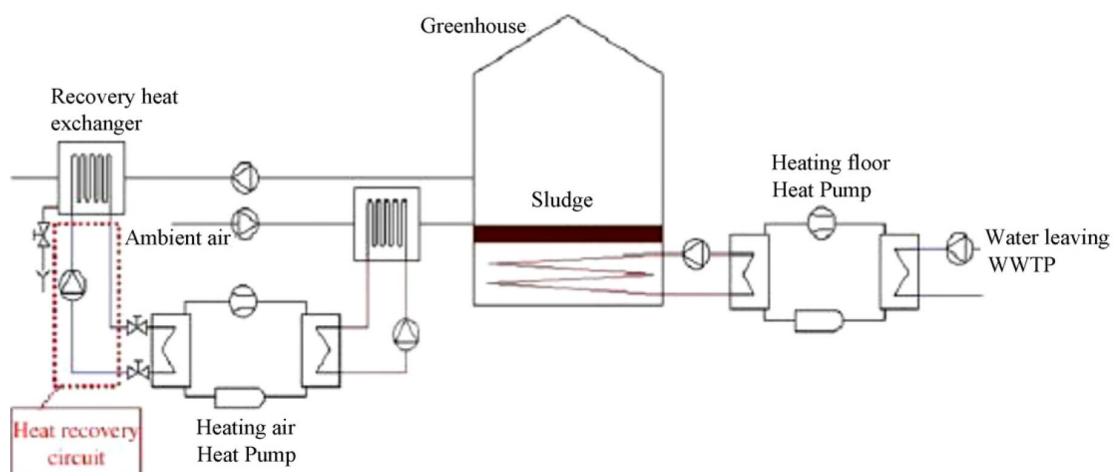


Figure 81. Greenhouse dryer combined with heat pump, installed in the west of France (Slim et al., 2008)

# APPENDIX C: ETHICAL CLEARANCE

---



UNIVERSITY OF  
KWAZULU-NATAL

INYUVESI  
YAKWAZULU-NATALI

RESEARCH OFFICE  
BIOMEDICAL RESEARCH ETHICS ADMINISTRATION  
Westville Campus  
Govan Mbeki Building  
Private Bag X 54001  
Durban  
4000  
KwaZulu-Natal, SOUTH AFRICA  
Tel: 27 31 2604769 - Fax: 27 31 260-4609  
Email: [BREC@ukzn.ac.za](mailto:BREC@ukzn.ac.za)  
Website: <http://research.ukzn.ac.za/ResearchEthics/BiomedicalResearchEthics.aspx>

03 April 2017

Mr TR Mugauri (212545105)  
Discipline of Chemical Engineering  
College of Agriculture, Engineering and Science  
[tendayimugauri@yahoo.co.uk](mailto:tendayimugauri@yahoo.co.uk)

Dear Mr Mugauri

Title: Drying and pasteurization of faecal sludge using solar Thermal energy. Or solar drying of faecal Sludge.  
Degree: MSc  
BREC Ref No: EXM200/17

I refer to your application to BREC received on 22 March 2017 and wish to advise that exemption of ethics review is granted for this study.

This exemption will be noted at the next Biomedical Research Ethics Committee meeting to be held on 11 April 2017.

Yours sincerely

  
Professor J Tsoka-Gwegweni  
Chair: Biomedical Research Ethics Committee

## APPENDIX D: EXPERIMENTAL SITE SOLAR ASSESSMENT

---

Before implementation of the drying rig, a solar resource assessment was done in order to characterize the solar irradiation available onsite.. The parameters employed in the solar assessment are:

- Global Horizontal Irradiation (GHI): total irradiation received in a plane surface, horizontal to the ground;
- Direct Normal Irradiation (DNI): irradiation from direct sunshine received in a plan surface, perpendicular to the sunrays;
- Diffusive irradiation (DIF): irradiation scattered by the atmosphere and received by a plane surface.

At first, solar source maps of South Africa and KwaZulu-Natal province were examined. The annual sum of GHI and DNI in Durban is around 1 750 and 1 550 kWh/m<sup>2</sup>. As seen in Figure 82 and Figure 83, these values are lower than most parts of the country and the region of KwaZulu-Natal, so Durban is one of the regions in South Africa that receives lower solar thermal energy. This could be explained by the high humidity and the considerable presence of cloudy along the year (with frequent rains in summer time). In terms of DIF, Durban has one of the highest values in the country, which is again related to the meteorological conditions (wet and cloudy weather).

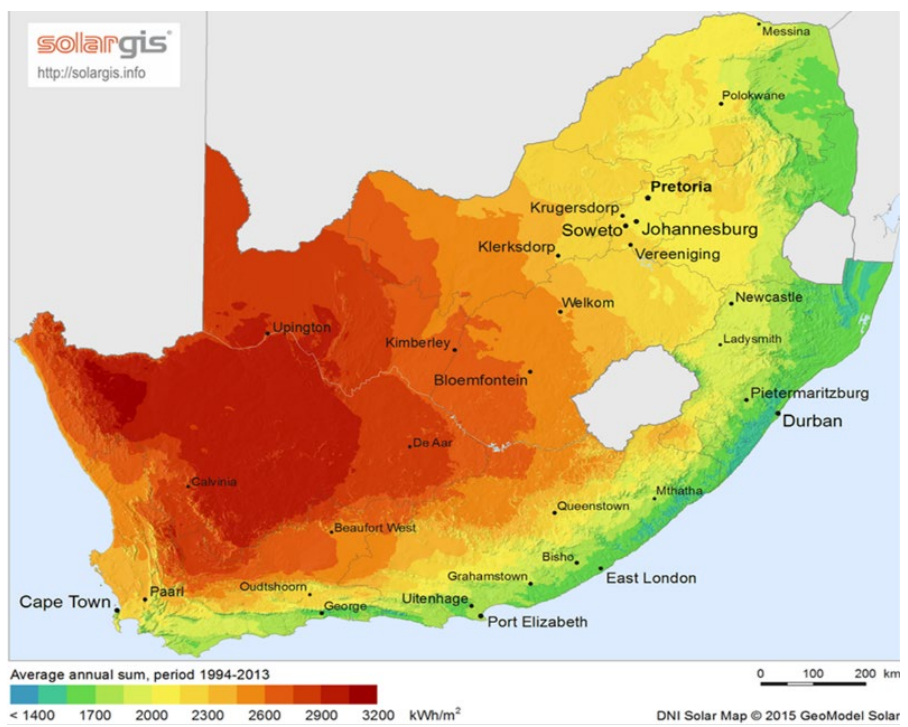
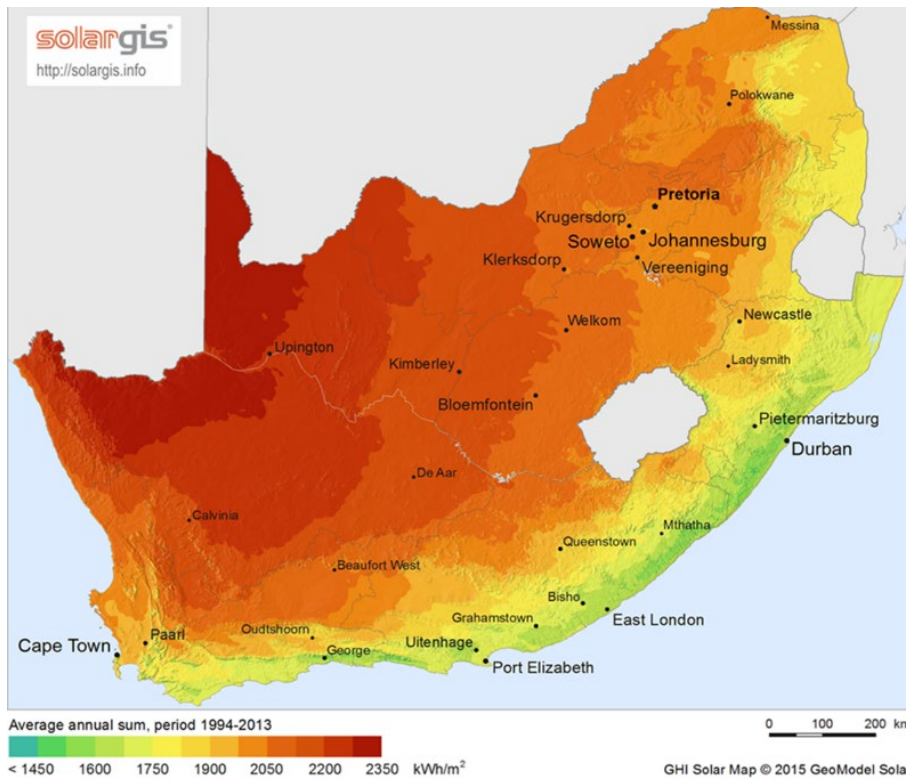


Figure 82. GHI (top image) and DNI (bottom image) maps in South Africa (source: <http://solargis.info>)

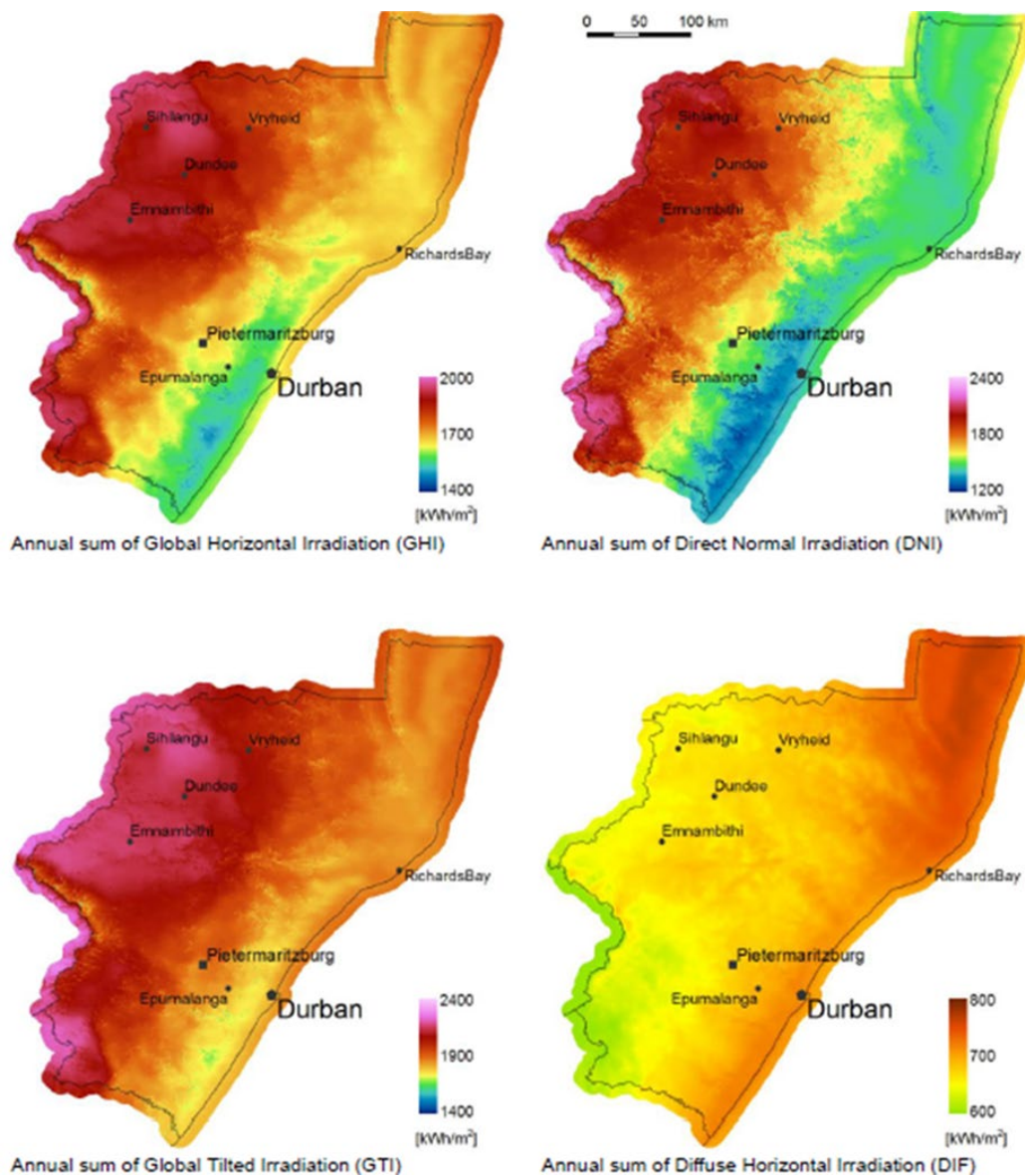


Figure 83. Solar maps in the region of KwaZulu-Natal

Thereafter, the solar conditions at the experimental site were studied using a tool designed for photovoltaic (PV) planners (at the website: <http://solargis.info/>). The experimental site is planned to be implemented in the roof of the Chemical Engineering building, at the University of KwaZulu-Natal. According to the analysis (Figure 84 and Figure 85), the sunshine conditions will widely vary according to the seasons:

- Winter : day length of 10 hours of day with an average air temperature of 17°C, GHI daily sum of 3 kWh/m<sup>2</sup> with a contribution of direct radiation of 2 kWh/m<sup>2</sup>-d;

- Summer : day length 14 hours of day with an average air temperature of 23°C, GHI daily sum of 5 kWh/m<sup>2</sup> with a contribution of direct radiation of 3 kWh/m<sup>2</sup>-d.

A short period of shading was detected at the planned experimental site during the sunrise (Figure 86). The length of this period is less than an hour, so it is possible to start experiments without any shading from 6 h in summer and 8 h in winter.

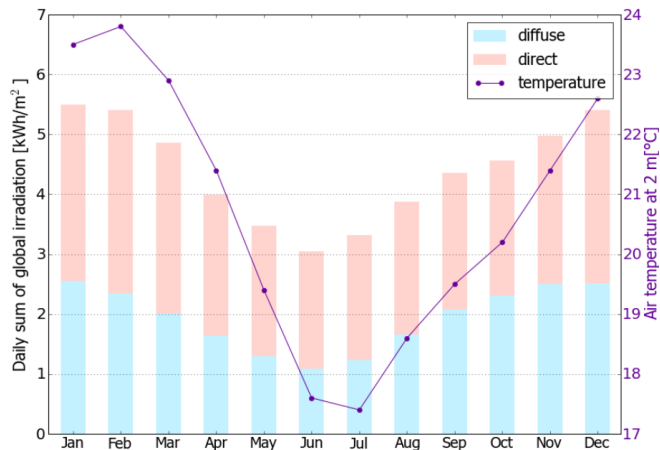


Figure 84. GHI daily sum with the diffusive and direct radiation contributions and air temperature during the day, at the roof of Chemical Engineering building (source: <http://solargis.info>)

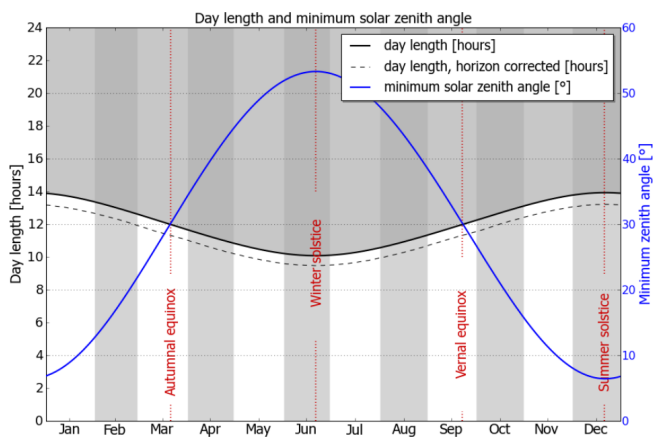


Figure 85. Day length and minimum solar zenith angle at the roof of Chemical Engineering building (source: <http://solargis.info>)

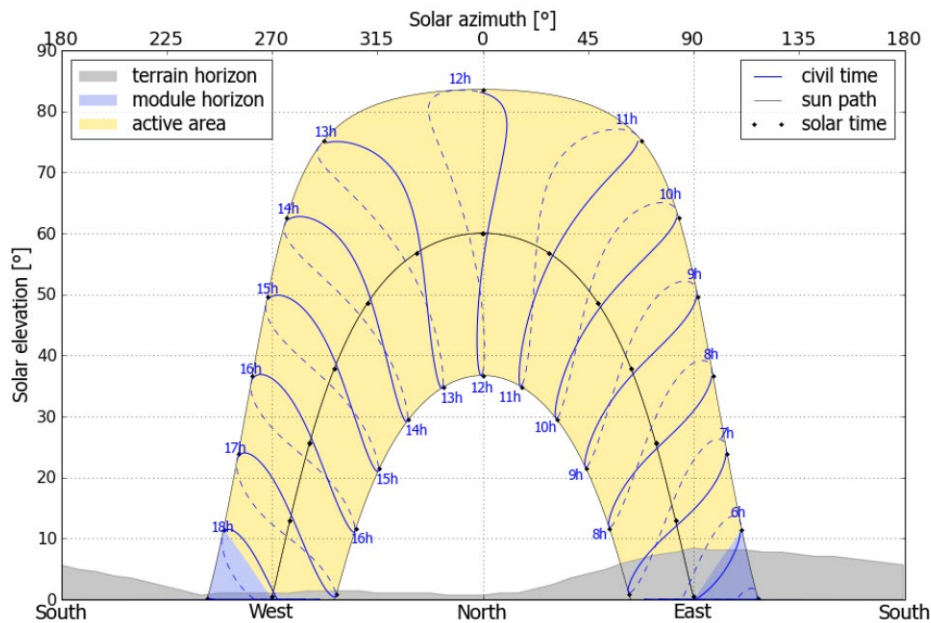


Figure 86. Position of the sun along the day at the roof of Chemical Engineering building (source: <http://solargis.info>)

In despite of the low irradiation levels in Durban with respect to the rest of the country, the irradiation levels are enough high to perform the experiments. The values are close to that of the south of Spain, where solar thermal energy is exploited at a commercial scale. However, the considerable presence of clouds in Durban can modify locally the irradiation levels, so it is very important to measure the irradiation on-site during experiments and not only rely on the nearby solar measurement stations. For example, a cloud could block the solar irradiation in the experimental site, while the sky will be clear above the solar measurement stations. This situation will lead to the overestimation of the irradiation parameters at the experimental site (particularly for the DNI), if only the values from the solar measurement stations will be considered.

## APPENDIX E: SELECTION OF THE MATERIAL OF THE DRYING CHAMBER

---

Different types of transparent materials could be used for the walls of the solar drying rig. Table 6 summarizes the transparent materials of interest with some of their properties. The transmissivities are high (ranging approximately from 80 to 90%) for all the transparent materials in the whole solar radiation spectrum (including visible light and shortwave IR radiation with a wavelength ranging between 700 to 2 250 nm). Appendix A shows how the transmissivities of the different materials were calculated.

Polymethyl methacrylate (PMMA) or acrylic glass (most commonly known as “plexiglass” or “perlex”) was selected as the material for the walls of the solar drying rig. This selection was based on the fact that acrylic glass is low-cost, readily available with local suppliers, resistant to shocks and easy to work on it in the workshop. Acrylic glass also offers a good thermal insulation (relative low thermal conductivity) and high transmittance. Acrylic has a suitable chemical resistance to possible gases released during the drying of faecal sludge, such as ammonia and hydrogen sulphide, due to the possible occurrence of anaerobic digestion and composting phenomena. However, acrylic has a low resistance to high temperatures. Acrylic has a relative low melting point (160°C), and its structure start to soften at temperatures around 100°C. Therefore, it is recommended to not expose the material to temperatures higher than 80°C.

In our case, this temperature limitation of the acrylic glass is acceptable during solar drying experiments where the drying chamber is exposed to solar radiation. However, in a later stage, experiments using solar radiation concentration or air with a temperature higher than are 80°C planned. Therefore, a second drying chamber will be built in silica glass, with identical characteristics to the first version in acrylic. Silica glass has a lower insulation ability and is less resistant to mechanical shocks than acrylic, but its cost is lower and it can stand higher temperatures (up to 500°C from where it starts to undergo physical changes). The second drying chamber will be built from silicate material that offers acceptable chemical resistance and transmissivities at the lower cost.

Both acrylic and silica glass are opaque at IR radiation with wavelength higher than 250 nm. Therefore, most of the radiation emitted by the sample during solar heating, which is mainly located in the mid and far IR zone (wavelength between 3 000 to 70 000 nm), will be captured in the drying zone, leading to a greenhouse effect.

*Table 6. Characteristics of transparent material of 2 -3 mm thickness*

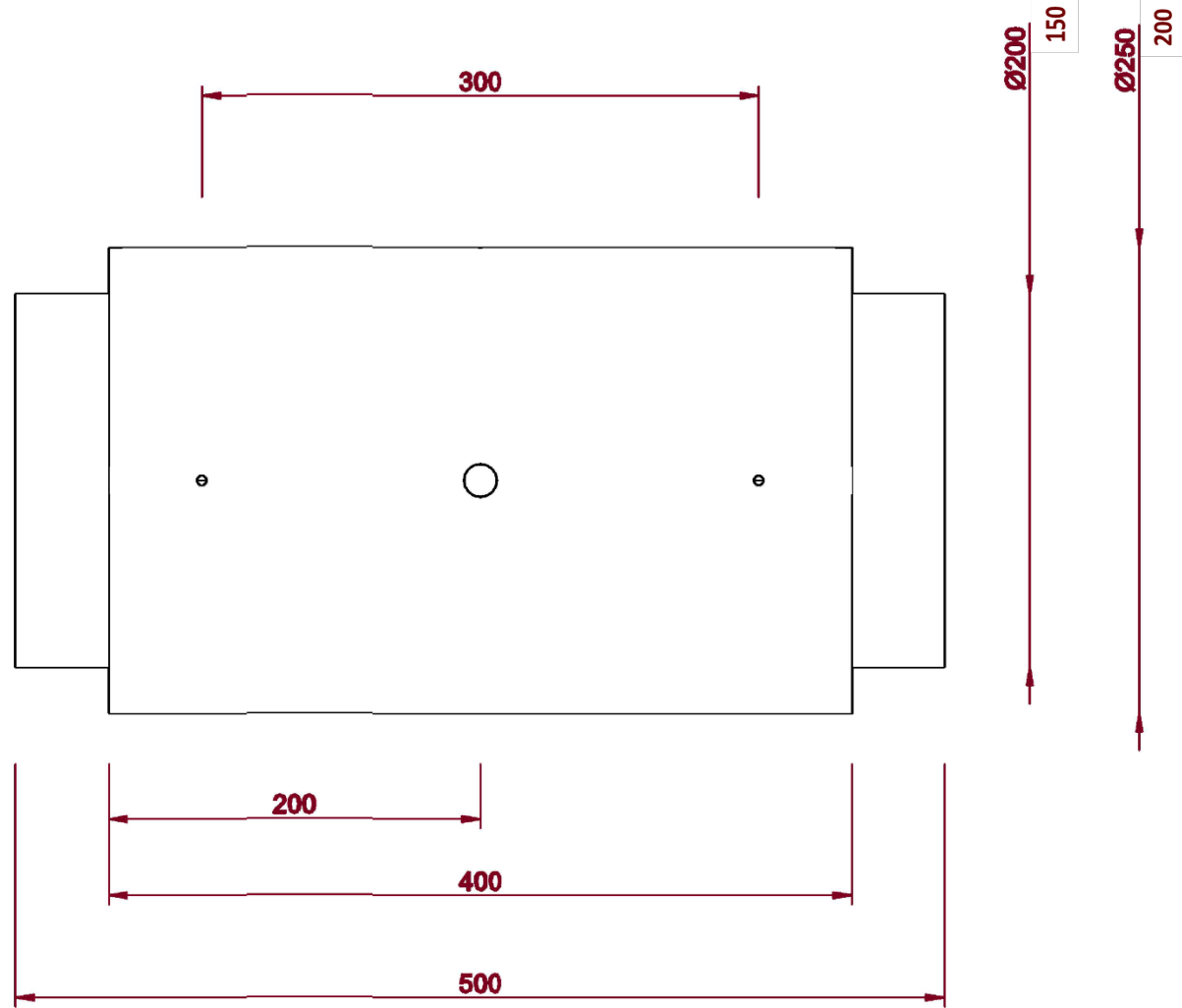
	<b>Cost</b>	<b>Density</b>	<b>Thermal conductivity</b>	<b>Specific Heat Capacity</b>	<b>Thermal Diffusivity</b>	<b>Transmittance</b>
	<b>US\$/kg</b>	<b>kg/m<sup>3</sup></b>	<b>W/m·K</b>	<b>J/g·K</b>	<b>m<sup>2</sup>/s</b>	<b>%</b>
Polycarbonate	~ 20	1310	0.20	1.10	1.39·10 <sup>4</sup>	79
Polyethylene Terephthalate	-	1595	0.29	2.30	7.91·10 <sup>5</sup>	82
Polyethylene (Molded)	-	925	0.30	2.20	1.47·10 <sup>4</sup>	82
Polymethyl Methacrylate	~ 10	1170	0.22	1.46	1.29·10 <sup>4</sup>	85
Polypropylene	~ 10	1070	0.12	2.00	5.61·10 <sup>5</sup>	-
Polyvinyl Chloride	~ 60	1245	0.18	1.20	1.20·10 <sup>4</sup>	-
Polycarbonate Aramid Fiber Reinforced	~ 100	1270	0.22	-	-	-
Silica Glass	~ 10	2180	1.38	0.75	8.44·10 <sup>4</sup>	89*

\* Value obtained for low-iron glass (high range glass with a reduced iron content in order to decrease the transmittance losses due to iron absorption)

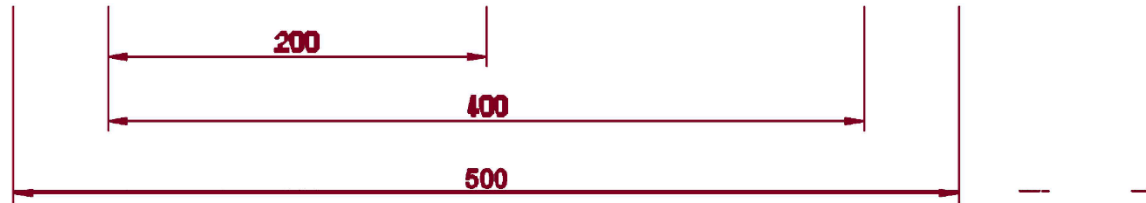
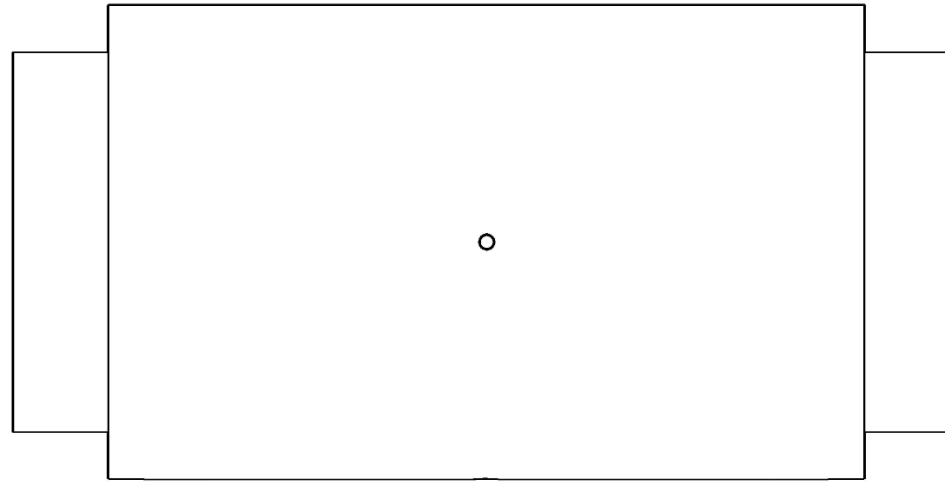
## **APPENDIX F: PLANS OF THE DRYING RIG**

---

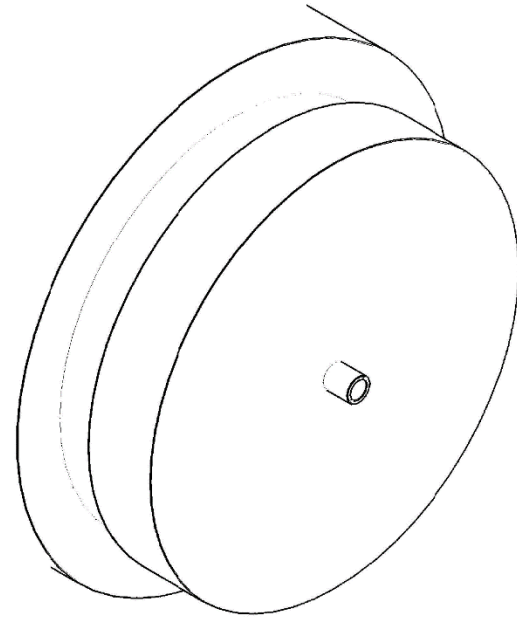
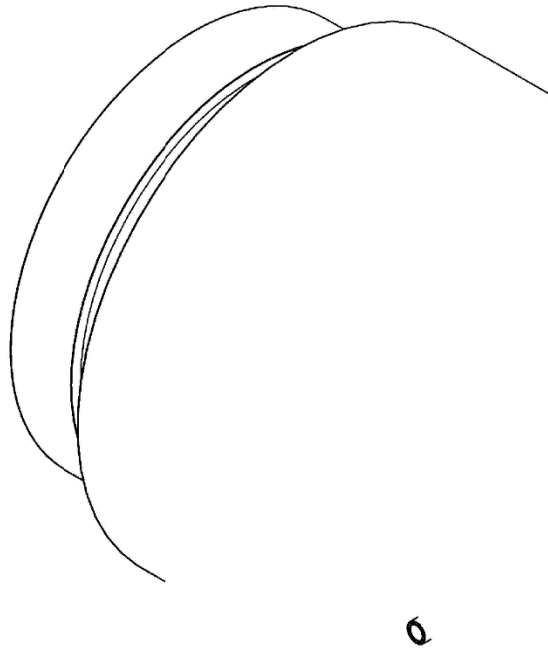
The plans of the drying box were performed in AutoCAD.



PROPRIETARY AND CONFIDENTIAL THE INFORMATION CONTAINED IN THIS DRAWING IS THE SOLE PROPERTY OF SANERGY LTD. ANY REPRODUCTION IN PART OR AS A WHOLE WITHOUT THE WRITTEN PERMISSION OF SANERGY LTD IS PROHIBITED	PROJECT TITLE _____		NAME	DATE	SIZE	A	DRAWING NO.	
		DRAWN	K. P. DUBE	30/01/2016	SCALE	1:1	REV	
	DRAWING TITLE	DESIGNED			DIMENSIONS	MM	SHEET	1 of 1
	DRAWING 1	CHECKED						



PROPRIETARY AND CONFIDENTIAL THE INFORMATION CONTAINED IN THIS DRAWING IS THE SOLE PROPERTY OF PRG. ANY REPRODUCTION IN PART OR AS A WHOLE WITHOUT THE WRITTEN PERMISSION OF SANERGY LTD IS PROHIBITED	PROJECT TITLE		NAME	DATE	SIZE	A	DRAWING NO.		
			DRAWN	K. P. DUBE	14/10/2016	SCALE	1:1	REV	
	DRAWING TITLE		DESIGNED			DIMENSIONS	MM	SHEET	1 of 1
	DRAWING 1		CHECKED						



6

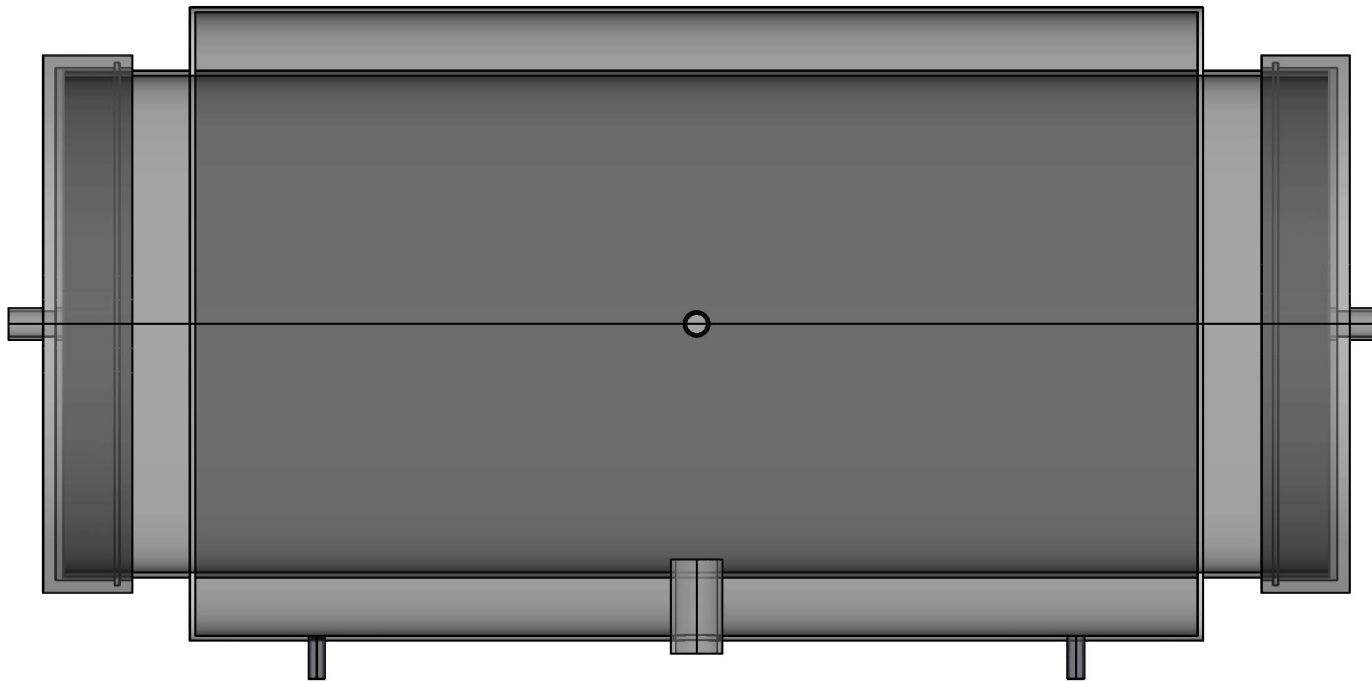
	PROPRIETARY AND CONFIDENTIAL THE INFORMATION CONTAINED IN THIS DRAWING IS THE SOLE PROPERTY OF SANERGY LTD. ANY REPRODUCTION IN PART OR AS A WHOLE WITHOUT THE WRITTEN PERMISSION OF SANERGY LTD IS PROHIBITED	PROJECT TITLE			NAME	DATE	SIZE	A	DRAWING NO.	
				DRAWN	K. P. DUBE	30/01/2016	SCALE		REV	
		DRAWING TITLE <b>DRAWING 1</b>		DESIGNED						
				CHECKED			DIMENSIONS	MM	SHEET	1 of 1



	PROPRIETARY AND CONFIDENTIAL THE INFORMATION CONTAINED IN THIS DRAWING IS THE SOLE PROPERTY OF SANERGY LTD. ANY REPRODUCTION IN PART OR AS A WHOLE WITHOUT THE WRITTEN PERMISSION OF SANERGY LTD IS PROHIBITED	PROJECT TITLE		NAME	DATE	SIZE	A	DRAWING NO.	
		DRAWING TITLE <b>DRAWING 1</b>	DRAWN	K. P. DUBE	30/01/2016	SCALE		REV	
			DESIGNED			DIMENSIONS	MM	SHEET	1 of 1
			CHECKED						



	PROPRIETARY AND CONFIDENTIAL THE INFORMATION CONTAINED IN THIS DRAWING IS THE SOLE PROPERTY OF SANERGY LTD. ANY REPRODUCTION IN PART OR AS A WHOLE WITHOUT THE WRITTEN PERMISSION OF SANERGY LTD IS PROHIBITED	PROJECT TITLE		NAME	DATE	SIZE	A	DRAWING NO.	
			DRAWN	K. P. DUBE	30/01/2016	SCALE		REV	
		DRAWING TITLE	DESIGNED			DIMENSIONS	MM	SHEET	1 of 1
		DRAWING 1	CHECKED						



	PROPRIETARY AND CONFIDENTIAL THE INFORMATION CONTAINED IN THIS DRAWING IS THE SOLE PROPERTY OF SANERGY LTD. ANY REPRODUCTION IN PART OR AS A WHOLE WITHOUT THE WRITTEN PERMISSION OF SANERGY LTD IS PROHIBITED	PROJECT TITLE		NAME	DATE	SIZE	A	DRAWING NO.	
		DRAWING TITLE <b>DRAWING 1</b>	DRAWN	K. P. DUBE	30/01/2016	SCALE		REV	
			DESIGNED			DIMENSIONS	MM	SHEET	1 of 1
			CHECKED						

## APPENDIX G: CFD SIMULATIONS

---

CFD analysis is used to simulate fluid flow mechanics models to test for feasibility and also ensure design success when in use and also to provide an insight into the expected results. The solar drying prototype uses air as the heat transfer medium as well as for moisture removal. Resulting in the generation of flow through the drying system. A CFD analysis was carried out to simulate the flow processes of the prototype at ret flowrates and dimensions for optimum drying

### General model information

- Mean inlet flow rate =  $0.088\text{m}^3/\text{s}$
- Outlet pressure = Atmospheric pressure.
- Number of fluid cells used by the final version of the CFD model;
- Multi-inlet with plate = 146 731
- Multi-inlet without plate = 108 555
- Singular inlet with plate = 125 010
- Singular inlet without plate = 89 472
- Number of partial cells used by the final version of the CFD model;
- Multi-inlet with plate = 256 012
- Multi-inlet without plate = 208 555
- Singular inlet with plate = 235 789
- Singular inlet without plate = 198 500
- Mean run time for the simulations: Multi-inlet with plate = 3254s
- Multi-inlet without plate = 2956s
- Singular inlet with plate = 2855s
- Singular inlet without plate = 2600s

### **Model development**

In the model development, it was assumed that constant flow rates a provided to the inlet valves. The flow was considered a constant density gas, with no significant change in properties. Due to the expected flow conditions, the flow was modelled as fully developed turbulent flow. There was assumed to be no expansion of the gas

through the chamber due to temperature change. Based on the calculation, flow after the inlet was assumed to be fully turbulent, to simplify the simulation of the model, K-Epsilon turbulence was employed with realizable two-layer treatment, as a result the K-Epsilon turbulence models were applied, and it was selected as it performs best for wall  $y^+$  values less than 300.

An internal analysis, which excluded cavities without flow conditions, with a fixed feature of the diffusive plate was implemented. For the flow analysis, thermodynamic conditions were considered to be at room temperature, with no present velocity parameters. Mesh resolution was set to 6, as this was a good compromise between mesh quality and computational time. A solid standard mesh type was applied. SI units were implemented.

Mesh models used were;

- Polyhedral Mesher
- Prism layer Mesher
- Surface Remesher

Polyhedral mesh model generated a volume mesh composed of cells shaped as polyhedrals. It was selected due to its efficiency to build and greater accuracy compared to tetrahedral mesh. As the surface mesh is of an acceptable quality, it also led to the selection of the mesh type. The results are more accurate and the computational time is less than that of tetrahedral meshes.

Prism layer mesher in-cooperates prismatic cell layers next to wall boundaries, it projects the core mesh into the wall boundaries to create the prismatic cells. The layer of cells improves the accuracy of the flow solution as a prediction of various flow features.

Surface remesher reconstructs the initial surface to provide a quality mesh suitable for CFD. Normally applied to triangulate the surface under inspection based on a target edge length, can also over look specific surfaces to preserve the original triangulation from the imported body.

Mesh density distribution is critical for the accuracy and convergence of the CFD analysis. 0.005m base size and prism layer stack size of 0.003m was used for the

surface meshing and a relative to base percentage of 33% was utilized for the model. The resulting surface mesh density was acceptable as it was capable of producing the required boundary layer resolution. The number of prism layers of 5 is utilized to accurately depict and analyse the flow through the system.

Boundary conditions applied were: Volume inlet. Environmental pressure conditions were applied to the lids covering the exit plate. This were considered as the opening to the environment. The body of the frame was considered as a real wall with adiabatic conditions. The inlet valves were considered as constant volume inlets. The geometry of the system was analysed before the analysis of the system. The flow field of the air was selected to be 3 dimensional. The fluid domain in assumed to be standard air with constant density. The material properties were incorporated into the system though the specification of the body material. The flow field of the air was selected to be three dimensional and steady, since an assumption was made that the physical properties are non-changing with respect to time. The fluid domain is assumed to be purely gas with constant density. Gradients of various fluctuating physical properties are incorporated into the CFD model. The flow was taken as fully turbulent hence K-Epsilon Turbulence, Liquid, Realizable K-Epsilon Two-Layer and Reynolds-Averaged Navies-Stokes models were applied. Two-layer all  $y^+$  wall treatment, was used for the analysis of the wall boundary layer. Gravity and coupled flow were also incorporated.

The physics models applied were:

- Constant Density
- Gas, specified to air with density= $1.18\text{kg/m}^3$  and dynamic viscosity= $1.86 \times 10^{-5}$  Pa-s
- Gradients
- Gravity
- K-Epsilon Turbulence
- Realizable K-Epsilon Two Layer
- Steady
- Three Dimensional

- Turbulent

Two-Layer All  $y^+$  Wall Treatment

## Results

Solution convergence is critical in a CFD analysis. The residuals plot is normally used to depict system convergence (Figure 87). Relating to the residuals plot, all the discrete conservation equations have been obeyed in all the cells, shown by the lack in changes over subsequent iterations. As a result, solution convergence has been achieved.

The  $y^+$  values have to be sized appropriately for the selected turbulence model:

$$D_h = 0.15\text{m}, \rho = 1.18\text{kg/m}^3, \mu = 1.983 \times 10^{-5}\text{m}^2/\text{s}$$

$$v = 1.0\text{m/s}, Re = \frac{vD}{\mu} = 8456$$

$$C_f = \frac{2 \times 0.036}{Re^{\frac{1}{5}}} = 0.0112, \tau_w = 0.5 C_f \rho v^2 = 0.0080\text{Pa}, U^* = \sqrt{\frac{\tau_w}{\rho}} = 0.082\text{m/s}, y^+ = 5$$

$$y = \frac{\mu y^+}{U^*} = 0.00121\text{m}, 2y = 2.42\text{mm}, \text{prism layer stack size} = 3\text{mm}$$

The prism layer size chosen is greater than the  $y$  value calculated, therefore the  $y^+$  value was appropriate for the selected turbulence model.

Figure 88 shows the velocity field obtained from CFD simulation using a single and multi-entry. It can be seen that a multi-entry inlet enables a better distribution of the air velocity along the cross-section. This conclusion was verified by measuring the air flowrate at different positions of the drying chamber cross-section, using an anemometer (Table 7).

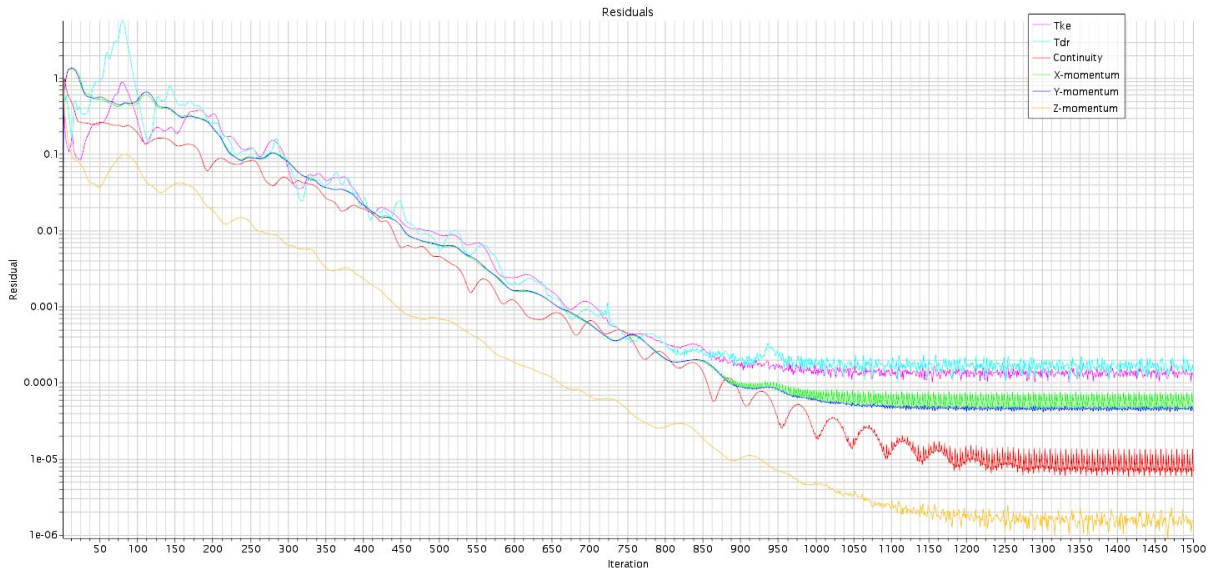
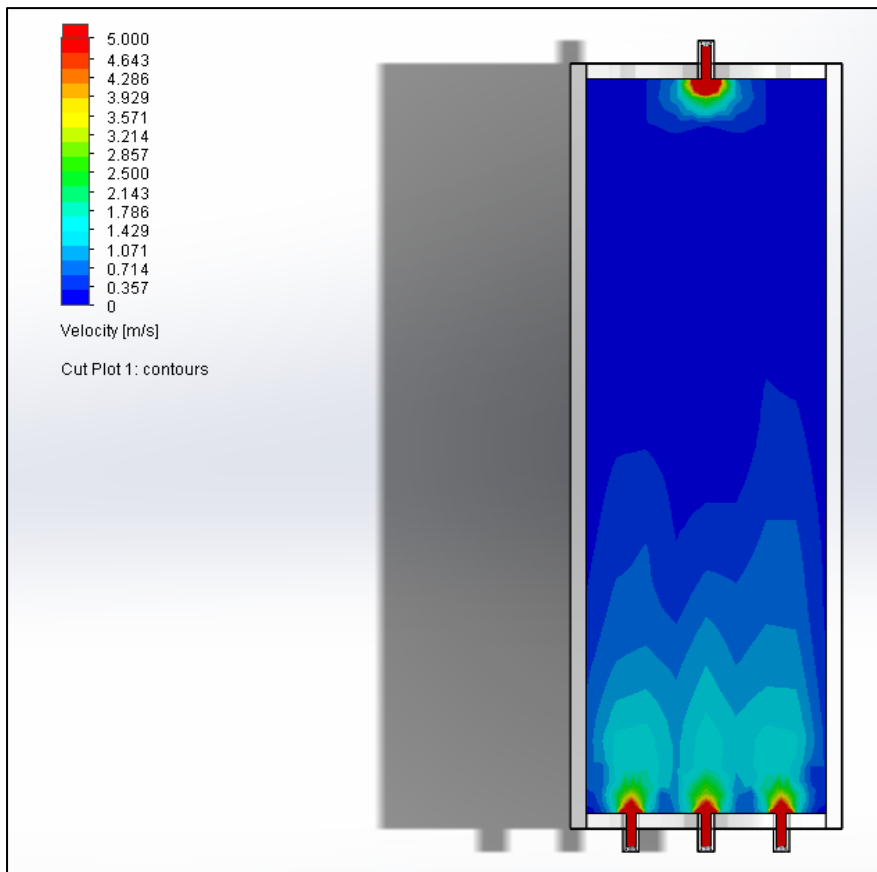


Figure 87. Residuals Plot



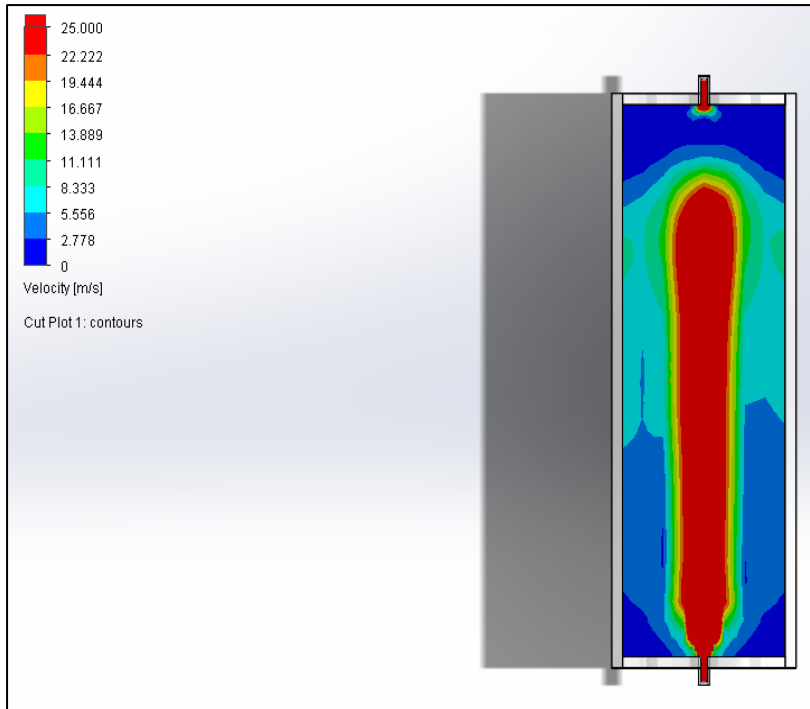


Figure 88. CFD simulations of the airflow within the drying chamber with multi-entries inlet (top) and single entry inlet (bottom)

Table 7. Air flowrates measured at different positions in the cross-section of the drying chamber, using a single and multi-entry inlet

Total flowrate (m <sup>3</sup> /s)	Inlet	Flowrate at different positions (m <sup>3</sup> /s)				
		Wall 1	Wall 2	Wall 3	Wall 4	Centre
0.01	Single entry	~	~	~	~	0.008
	Multi-entry	0.002	0.002	0.002	0.002	0.003
0.05	Single entry	0.002	0.001	0.002	0.004	0.04
	Multi-entry	0.009	0.01	0.01	0.009	0.011
0.09	Single entry	0.003	0.003	0.002	0.004	0.07
	Multi-entry	0.018	0.018	0.016	0.019	0.022

## APPENDIX H: PRELIMINARY TESTS

A preliminary experiment in the solar drying rig was done using a tissue that was previously wet, in order to test the functionality of the equipment.

### Irradiance data

Figure 89 shows the solar irradiance measured by the pyranometer between 10:30 AM and 2:30 PM during the experiment. The irradiance was at a quite constant value of 450 W/m<sup>2</sup> until 11:30 AM, from when it increased to reach an irradiance highly fluctuating between 600 to 900 W/m<sup>2</sup>. After 12:30 PM, the irradiance decreased smoothly until arriving at 200 W/m<sup>2</sup> at the end of the measurements. The solar irradiance values obtained during the experimentation day were predominantly higher than the typical value expected in August 300 W/m<sup>2</sup>.

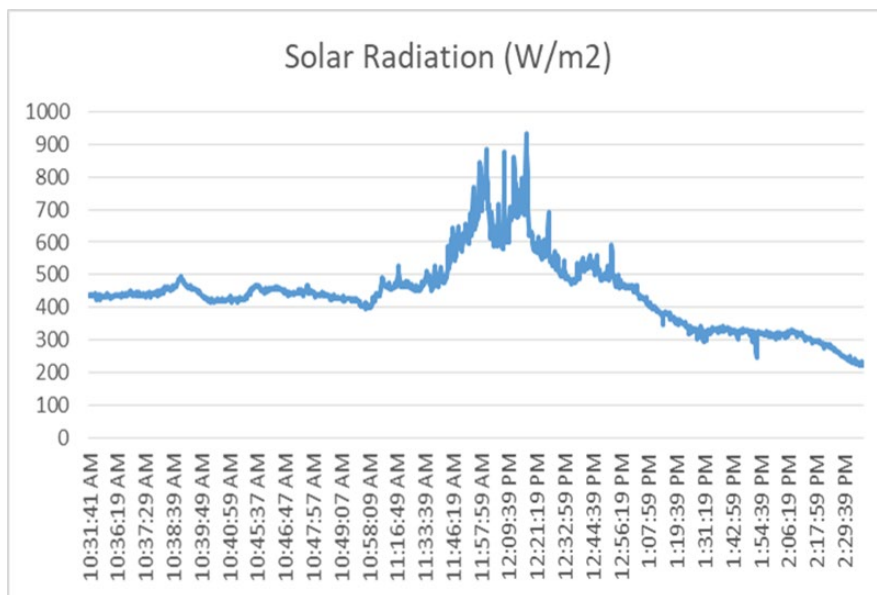
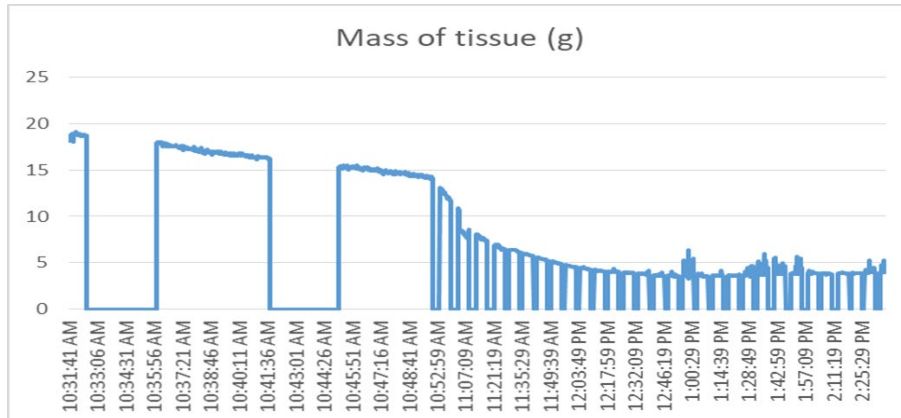


Figure 89. Solar irradiance measured by the pyranometer

## **Mass evolution**

The plot of tissue mass variation is presented in Figure 90. It can be seen that the mass reading frequently dropped in a drastic way, which was caused by the auto-calibration of the balance. In fact, the balance has a very sensitive auto-calibration system that even a small perturbation can trigger. In despite of the data missing during the calibration periods, it is possible to observe the mass evolution trend with time. During the periods when the mass was recorded, the measurements looked quite stable and not being perturbed by external conditions as the wind.

It can be seen that the mass of the tissue decreased slowly at the beginning of the experiment. At around 10:50 AM, the loss of mass suddenly dropped during some minutes, and after this it continued to decrease at a slow rate again. The mass stabilised at approximately 12:40 PM, from where drying can be considered to be achieved. The duration of drying was approximately of 2 hours and 15 g of water was evaporated.



*Figure 90. Mass variation of the wet tissue in the solar drying rig*

Typically, the drying rate at the beginning is constant until achieving the critical moisture content, from which it starts to decrease. In our experiments, the constant rate period appeared to occur until 10:50 AM. After this moment, the drying rate suddenly increases, contradicting the theory that expected rather a decrease. A phenomenon non-predicted in the conventional drying theory may have been the cause, leading to the acceleration of the process. We can discard the assumption of

an increase of solar irradiance during the experiment, as this occurred after the drying rate increase (around 11:30 AM).

### **Temperature evolution**

Figure 91 shows the temperature measured at different points in the solar drying rig. The ambient temperature (yellow plot) presented a relative constant value at 25°C, followed by an increase until a temperature fluctuating around 30°C, and finally a decrease up to 25°C. This temperature evolution was quite synchronized with respect to the solar irradiance variation. This result could be expected as solar radiation conditions have a great influence on the ambient temperature.

The temperature in the protection box (blue plot) was the same than the ambient temperature. This demonstrates that the box didn't not allow an overheating nearby the balance, which could damage it.

The temperature inside the drying chamber (grey plot) was a few degrees lower than the ambient temperature. At around 11:30 AM, the trend was inversed and the temperature inside the drying chamber was slightly higher than the ambient temperature.

The temperature within the tissue (orange plot) was considerably lower than the ambient temperature during the first half of the experiment. It was at constant value of 15°C, which should correspond to the wet bulb temperature (temperature at which the constant rate period occurs). At around 11:10 AM, the temperature started to increase sharply until reaching the ambient temperature at 12:00 PM and exceeding it of a few degrees for the rest of the experiment. The temperature increase can be attributed to the fact that at 11:10 AM, the core of the tissue starts to be considerably dried. By consequence, the effect of moisture evaporation on the temperature weakened and the solid starts to be heated from the solar radiation.

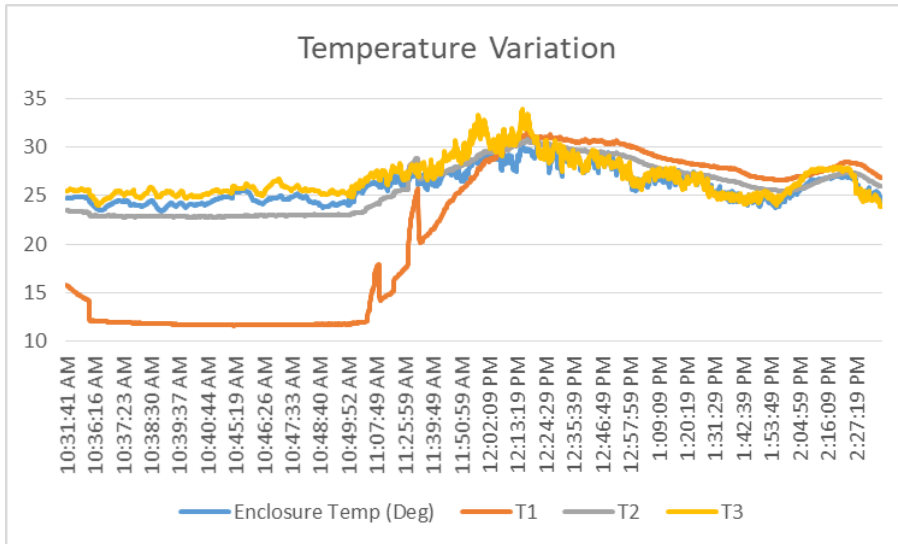


Figure 91. Temperature variation during solar drying (blue plot: temperature in the protection box; orange plot: temperature of the tissue; grey plot: air temperature inside the drying chamber; yellow plot: ambient temperature)

## **Conclusion**

The functionality of the solar drying rig was tested with encouraging results. A stable operation was obtained after four hours of experimentation. The measurement of the solar irradiance and temperature were done without any issue. The data was logged with success into the computer. The mass measurement was stable in despite of the wind, and no overheating of the balance occur. The protection box ensured, like this, its role to protect the balance from external conditions. Nevertheless, the balance tended to auto-calibrate frequently, probably due to small perturbations that the protection box could not avoid, leading to the loss of data during the calibration time. In fact, the balance has a very sensitive auto-calibration system that even a small perturbation can trigger. This problem was solved by replacing the balance to one device with manual calibration.

# APPENDIX I: SOLAR AIR HEATING CHIMNEY

---

## **Concept**

A solar heating chimney was designed and constructed in order to heat air using thermal solar energy for drying purposes. This work is conducted on collaboration with Dr. Herbert W. Bernhardt from the Chemical Engineering department at UKZN. The purpose of the solar heating chimney is to couple this device with the solar drying rig, after determination of the optimal design, and test its efficiency for drying.

Two laboratory undergraduate projects have been conducted in order to test the functionality of the chimney and improve its design. During the first laboratory undergraduate projects (March to May 2016), the concept was validated but it was noted that the solar heating chimney was strongly influenced by the meteorological conditions, in particular the wind. During windy days, the performance of the device dropped drastically with respect to sunny days. This was related to a poor insulation, leading to high heat losses by convection with the wind. In addition, the air flowrate at the exit of the chimney was very low, putting into evidence a weak effect of natural convection as the flow driven force.

## **Modifications of the prototype**

In order to cope the aforementioned limitations, some modifications were performed in the solar chimney:

- **Modified version1:** The surface receiving the irradiation (metallic surface painted in black) was replaced by a transparent acrylic sheet. The inner surface of the chimney was painted in black (not painted at that point) in order to increase its absorbance. This surface will play the role of absorber. The acrylic sheet will create a greenhouse effect by trapping part of the radiation emitted by the inner walls (transparent materials are usually opaque to longwave infrared radiation, which is the one usually emitted by bodies at temperatures lower than 100°C).

- Modified version 2: A polystyrene thermal insulation layer was added on the metallic outer walls of the chimney in order to reduce the heat losses into the environment.
- Modified version 3: A ventilation fan was added at the outlet of the chimney in order to induce higher flowrates by forced convection.
- Modified version 4: The baffles were removed.
- Modified version 5: The interior of the chimney was filled with stainless steel wool, in order to increase the contact area with the air and create more turbulences, with the expectations to improve the heat transfer.

Figure 92 shows some photographs of the chimney after the modifications. Note that in the photograph at the bottom left, part of the insulation material went off the surface of the chimney.



*Figure 92. Photographs of the solar heating chimney*

### **Results obtained**

Table 8 summarizes the results from the solar heating chimney from the initial version to the last modified version. The initial design was tested in 2016 (end of March and

April), while the tests for the modified versions were held in 2017 (beginning of March for modified version1, beginning of April for modified version 2 and middle of April for modified version 3). During the tests, the ambient temperature was mainly comprised between 25 and 30°C, and tended to decline of a few degrees from March to April. The same trend was observed for the solar irradiance.

*Table 8. Summary of the results obtained in the solar heating chimney from the initial design to the modified versions*

	<b>Air temperature increase (°C)</b>	<b>Air flowrate (kg/s)</b>	<b>Solar irradiance power (W)</b>	<b>Power absorbed by the air (W)</b>	<b>Efficiency (%)</b>
<b>Initial design</b>	15-35	~ 0.01	~ 1200	150-450	12-38
<b>Modified version 1</b>	19-25	~ 0.01	~ 1350	~ 250	~ 19
<b>Modified version 2</b>	22-26	~ 0.01	~ 1100	~ 250	~ 23
<b>Modified version 3</b>	9-14	~ 0.04	~ 1000	350-600	35-60

As it can be seen in Table 8, the heating of the air in the initial version of the chimney varied widely, as it was greatly influenced by the ambient condition. In favourable conditions (sunny and no wind), the increase of temperature can go up to 35°C, which is higher than any of the outflow air temperatures measured in the chimney after the modifications. However, if the weather conditions were cloudy and windy, the rise of temperature was as low as 15°C. By changing the metallic front of the chimney to acrylic (modified version1), the heating of the air was much less influenced by the ambient conditions, increasing its robustness. However, the maximum temperature attained by the air was lower than that from the initial version, probably due to a reduction of the heated surface area (the surface in acrylic does not get as hot as the

metallic surface). The addition of thermal insulation (modified version2) led to a slight increase of efficiency.

In sunny conditions without wind, the initial design of the chimney has a better performance than the first two modified versions, with a higher outflow air temperature and efficiency. Nonetheless, the presence of clouds and wind will lead to a drop of its performance, and the trend will be inversed. The original version of the chimney will be more suitable to use for locations where the weather conditions are stable, with permanent sunshine with clear sky and low winds. The version with the modifications will be more adapted to a location with varying weather conditions (as Durban).

The addition of the ventilation fan (modified version 3) led to a significant increase of the amount of air flowing in the chimney, by quadruplicating the flowrate. The outflow air temperature was lower than in the other chimney versions, which is a consequence of the increase of the mass of air to heat. Nevertheless, the efficiency of the third modified version of chimney was considerably higher than the other cases, reflecting a more efficient heat transfer in despite of a decrease of the residence time. The highest efficiency achieved by this system was about 60%, thereby approaching to the maximum theoretical efficiency value of approximately 80% (which is based on the solar irradiance transmissivity efficiency of acrylic and considering a perfect thermal insulation).

Note that the efficiency of the modified chimney version 3 exhibited a wide variation. Efforts have to be made in order to understand this variability, which could be issued from the experimental measurements.

### **Current status**

The modified version 4 and 5 are in course to be tested.

# APPENDIX J: RISK ASSESSMENT OF THE EXPERIMENTAL RIG

*Pollution Research Group*  
**Hazard Identification Risk Assessment**

*Task Safety Analysis: Solar Drying rig*

List Major Hazards	What are the Risks	Present Risk Level	Probability Level	Control Measures	Risk Level after control
Biological	Infection originated from faecal sludge	High	High	Vaccination against Typhoid, Hepatitis A & B, Tetanus, Polio Use of personal protection equipment	Low
Physical	Shed blown away due to wind	High	Low	Support shed with heavy supports, e.g. bags of sand	Low
Fire	Fire of shed	Medium	Medium	Extincter near the cabinet	Low
Electrical	Electrocution	High	Medium	Use of personal protective equipment and switch off electricity during an intervention in the electrical components	Low
Physical	Sunstroke	Medium	High	Setup of a shaded place and availability of drinking water at proximity of the solar drying rig	Low
Physical	Burning	Medium	High	Avoid touching surfaces exposed to solar irradiation or use of thermal insulated gloves	Low
Physical	physical harms due to material falling on the ground	Medium	High	Use of mechanically reliable support for the stand of the material	Low
Physical	physical harms due to moving	Medium	High	Ask assistance to move the material and use adequate transporting material	Low

*Determining Needs to Perform the Task Safely*

PPE REQUIRED	X	SPECIALISED PPE	X	GENERAL SAFETY	X	FIRE PROTECTION	X
Lab coat		Chemical resistant lab coat		Extraction		Fire hydrant/extinguishers available	X
Latex powder free gloves		Heat resistant gloves		Fume hood		Emergency escape route identified	
Safety shoes	X	Face Shield		Temp controlled environment		Assembly points identified	
Safety glasses	X	Dust mask		Chemical resistant working surface		Emergency numbers available	
		Respirator		Heat resistant working surface			

# APPENDIX K: IRRADIANCE MEASURED DURING THE EXPERIMENTS

---

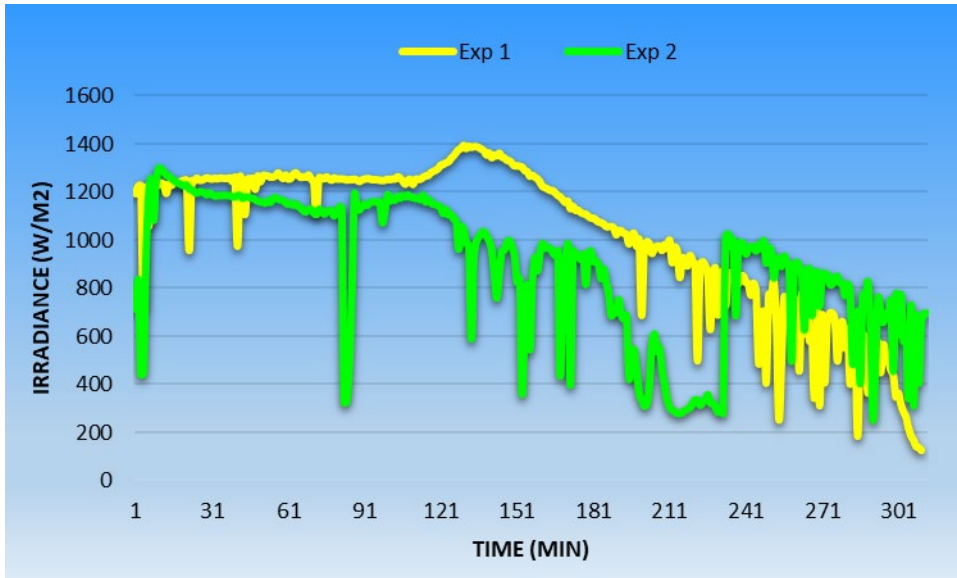


Figure 93. Irradiance during solar drying of a sample of 60 mm diameter and 5 mm thickness, in a sunny day, with an airflow velocity of 0.5 m/s within the drying chamber and no pre-heating

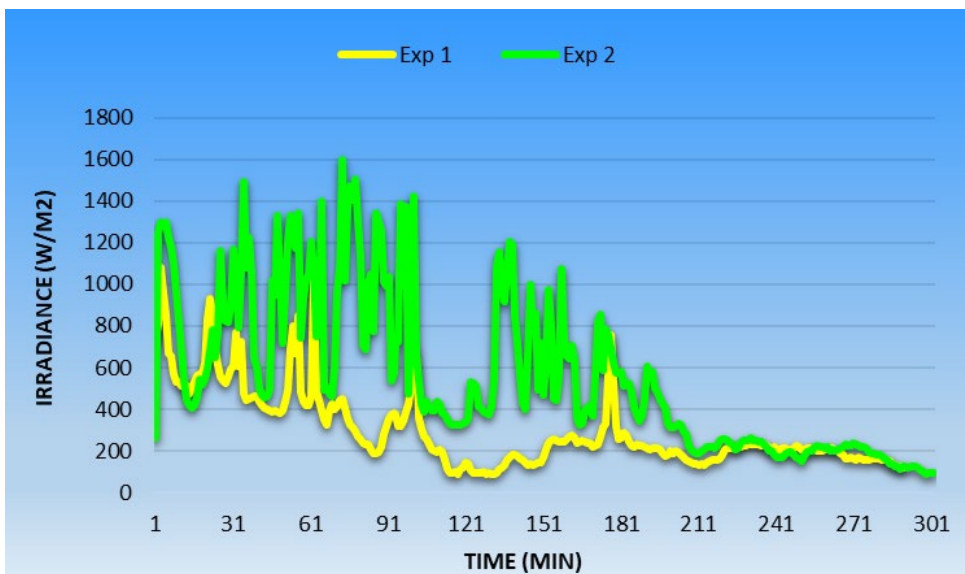


Figure 94. Irradiance during solar drying of a sample of 60 mm diameter and 5 mm thickness, in a cloudy day, with an airflow velocity of 0.5 m/s within the drying chamber and no pre-heating

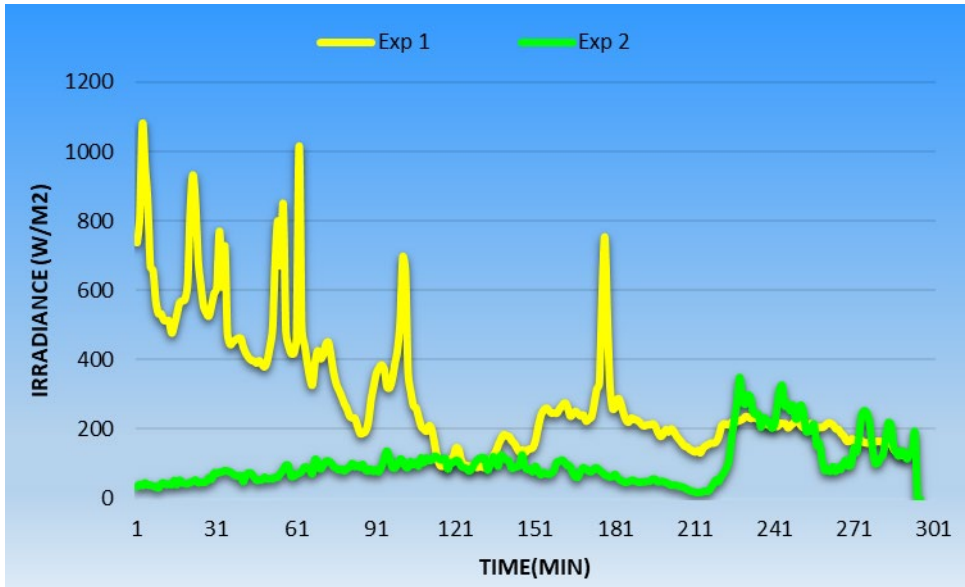


Figure 95. Irradiance during solar drying of a sample of 60 mm diameter and 5 mm thickness, in an overcast day, with an airflow velocity of 0.5 m/s within the drying chamber and no pre-heating

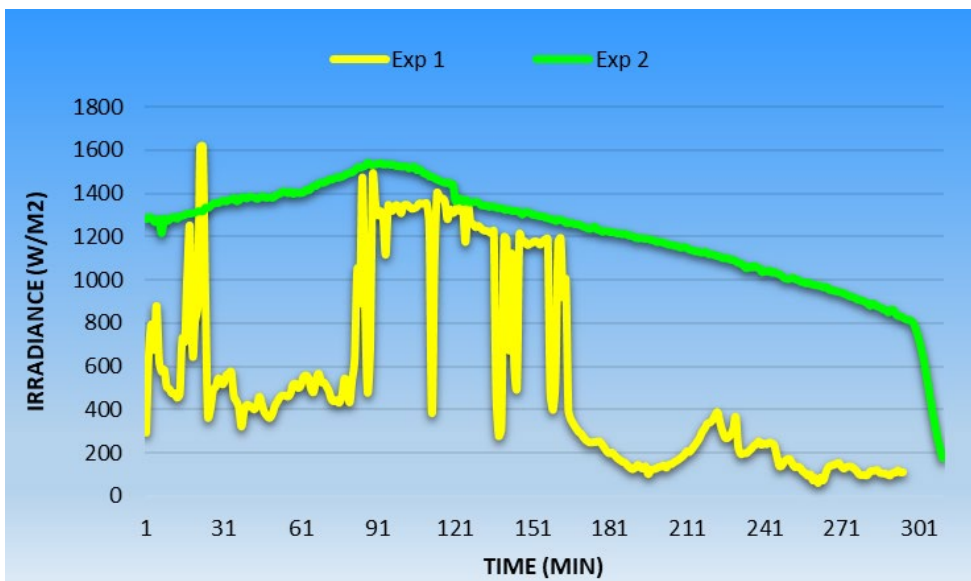


Figure 96. Irradiance during solar drying of a sample of 60 mm diameter and 10 mm thickness, in a sunny day, with an airflow velocity of 0.5 m/s within the drying chamber and no pre-heating

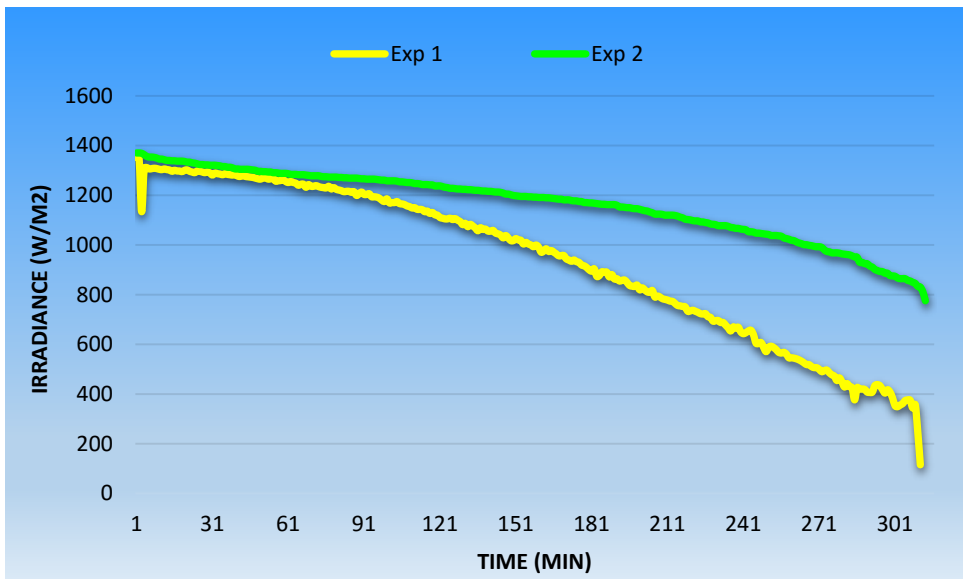


Figure 97. Irradiance during solar drying of a sample of 120 mm diameter and 5 mm thickness, in a sunny day, with an airflow velocity of 0.5 m/s within the drying chamber and no pre-heating

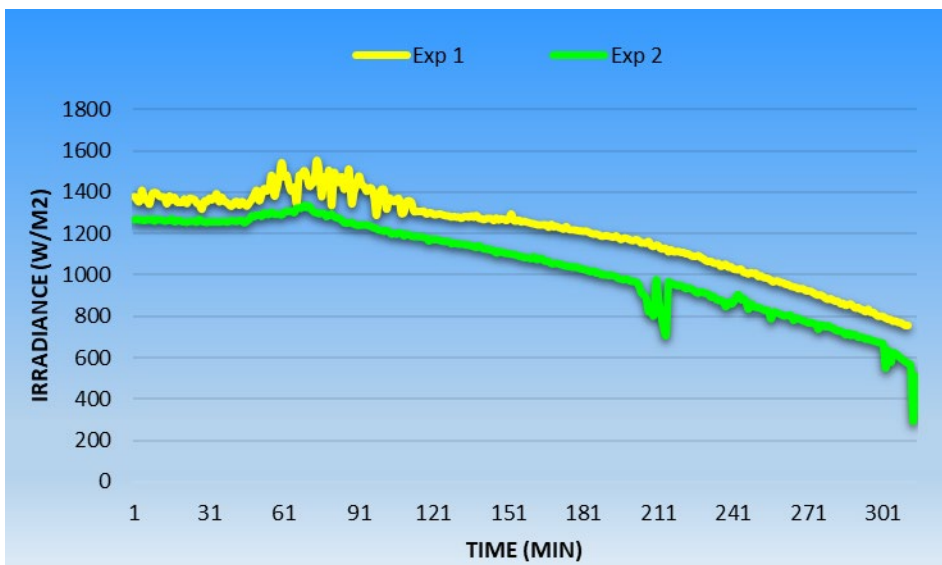


Figure 98. Irradiance during solar drying of a sample of 60 mm diameter and 5 mm thickness, in a sunny day, without airflow introduction

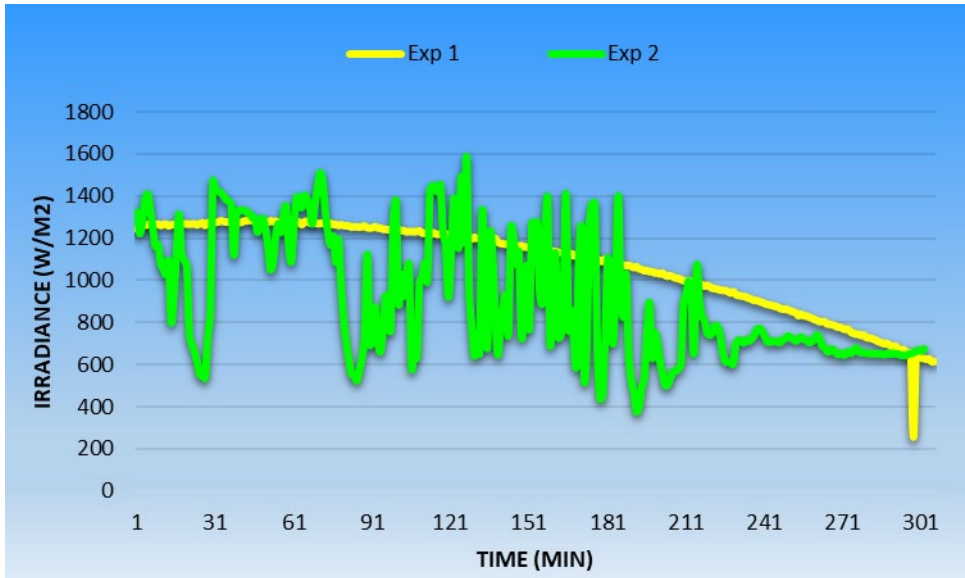


Figure 99. Irradiance during solar drying of a sample of 60 mm diameter and 5 mm thickness, in a sunny day, with an airflow velocity of 1 m/s within the drying chamber and no pre-heating

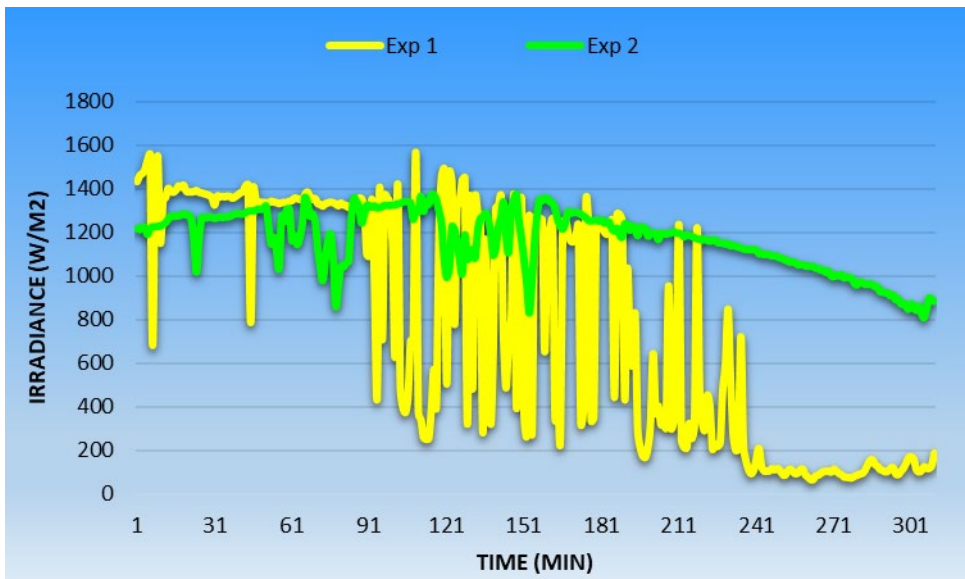


Figure 100. Irradiance during solar drying of a sample of 60 mm diameter and 5 mm thickness, in a sunny day, with an airflow velocity of 0.5 m/s within the drying chamber and pre-heated at 30°C

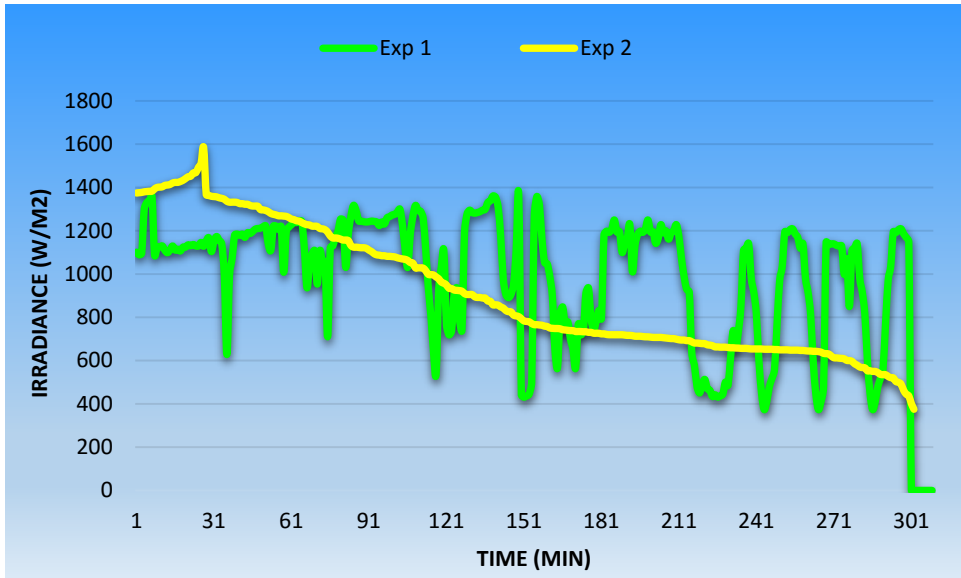


Figure 101. Irradiance during solar drying of a sample of 60 mm diameter and 5 mm thickness, in a sunny day, with an airflow velocity of 0.5 m/s within the drying chamber and pre-heated at 60°C

# APPENDIX L: TEMPERATURES MEASURED DURING THE EXPERIMENTS (AMBIENT AND DRYING CHAMBER)

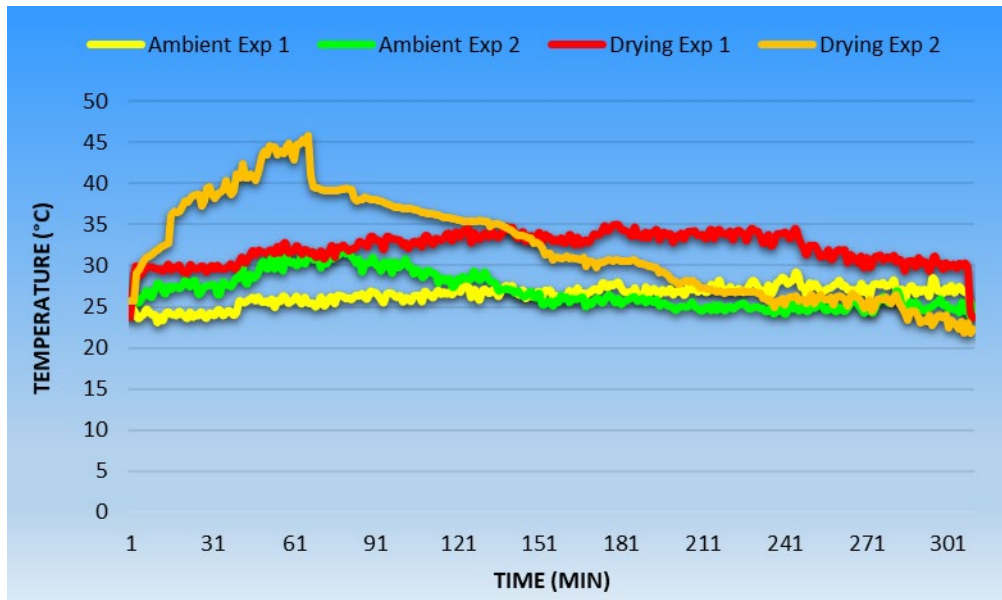


Figure 102. Ambient temperature and temperature in the drying chamber during solar drying of a sample of 60 mm diameter and 5 mm thickness, in a sunny day, with an airflow velocity of 0.5 m/s within the drying chamber and no pre-heating

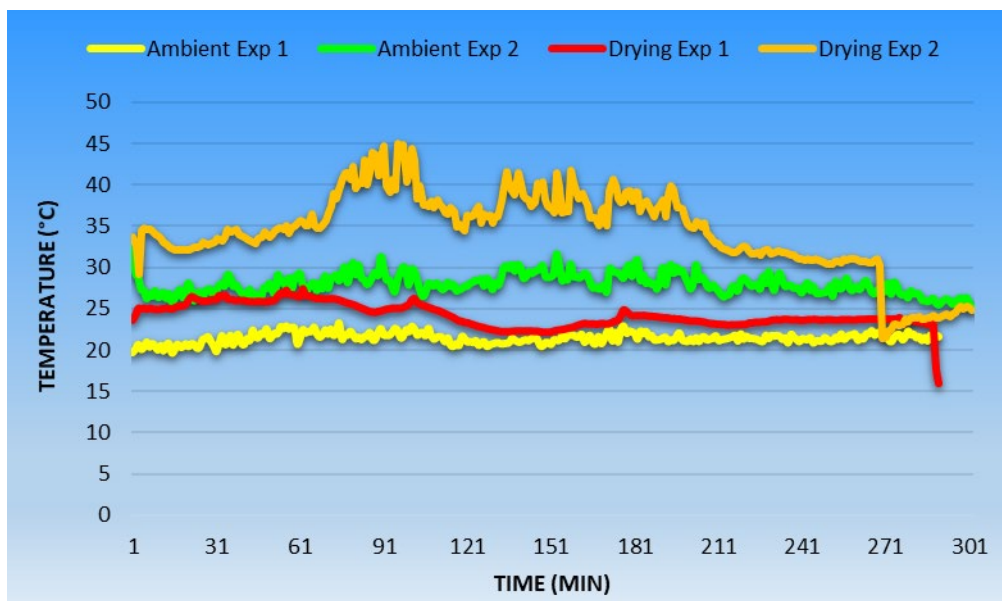


Figure 103. Ambient temperature and temperature in the drying chamber during solar drying of a sample of 60 mm diameter and 5 mm thickness, in a cloudy day, with an airflow velocity of 0.5 m/s within the drying chamber and no pre-heating

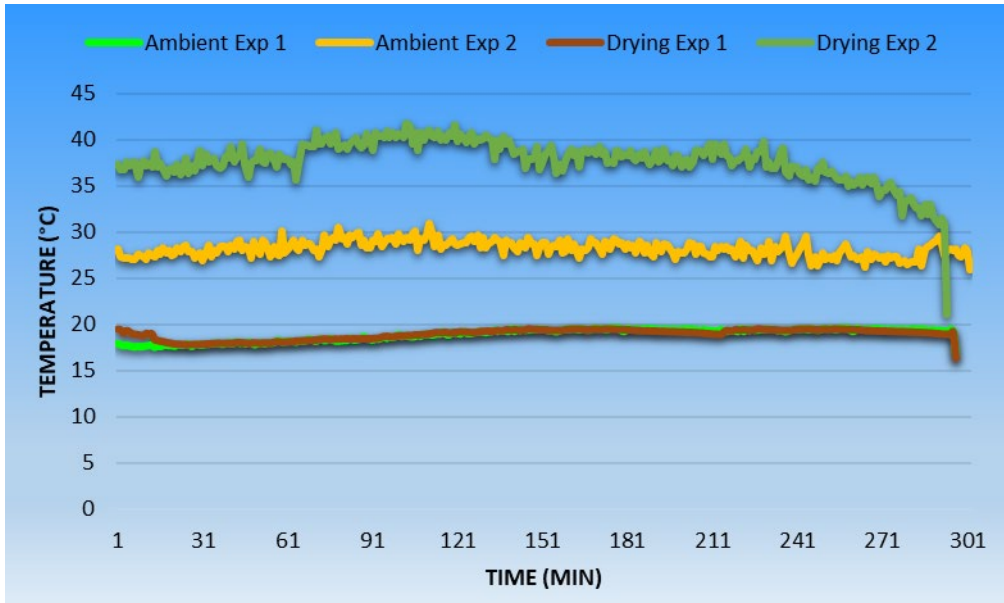


Figure 104. Ambient temperature and temperature in the drying chamber during solar drying of a sample of 60 mm diameter and 5 mm thickness, in an overcast day, with an airflow velocity of 0.5 m/s within the drying chamber and no pre-heating

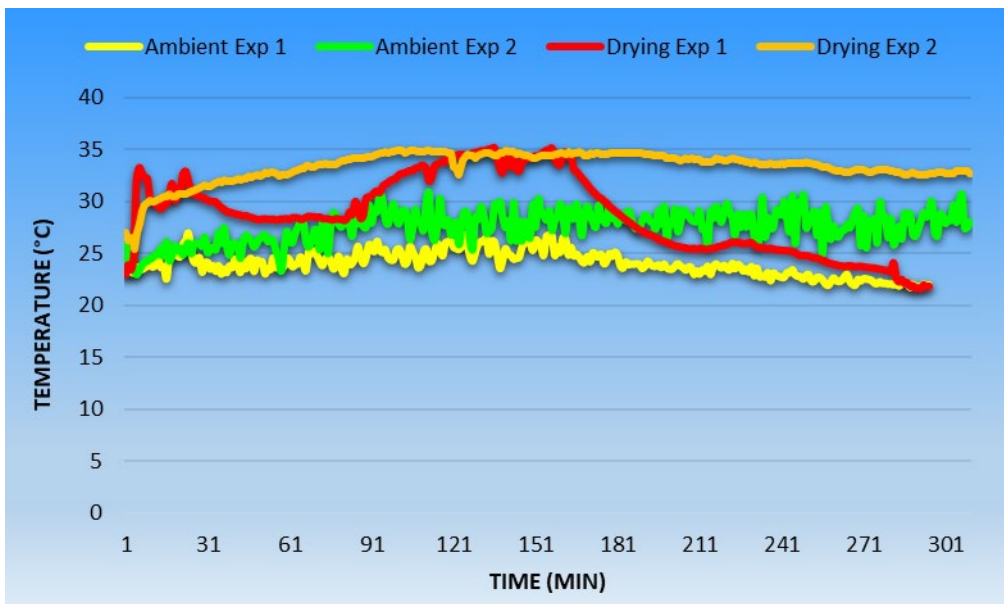


Figure 105. Ambient temperature and temperature in the drying chamber during solar drying of a sample of 60 mm diameter and 10 mm thickness, in a sunny day, with an airflow velocity of 0.5 m/s within the drying chamber and no pre-heating

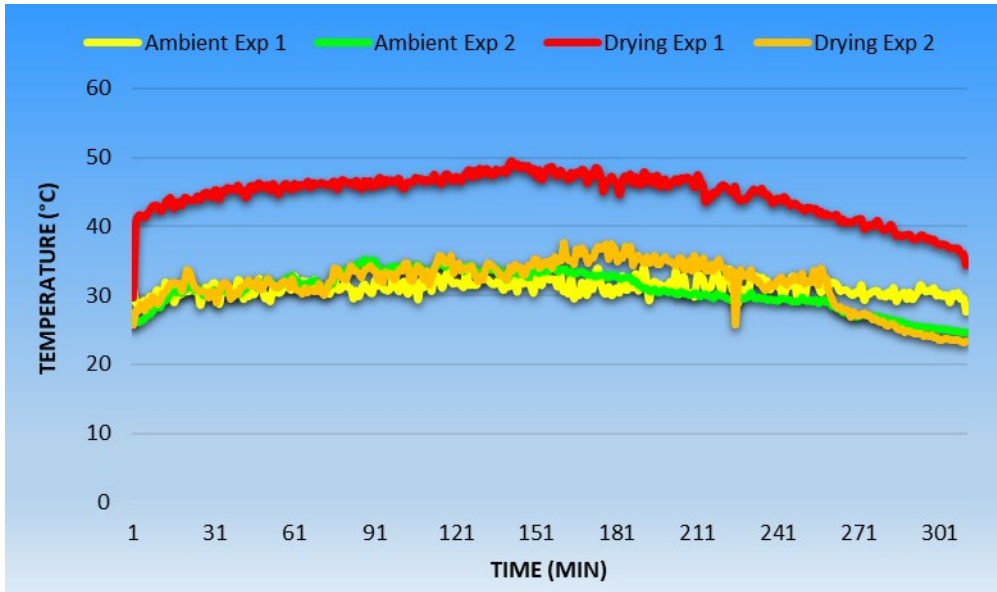


Figure 106. Ambient temperature and temperature in the drying chamber during solar drying of a sample of 120 mm diameter and 5 mm thickness, in a sunny day, with an airflow velocity of 0.5 m/s within the drying chamber and no pre-heating

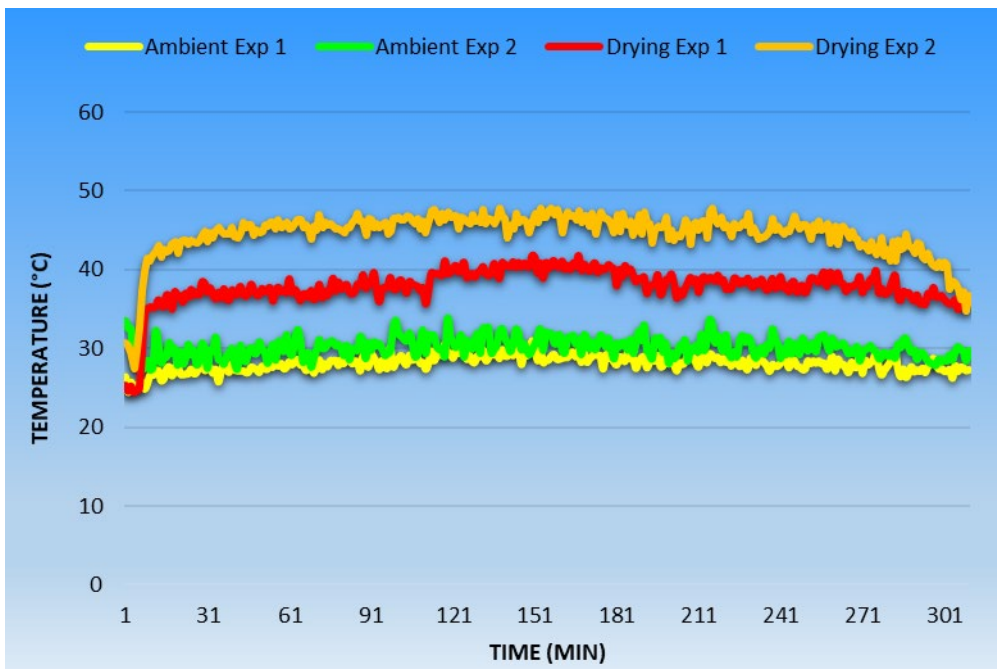


Figure 107. Ambient temperature and temperature in the drying chamber during solar drying of a sample of 60 mm diameter and 5 mm thickness, in sunny day, without airflow introduction

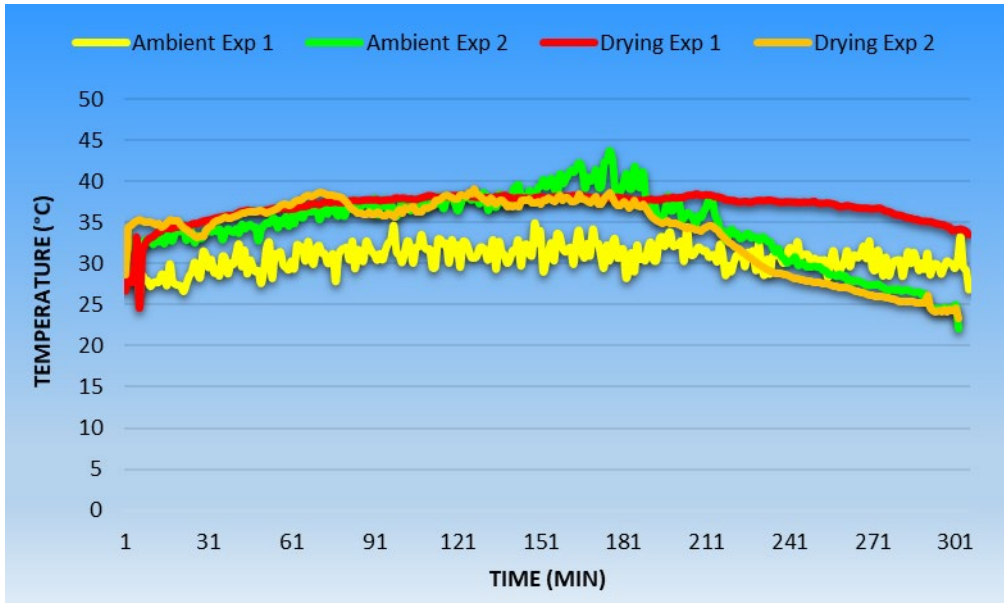


Figure 108. Ambient temperature and temperature in the drying chamber during solar drying of a sample of 60 mm diameter and 5 mm thickness, in a sunny day, with an airflow velocity of 1 m/s within the drying chamber and no pre-heating

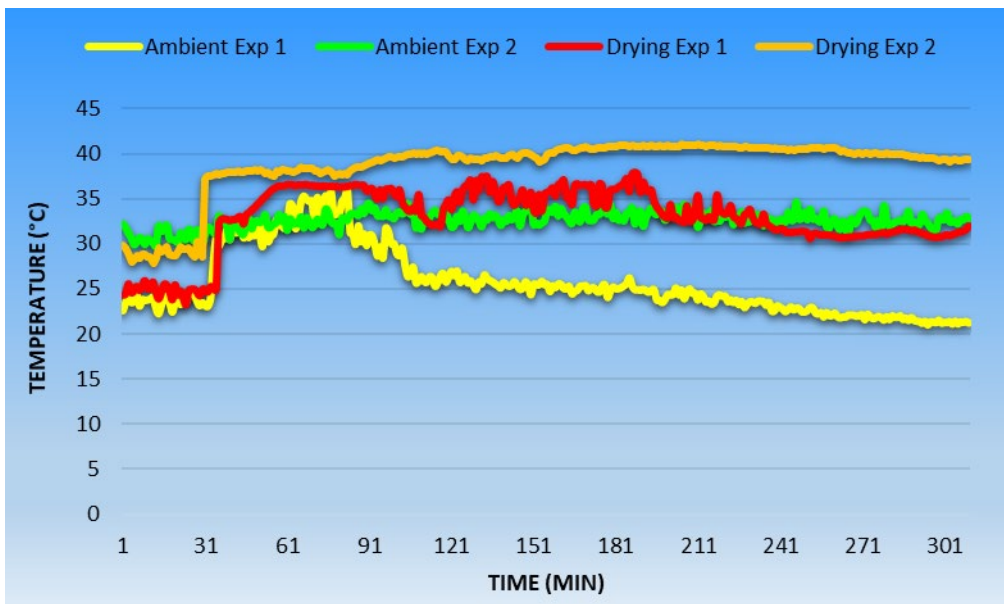


Figure 109. Ambient temperature and temperature in the drying chamber during solar drying of a sample of 60 mm diameter and 5 mm thickness, in a sunny day, with an airflow velocity of 0.5 m/s within the drying chamber and pre-heated at 30°C

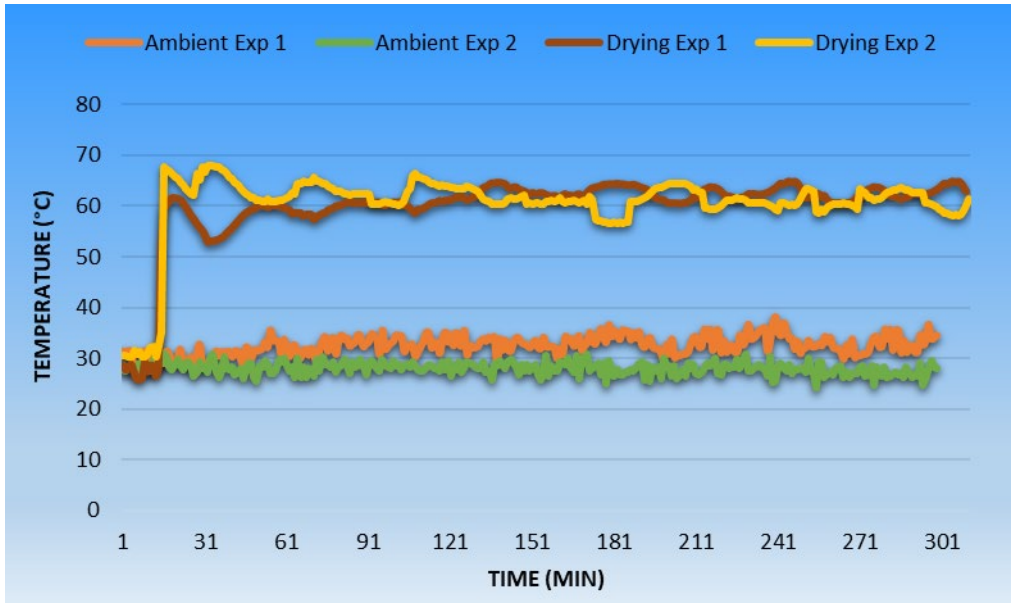


Figure 110. Ambient temperature and temperature in the drying chamber during solar drying of a sample of 60 mm diameter and 5 mm thickness, in a sunny day, with an airflow velocity of 0.5 m/s within the drying chamber and pre-heated at 60°C

## APPENDIX M: NUTRIENT ANALYSIS

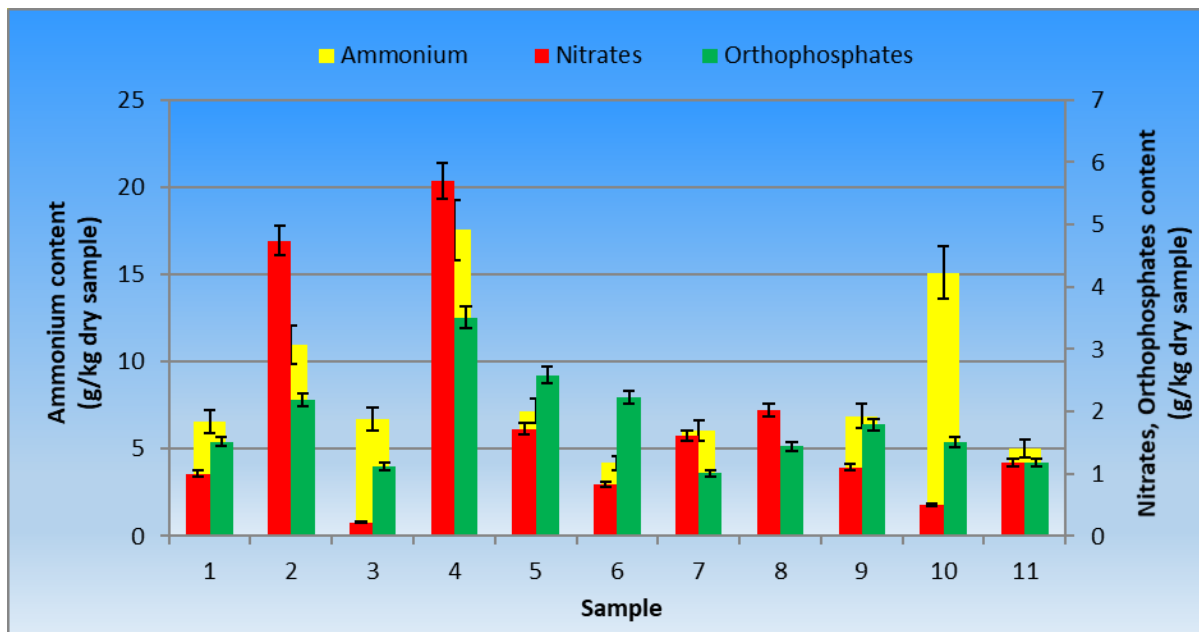


Figure 111. Ammonium, nitrates and orthophosphates content of the sludge samples

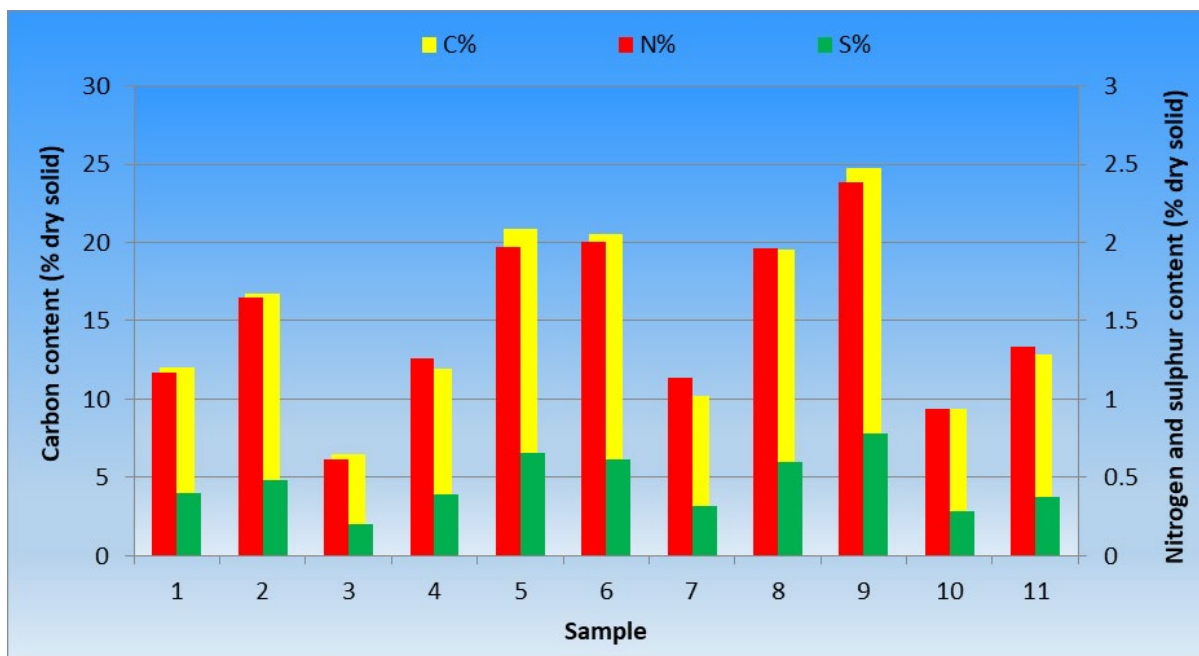


Figure 112. Carbon, nitrogen and sulphur content of the sludge samples